LUND UNIVERSITY

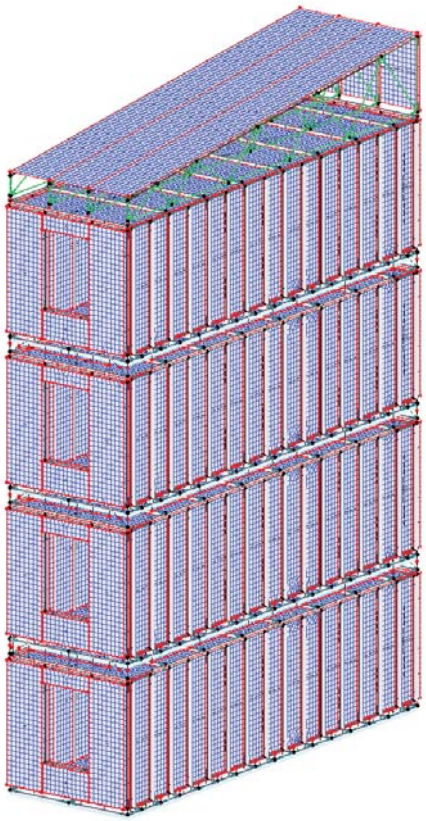

LATERAL STABILISATION IN MULTI-STOREY TIMBER VOLUME ELEMENT BUILDINGS

ELIN JÖNSSON

Structural Mechanics

Master's Dissertation

DEPARTMENT OF CONSTRUCTION SCIENCES

DIVISION OF STRUCTURAL MECHANICS

ISRN LUTVDG/TVSM--19/5231--SE (1-108) | ISSN 0281-6679

MASTER'S DISSERTATION

LATERAL STABILISATION IN MULTI-STOREY TIMBER VOLUME ELEMENT BUILDINGS

ELIN JÖNSSON

Supervisors: Professor **ERIK SERRANO** and Dr **HENRIK DANIELSSON**,
Division of Structural Mechanics, LTH.

Examiner: Professor **PER JOHAN GUSTAFSSON**, Division of Structural Mechanics, LTH.

Printed by V-husets tryckeri LTH, Lund, Sweden, March 2019 *(Pl)*.

For information, address:
Division of Structural Mechanics,
Faculty of Engineering LTH, Lund University, Box 118, SE-221 00 Lund, Sweden.

Homepage: www.byggmek.lth.se

Abstract

The use of timber volume elements (TVEs) in residential multi-storey buildings is increasing in popularity. Manufacturing methods and building processes have been streamlined to improve product quality. However, further streamlining still remains concerning the efficiency of current calculation methods, as many developers still use simple hand calculations. The objective with this dissertation was to create a three-dimensional numerical calculation model of a TVE building system from a well-known TVE developer. The dissertation aimed mainly at providing further knowledge about lateral stabilisation for TVE systems, since this is one of the current challenges for the developer. The focus was on how connections within and between TVEs affect the overall stability of the structural system, and what advantages could be gained from using a three-dimensional numerical model compared to analytical methods.

Numerical models of TVEs were developed using the finite element method. Firstly, individual TVE models were assembled and stiffnesses gained from regarding three-dimensional effects were compared to those obtained from analytical methods. Secondly, the TVE models were assembled into the tallest and most slender configuration possible in regards to lateral stability. Assumptions made in previously performed analytical calculations were tested, as well as further three-dimensional effects from regarding the complete structural system.

The analysis of the individual TVEs resulted in a 30 % stiffness increase compared to analytical methods, mainly from load-sharing between parallel shear walls through the roof. The assembled model of the building system resulted in transverse walls having a significant impact on load-sharing, as rotations and out-of-plane displacements in shear walls increased with increasing building height. Depending on wind load direction and model configuration, 17-40 % of lateral loads were shared with the transverse walls. Overall, the numerical model provided sufficiently accurate depictions of connection force distributions. Thus, further experimental calibrations are required to take full advantage of the three-dimensional structural behaviour.

Preface

This thesis concludes my years as a Civil Engineering student at the Faculty of Engineering. It was carried out at the Division of Structural Mechanics, Lund University. I would like to thank my supervisor, Prof. Erik Serrano, who helped formulate the framework for the thesis. I am grateful for all his valuable input, support and guidance throughout the process. I would also like to thank my assistant supervisor, Dr. Henrik Danielsson, for his input.

Elin Jönsson

Lund, February 2019

Contents

1 Introduction **1**
- 1.1 Background . . . 1
- 1.2 Aims and objectives . . . 2
- 1.3 Methods . . . 2
- 1.4 Limitations . . . 3
- 1.5 Outline of the report . . . 3

2 Timber volume element building systems **5**
- 2.1 Background . . . 5
  - 2.1.1 History . . . 5
  - 2.1.2 Incentives for further development . . . 5
- 2.2 Structural system . . . 6
  - 2.2.1 The tallest configuration . . . 7
  - 2.2.2 Timber volume element structure . . . 7
- 2.3 Load transfer . . . 10
  - 2.3.1 Vertical loads . . . 10
  - 2.3.2 Lateral stabilisation . . . 10
  - 2.3.3 Structural limitations . . . 12

3 Literature study **13**
- 3.1 Shear walls . . . 13
  - 3.1.1 Rigid and hinged connections . . . 14
  - 3.1.2 Springs . . . 14
  - 3.1.3 Simplifications . . . 16
- 3.2 Three-dimensional models . . . 16
  - 3.2.1 Transverse walls . . . 17
  - 3.2.2 Horizontal diaphragms . . . 18
  - 3.2.3 Intercomponent connections . . . 18

4 Analyses methods **21**
- 4.1 The finite element method . . . 21
  - 4.1.1 Nonlinear static analysis . . . 21
- 4.2 Verification of static equilibrium . . . 22
  - 4.2.1 Wind pressure loads . . . 22

5 Numerical modelling **25**
- 5.1 Pre-study . . . 25
  - 5.1.1 Modelling methods . . . 25

5.1.2 Substructuring . . . 26
5.1.3 Remarks . . . 27
5.2 Finite element models . . . 27
5.2.1 Shear wall stiffness calibration . . . 28
5.2.2 Timber volume elements . . . 33
5.2.3 Roof . . . 38
5.2.4 Connections between TVEs . . . 39
5.2.5 Configurations and load cases . . . 41

6 Numerical analyses **45**
6.1 Visualisation of increased stiffness . . . 45
6.2 Wind load cases analyses . . . 46
6.2.1 Data selection . . . 47
6.2.2 Support reaction forces distributions . . . 48
6.2.3 Two- and three-dimensional modelling . . . 49
6.2.4 Load-sharing between adjacent modules . . . 55
6.2.5 Load transfer between adjacent shear walls . . . 57
6.2.6 Friction model . . . 58

7 Concluding remarks **61**
7.1 Summary of results . . . 61
7.2 Discussion . . . 62
7.3 Suggestions for further research . . . 63

Bibliography **65**

A Connection and material properties **67**
A.1 Connection stiffness calculations . . . 67
A.1.1 Walls and horizontal diaphragms . . . 67
A.1.2 Intercomponent connections . . . 68
A.2 Timber properties . . . 69
A.3 Fictitious shell matrices . . . 69

B Analyses results - Wind loads towards building long side **73**
B.1 Support reaction forces . . . 73
B.1.1 Complete model . . . 73
B.1.2 Reduced model . . . 75
B.1.3 Reduced model with only shear walls . . . 76
B.1.4 Reduced model with friction . . . 77
B.2 Displacements . . . 78
B.2.1 Complete model . . . 78
B.2.2 Reduced models . . . 79
B.3 Connection forces . . . 81
B.3.1 Vertical connection forces distributions within modules . . . 81
B.3.2 Horizontal force distribution in shear walls . . . 91
B.3.3 Connection forces between modules . . . 93

C Analyses results - Wind loads towards building short side **95**
C.1 Support reaction forces . . . 95

C.1.1 Complete model 95
C.1.2 Complete model with only shear walls 96
C.2 Displacements 97
C.3 Connection forces 98
C.3.1 Vertical connection force distributions 98
C.3.2 Horizontal force distributions in shear walls 102
C.3.3 Horizontal connections between TVEs 104
C.3.4 Vertical connections between TVEs 105

Chapter 1

Introduction

The use of timber volume elements (TVE) in multi-storey buildings is increasing in popularity. For the past two decades, TVE manufacturers have developed and streamlined their production techniques to achieve efficient manufacturing methods and building processes. Today, an additional focal point is further streamlining of the design process.

1.1 Background

Timber volume elements (TVE) have been developed with the objective to reduce on-site construction. A reduced on-site construction gives developers a greater control of the production costs, the quality of the finished product and the overall construction time. It also results in more efficient moisture protection and an improved work environment for builders. Manufacturing methods have been developed for many decades to streamline the construction process, however challenges still remain concerning the efficiency of the design methods.

A well-known timber volume element developer, who due to risks of disclosing company secrets to other developers in the industry has chosen to stay anonymous, is one of the companies wishing to further streamline its design process. The main concern at the moment is lateral stabilisation. Today, the TVE developer uses the same methods for checking stabilisation against lateral loads in their multi-storey TVE buildings as for traditional multi-storey buildings. Simple two-dimensional calculation models are used for determining the capacity of the system. Calculations regarding lateral stabilisation are performed for the ”worst” configuration of the TVE system, i.e. the tallest and most slender configuration possible.

Therefore, new calculations starting from scratch have to be performed for any change in the configuration of the TVE system. This approach is inefficient and time consuming compared to otherwise streamlined production methods. TVEs function as three-dimensional ”boxes”, resulting in an increased stiffness compared to traditional buildings. However, simple two-dimensional methods do not efficiently utilise this increase in stiffness. A further streamlining of the planning process and a utilisation of the increased stiffness would be possible with a three-dimensional calculation model of the TVEs.

1.2 Aims and objectives

The aim of the dissertation is to attain further knowledge about lateral stabilisation for multi-storey TVE buildings. The objective is to create a numerical calculation model of the building system used by the TVE developer, and compare the results to the current approach. What conclusion can be drawn from the FE models regarding stability compared to analytical calculations? The dissertation is carried out in collaboration with the TVE developer and the aim is for the company to be able to use the model when evaluating new configurations of its building system, e.g. changes in the number of TVEs, changes in materials and components or changes in the connections between components. The TVE models are to be used for product development purposes, hence a fairly detailed depiction of the TVEs have to be obtained in the calculations. The models are to be used for determining force distributions, stress distributions, displacements and stiffnesses of the structure, of individual components and of connections.

The TVE developer is particularly interested in attaining further knowledge about the behaviour of the connections between components within the TVEs, as well as the connections between TVEs. Another objective is therefore to investigate how the different connections affect the overall stiffness of the structural system. The developers vision for the future is to implement even more variables in the model and to use it as a tool in its product development.

1.3 Methods

A significant part of the work consisted of gaining insight into and understanding the industrial building system that is used by the TVE developer. Industrial building systems are fundamentally different from traditional building methods since the structural system has been developed for both transport and on-site construction. A literature study was also conducted to establish a knowledge base about multi-storey timber buildings stabilised with shear walls. The literature study mainly focused on different numerical modelling techniques to set a base for developing a numerical calculation model.

A numerical model was developed using the finite element method. A pre-study was firstly carried out using the finite element software Abaqus [1]. The numerical model in Abaqus was then adapted for FE software used by the TVE developer, FEM Design [2], to enable the company to utilise the results and the finished models. Simple three-dimensional models of shear walls were validated using experimental data from previous tests on prototypes of shear walls from the building system. Detailed models of the timber volume elements were then developed using the modelling techniques from the simple shear wall model and theoretical connection stiffness calculations using Eurocode [3].

The validity of the calculations were tested by assembling the TVE models into the ”worst” configuration in regards to lateral stability and comparing it with analytical calculation results currently used by the TVE developer. The TVE models and the assembled configuration models were tested in various ways to determine the impact from different connections within and between the modules. Calculations were performed using nonlinear static anlyses according to the first order theory.

1.4 Limitations

For the work to be executable within the requisites and the time frame for a masters dissertation, some limitations had to be implemented. The numerical models were only developed for studying lateral stabilisation, and analyses were only carried out using static analysis according to the first order theory. Aspects concerning second order theory, such as buckling, is therefore not covered in the analyses.

The overall objective was to study the force distribution in the structural system when regarding the complete three-dimensional behaviour of the TVEs, compared to two-dimensional calculations. The analyses did therefore not aim to design any components or connections. Displacements and forces were only compared between different models, and not to any requirements or design values. Further analyses are required to design the building system, including additional load cases and load combinations, thus this was not covered in the report.

1.5 Outline of the report

Chapter 2 gives an introduction to industrial building systems and describes the building system used by the TVE developer. The structure of the TVEs and the assembled configuration are described, along with explanations of how loads are transferred within and between modules. In chapter 3, the results from the literature study on numerical analyses is presented. The focus is different modelling techniques for buildings stabilised with stud walls, and the different techniques' validity compared to experimental tests on shear walls. Chapter 4 describes the analyses methods used in the numerical analyses, and the development of the numerical models in Abaqus and FEM Design. The results from the numerical analyses are presented and discussed in chapter 5. Chapter 6 contains a summary and discussion regarding the main conclusions drawn from the analyses and suggestions for further work. Detailed results from the work is presented in Appendices B and C.

Chapter 2

Timber volume element building systems

The chapter is an introduction to the industrial production methods used by the TVE developer. The structure and load transfer for its current building system is presented.

2.1 Background

Prefabricated timber elements were invented for streamlining the production of single-family houses, but have been developed to also be used in multi-storey residential buildings. Today, the demand for sustainability in the construction process and the increasing need for more dwellings have made the TVE concept even more popular.

2.1.1 History

The idea of prefabricated houses emerged in the end of the 1920s, with minimising living space as the main objective [4]. In Sweden, the development of prefabricated timber houses started in the 1960s when the first single-family houses with prefabricated timber frames were produced [5]. Due to strict fire regulations, the development from single-family houses to multi-storey residential buildings took several decades. The strict fire regulations were changed in 1994, and new regulations that focus on performance during fire for the entire building rather than the combustibility of the materials were implemented [5]. With the new regulations, multi-storey timber buildings started to increase in popularity. Mainly constructed with traditional methods at first, but prefabricated elements were quickly implemented [5].

2.1.2 Incentives for further development

The decades without any practical experience or development of design methods for multi-storey timber buildings has resulted in challenges with the design process. For timber buildings, further knowledge about lateral stabilisation and deformations is crucial. The

higher the building, the greater the wind loads, resulting in an increased demand for lateral stabilisation. The simple methods developed for checking stabilisation of single-story houses are often not sufficient for designing complex multi-storey timber buildings. The same applies for deformations, where more detailed calculation models are required to more accurately predict deformations when designing high-rise buildings. When using TVEs, simple analytic calculation models are also inefficient due to inabilities to account for their three-dimensional structural behaviour.

Despite the challenges, there are strong incentives for continuing to develop industrial building systems with timber as the main component. One of the primary incentives is the increasing demand for more dwellings. Estimations have shown that there will be a need for 600 000 new dwellings (mainly apartments) in Sweden until 2025 [6] and a further industrialisation of the construction process could be a possible solution. However, there is also an increasing demand for reducing CO_2 emissions in the building industry and to produce more sustainable buildings [7]. Using timber as structural material is an efficient strategy to achieve a reduction. For example, a timber based multistory residential building has a 40 % lower CO_2 emission compared to a similar concrete building during the building process [7].

Figure 2.1: Module lifted into place at a TVE building site.

2.2 Structural system

The building system used by the TVE developer consists of a variety of standardised timber volume elements. Each TVE contains one to two rooms, and the modules can currently be combined to form apartment buildings with up to four storeys. All of the TVEs are manufactured in factories and transported to building sites. Figure 2.1 shows a TVE lifted into place at a TVE building site.

2.2.1 The tallest configuration

Figure 2.2 shows an illustration of the tallest and most slender configuration possible for the building system today in regards to lateral stability. The configuration contains one-bedroom apartments and three-bedroom apartments in four storeys. The one-bedroom apartment consists of two modules: an entrance module (En) containing a bedroom and a bathroom, and a small kitchen module (K1) containing a kitchen and a living room. The three bedroom apartment consists of three modules: an entrance module (En), a large kitchen module (K3) and a bedroom module (B3) with two additional bedrooms. Apartments are accessed via exterior corridors with staircases on the long side of the building. Balconies can be attached to modules K1 and K3.

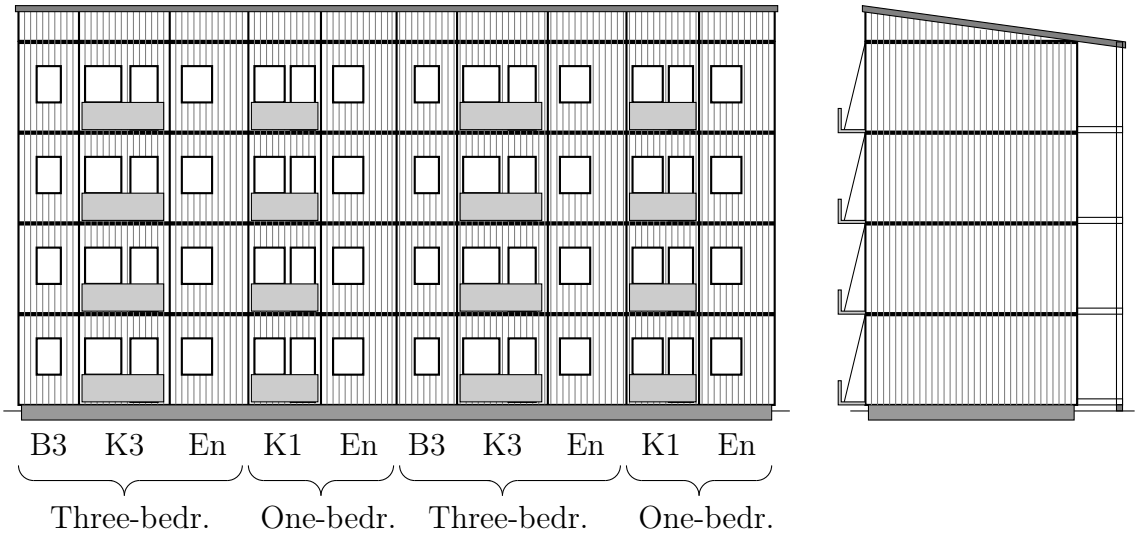

Figure 2.2: Illustration of the tallest and most slender configuration of the building system in regards to lateral stability.

In regards to lateral stability, four storey buildings require a minimum of ten modules along the long side. Three storey buildings require 8 modules and two storey buildings require 5 modules. The building system can be built with either a saddle roof or a mono-pitch roof. The mono-pitch roof (showed in Figure 2.2) will result in the "worst" case in regards to lateral stability since it has the lowest weight in comparison to the uplifting forces generated by wind loads, and is hence used in the analyses.

2.2.2 Timber volume element structure

The structure and size of the TVEs have been adapted for an efficient transport and on-site assembly. The modules are almost 3 meters high and about 9 meters long. The width vary depending on the module type. B3 is the smallest module, 2.6 meters wide, and K3 is the largest module, 3.8 meters wide. The load-bearing system consists of timber frames, with different types of gypsum and wood-based boards. Figure 2.3 presents an illustration of the structure in a typical TVE, with close-ups of important connections.

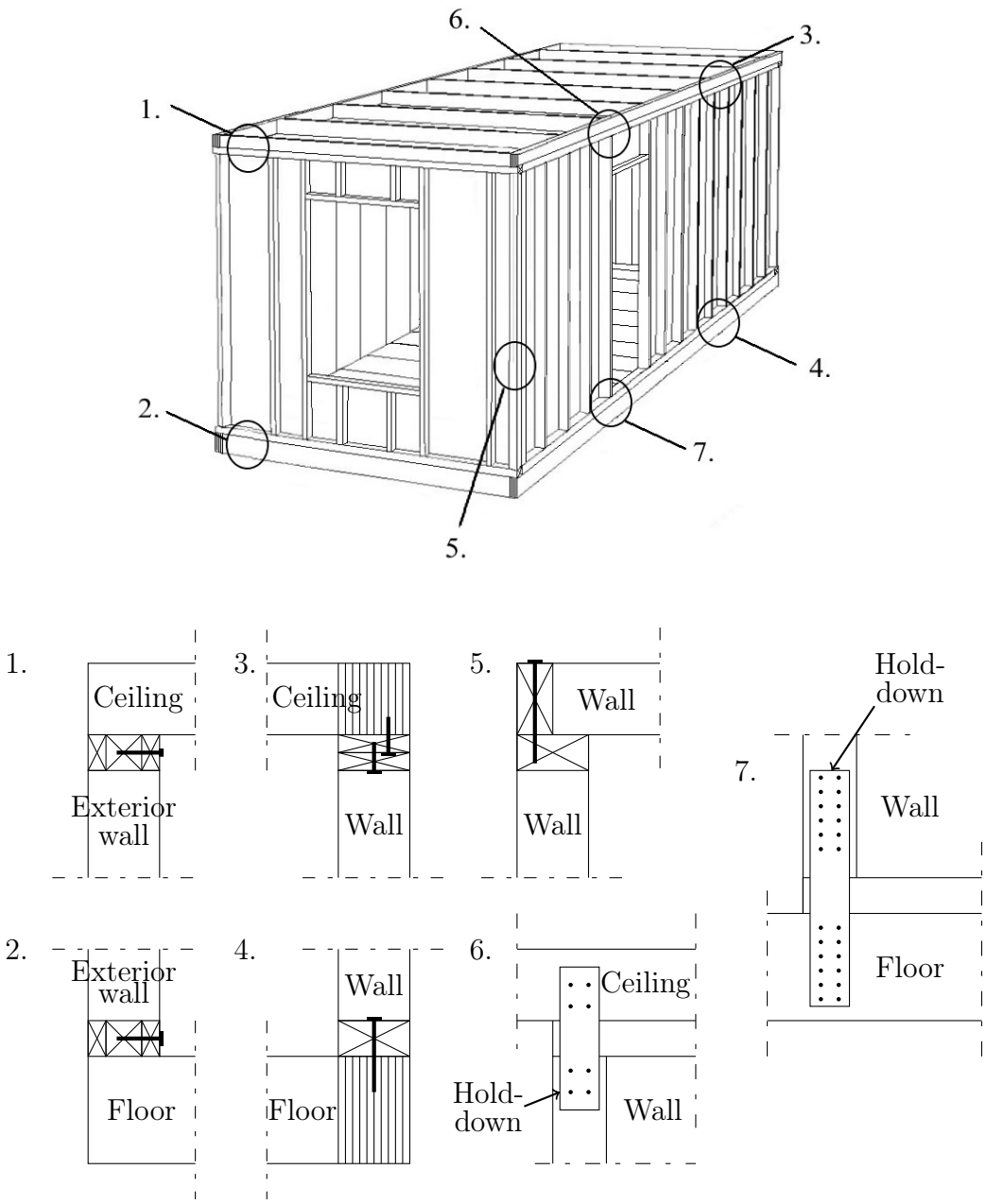

Figure 2.3: illustration of the load-bearing structure in a TVE with close-ups of important connections between components.

Connections within TVEs

Gypsum sheaths and wood-based boards are screwed to the wall, ceiling and floor frames to create stable diaphragms. Connections between components are important for the overall stability of the modules. As can be seen in Figure 2.3, different connections between walls, floors and ceilings are used depending on position within the modules. The connections between the exterior walls (connections 1 and 2) distribute wind loads from the wall to the ceilings and floors. In the walls between modules, simple screwed connections (3 and 4) are sufficient for holding the walls in place. To prevent separation between the walls and floor/ceiling around door openings, hold-downs connect the studs in the wall frames to the floors and ceilings (connections 6 and 7).

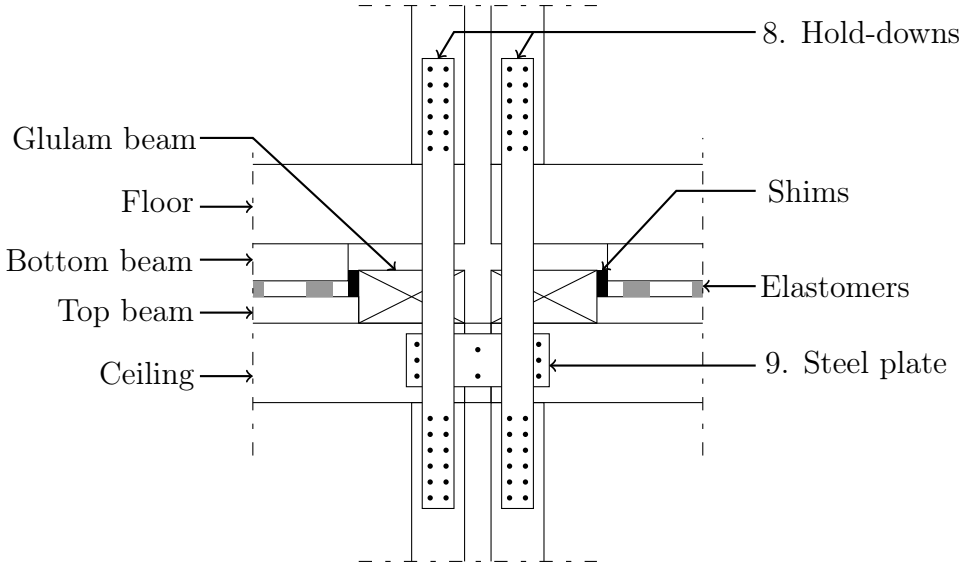

Figure 2.4: Connection between the short sides of four modules.

Connections between TVEs

An illustration of a connection between modules is presented in Figure 2.4. Hold-downs (connection 8) prevent uplift in the walls on the short side of the modules. The steel plate prevents modules from separating and transfer lateral loads between adjacent modules (connection 9). The contact between the glulam beam and the bottom beam prevents the TVEs from moving laterally when the building is subjected to wind loads on the long side of the building. After the module has been lifted into place at the building site, shims are added between the beams to further prevent movements.

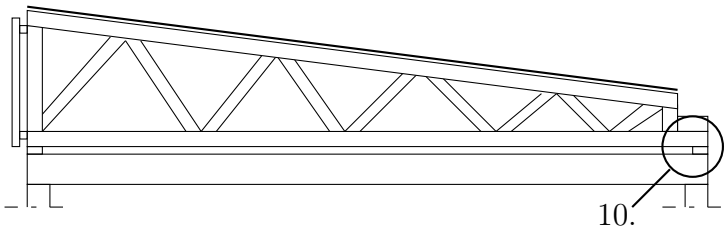

Figure 2.5: Visualisation of a roof truss for the mono-pitch roof, and its connection to the ceiling of the top TVE.

Roof

The roofs in the building system consist of prefabricated truss structures, see Figure 2.5. The roof trusses are connected with a wood panelling on the top (covered with roofing felt), and the sides are covered with windbreak plates. The trusses are connected to the top beam on the short side of the TVE ceiling. Two angle brackets are screwed on each side of the trusses to the ceiling structure, see connection 10 in Figure 2.6. Adjacent modules are also connected through the roof trusses with steel sheets screwed to the trusses, see connection 11 in Figure 2.6.

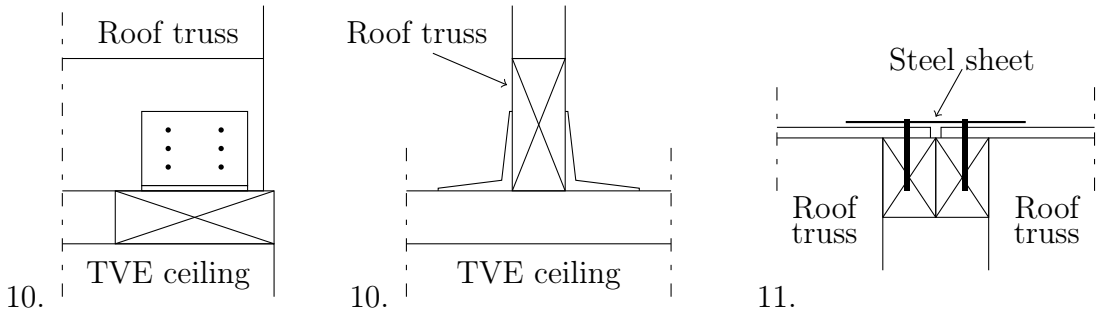

Figure 2.6: Visualisation of angle brackets between the top TVE and the roof trusses (connection 10), and steel sheets between adjacent roof modules (connection 11).

2.3 Load transfer

The load transfer within the building system is affected by the fact that it consists of several small "boxes". The load paths in and between modules are unaffected by the number of modules in the system, resulting in a versatile and easily modified structure.

2.3.1 Vertical loads

Vertical loads from the roof are transferred to the exterior walls on the short side of the TVEs (long side of the building) through connection 10 presented in Figure 2.6. In the modules, vertical forces are transferred through the walls that separate modules from the outside and from other modules. None of the walls within the modules are load-bearing. Between TVEs, loads are transferred through elastomers. The purpose of the elastomers is to prevent noise and vibrations from propagating between apartments. Figure 2.4 shows the connection on the short side, but the same method is used on the long side. Vertical loads from the floor structure is transferred to the bottom beam, through elastomers, and to the top beam in the ceiling structure. No vertical forces are transferred in the corners (through the glulam beams) to further prevent noise and vibration propagation.

2.3.2 Lateral stabilisation

In non-seismic areas, lateral stabilisation primarily means stabilisation against wind loads. Stabilisation becomes increasingly important the higher a building is relative to its width. Insufficient stabilisation can create problems with deformations, noise and vibrations. Several different strategies are available for stabilising multi-storey timber buildings, whence the TVE developer's building system utilises shear walls. Figure 2.7 presents a simple sketch of the lateral load transfer within a TVE. The large arrows represent external wind pressure loads and the small arrows represent the resisting forces from the structure. The ceiling distributes wind loads from the wall on the windward side to the shear walls. The shear walls then direct the loads through the building down to the foundation. Only exterior walls and walls separating modules (not any walls within the modules) are stabilising.

The stability for a shear wall building depends on the position and the load carrying

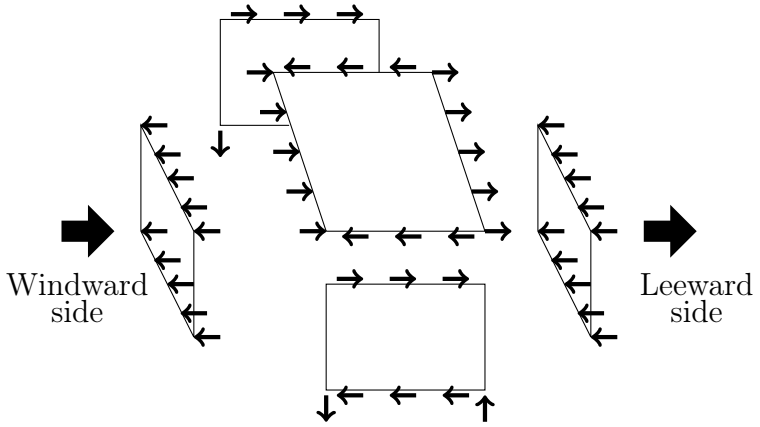

Figure 2.7: Lateral load transfer within a TVE. Source: Adaption from: [8].

capacity of the walls. For an efficient load transfer, shear walls should be placed along all sides of the building and preferably as far away from the centre as possible. A building can be regarded as structurally stable if it contains at least three walls that are not parallel to each other and that do not have a point of intersection. This concludes that each module can be regarded as a stable box. The shear walls enable multiple modules to be stacked whilst maintaining a stable building, since the load paths within each box is unaffected by the number of boxes. Figure 2.8 illustrates the lateral load transfer between modules for wind loads towards the long and short sides of a small TVE building.

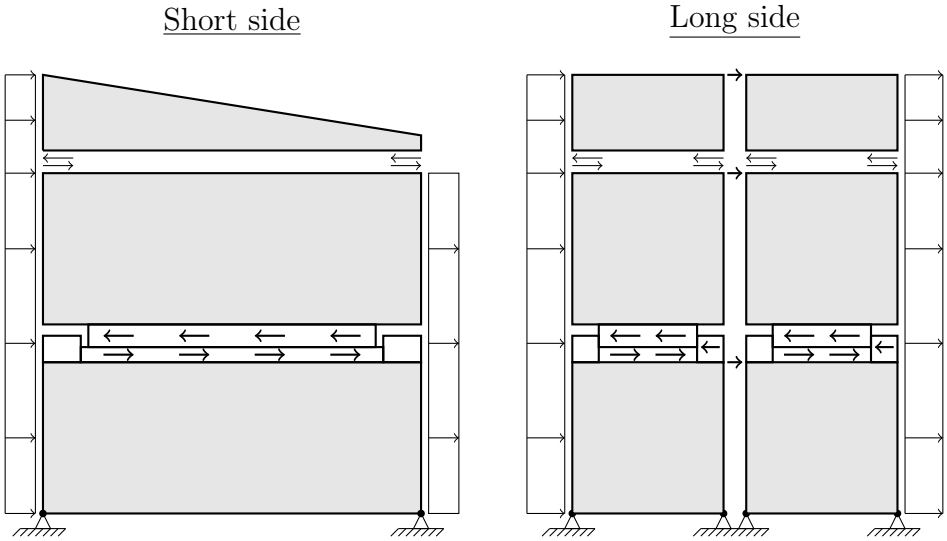

Figure 2.8: Lateral load transfer between TVEs for wind loads against the short and long sides of the modules.

Wind loads towards the roof are directed to the top TVE through the angle brackets illustrated in Figure 2.6. For wind loads towards the long side of the modules, TVEs are prevented from moving laterally by the contact between the glulam beam and the bottom beam. Shims are added between the beams to make the connection stiffer to further prevent movements. Lateral movements are also prevented through friction between the elastomers and the bottom beam (see Figure 2.4). Lateral loads are transferred between adjacent modules through the steel plate (see Figure 2.4). Load-sharing between TVEs is

crucial for wind loads against the long sides of the modules, since the short exterior wall shear capacity in a single TVE is not sufficient to withstand wind loads for a multi-storey building. The steel plates distribute wind loads along all of the exterior walls on the same floor, enabling the individual TVEs to function as one cohesive building.

For wind loads towards the short side of the modules, lateral movements are primarily prevented through friction between the elastomers and the bottom beam. Shims can only be added between beams on the long side of the modules for the first TVE placed, and then only for the outermost long side in the other modules on the same floor. This results in a small gap between the glulam beam and the bottom beam in most of the TVEs in the configuration. On the short sides, shims can be added to all TVEs regardless of position in the configuration, hence enabling a stiffer connection. The TVE buildings are placed on a concrete foundation, and the bottom TVEs are pinned in all four corners with brackets screwed into the concrete. This prevents lateral movements between the foundation and the bottom TVE.

2.3.3 Structural limitations

Using shear walls for stabilisation is very useful in industrial building systems. Modules can easily be added to the structure without a change in load transfer in the individual TVEs. In regards to lateral stability, the maximum number of modules added vertically is limited by the shear capacity of the walls on the long side of the modules, and the minimum number of TVEs required to be added horizontally is limited by the shear capacity of walls on the short side of the modules. The stability also depends on connection stiffnesses for connections within and between TVEs, as well as the largest acceptable displacements.

For a complete design of the structural system, further limitations have to be considered. The load-bearing capacity of connections and components as well as requirements concerning fire protection also influence structural limitations. Furthermore, the use of timber as structural material combined with long span widths (none of the interior walls are load-bearing), require analyses on long-term deformations.

Chapter 3

Literature study

The chapter presents conclusions drawn from the literature study on numerical analyses. The modelling technique affects the complexity and the accuracy of the model, as well as the calculation time. To obtain a usable model, a balance between details and calculation efficiency has to be accomplished. The chapter mainly focuses on different modelling techniques for components and connections, as well as how the different techniques affects the complexity of the model and its validity compared to experimental tests on actual shear walls.

3.1 Shear walls

A number of different studies have been conducted on shear walls. The majority focus on connections rather than components, since the connection stiffness determines the shear wall stiffness. In most studies, the studs and rails are modelled with beam elements and the gypsum or particle boards with shell elements. The frame and sheathing can be given linear elastic behaviour, but the behaviour of the connections are more complex. Nailed and screwed connection behaviours are approximated with springs or other connecting elements calibrated with experimental tests.

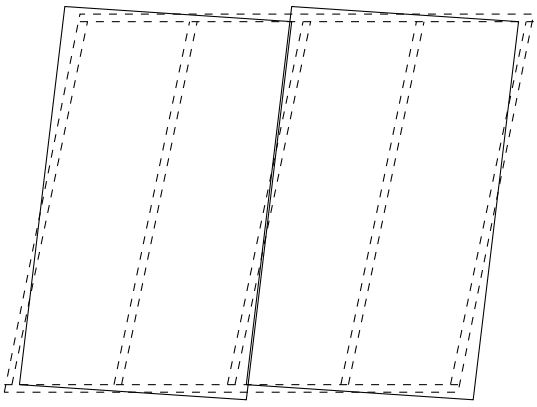

Figure 3.1: Displacement behaviour for a shear wall subjected to lateral loads. Source: Adaption from: [9].

Figure 3.1 illustrate the displacement in a shear wall subjected to lateral loads. The frame (dotted lines in the figure) resists the out-of-plane bending and the vertical loads, and the sheathing (continuous lines) resist most of the in-plane shear [10]. Several separate studies have shown that the connections between the frame and the sheathing are crucial for the shear wall stiffness [9] [11] [12] [13] [14] . The framing to sheathing connection is the weak link in shear walls, failing by nails pulling out of the frame, pulling through the sheathing or simply breaking [9].

3.1.1 Rigid and hinged connections

The simplest possible modelling technique for connections between studs and rails is assuming completely rigid connections. Components are unable to translate and rotate, both vertically and horizontally. Another simple option is to model connections as hinged. A hinged connection enables rotation, but prevents translation. Neither options will result in a realistic model since separation between components is prevented [13]. This results in a significantly higher shear capacity in FE models compared to actual tests on shear walls [13].

3.1.2 Springs

To attain a more realistic numerical model compared to hinged and rigid connections, one approach is to model the joints with springs. Springs are often used in numerical models because of their simplicity and the easy calibration using results from experimental tests. Figure 3.2 presents three different spring models that can be used for modelling compression, tension and shear behaviour for the stud to rail joints and the framing to sheathing joints. The spring stiffness, $\mathbf{K}$, can be expressed in terms of the total forces, $\mathbf{P}$, and the displacements, $\mathbf{u}$, according to

$$\mathbf{P} = \mathbf{K}\mathbf{u} \tag{3.1}$$

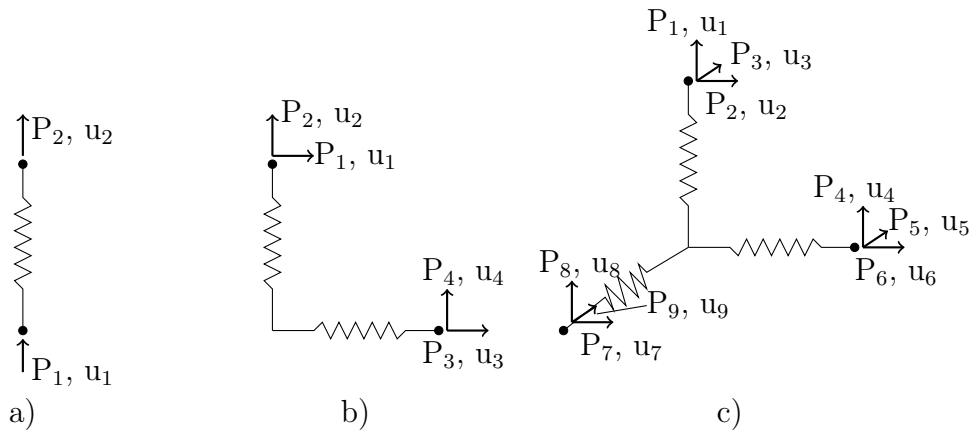

Figure 3.2: Visualisation of springs in a) one , b) two and c) three directions used for modelling compression, tension and shear for connections.

Spring model a in Figure 3.2 gives a sufficient approximation for small deformations and results in an underestimation of the load carrying capacity, making it a safe choice [13]. Larger deformations often result in a change in the spring orientation, causing the behaviour of the entire connection to change [13]. For larger deformations, spring model b in 3.2 with two perpendicular springs has proven to be more accurate when comparing FE model to tests on actual shear walls [13]. The difficulty with using two springs is that the calibration becomes more complicated and the risk of overestimating the stiffness increases [13].

According to Andreasson [15], one or two springs are generally sufficient for modelling connections between the studs and rails. Shear behaviour perpendicular to the plane has secondary importance for shear walls since the forces mainly act in the plane. However, this conclusion is based on a two-dimensional model with loads only in the plane. For the connectors between the frame and the boards, the single spring is too simple for accurately depicting their behaviour since there are loads acting in at least two directions (in a two-dimensional model) [13]. To accurately model shear, tension and compression behaviour between beams and boards, two or three perpendicular springs are generally required [13].

Elastic or plastic behaviour

Springs can be modelled as either elastic or plastic. In elastic springs, the unloading curve follows the reverse load-displacement curve [13]. Plastic springs have an unloading curve determined by the initial stiffness of the load-displacement curve, resulting in permanent deformations of the spring [13]. Plastic springs are therefore mainly used for cyclic loads (e.g. seismic design in regards to earthquakes), since permanent deformations largely impact the load-displacement curve [10]. Vessby [13] concluded that for shear walls with lateral loads, plastic and elastic springs for the frame to sheathing connection will result in similar load-displacement curves [13]. However, the unloading behaviour for diagonal loads are affected by the plasticity to a greater extent [13]. This could imply that spring plasticity becomes more important for high-rise buildings with large vertical loads.

Nonlinear or linear elastic

Elastic springs can be modelled with either linear or nonlinear behaviour. Linear elastic springs are assumed to have a linear load-displacement curve, whilst nonlinear elastic springs have a nonlinear curve. Nonlinear springs have an advantage over linear springs, providing the possibility to include different behaviours in different directions. Andreasson [15] studied the behaviour for joints between studs and rails, and frame to sheathing joints, using small specimen tests. Examples of mechanical properties from the tests are presented in Table 3.1. The frame to sheathing joints have the same stiffness in all directions due to difficulties distinguishing between different behaviours (tension and shear acting coincidentally). The stiffness generally does not depend on timber grain orientation, but rather the nail properties [9].

Table 3.1: Examples of stiffnesses for elastic springs from Andreassons small specimen tests [15].

Fastener type	Stiffness [kN/m]			
	Shear	Tension	Compression	Uniaxial
Framing joint	370	67	4545	-
Frame to sheathing joint	-	-	-	90
Weak (e.g. nails)	-	-	-	300
Semi-rigid (e.g bracket in frame)	-	-	-	1240
Rigid (e.g. bearing cross grain joist)	-	-	-	8100

Coupled or uncoupled behaviour

In models with two and three springs, the springs can be coupled or uncoupled [16]. The individual springs are not affected by the load or the displacement in the other springs in an uncoupled model, but are in a coupled model [16]. Uncoupled spring models therefore overestimate the stiffness and should be used with caution [16]. Coupled spring models underestimate stiffness, but also result in more complicated calibrations for the individual springs [16]. For simple linear elastic shear wall models, uncoupled spring models have been found to be sufficient for attaining realistic behaviours [13].

3.1.3 Simplifications

For models larger than a single wall, using individual springs for all connections will likely result in a very time-consuming modelling process. For large buildings, the internal forces and displacements in each component have secondary importance compared to the overall behaviour of the walls. Consequently, some simplifications of the model are generally advantageous. Vessby [13] suggested modelling the frame to sheathing connection with an elastic medium instead of single springs, creating a glue-like contact between the frame and the sheathing.

Another simplified shear wall model was suggested by Kasal och Lechti [17], who divided their shear wall model into smaller substructures instead of components. Important degrees of freedom in the shear wall were identified and an equivalent model was created using beam elements and a nonlinear elastic spring [17]. The vertical load-bearing capacity was determined by the beams and the horizontal load-bearing capacity by the spring [17]. The spring stiffness corresponded to the global stiffness of the wall, including sheathing, frame to sheathing connections and openings [17]. The substructure technique has later been used in several other studies on large structures with shear walls, e.g. in Collins, Kasal, Paevere and Folientes [18] [19] 3D model of a house.

3.2 Three-dimensional models

Studies on single shear walls, and the analytical methods used for determining shear wall stiffness, are two-dimensional and fail to account for the combined three-dimensional behaviour of a building. Effects from the geometry of the building, such as anchoring

the shear walls to transverse walls and to horizontal diaphragms have a large effect on load distribution, uplift at shear wall ends and general load-displacement behaviours. Regarding the TVEs, the intercomponent connections between floors, ceilings and walls are especially important for obtaining its characteristic box behaviour.

3.2.1 Transverse walls

Transverse walls are oriented with their length perpendicular to the length of the shear walls. The purpose of anchoring shear walls to transverse walls is to prevent uplift and therein increase stability. Figure 3.3 illustrates the load transfer in the connection between a shear wall and transverse wall. The risk of uplift increases with decreasing shear wall length. Including transverse walls in calculation models accounts for the entire 3D effect of the building and not only the shear wall capacity. This has been investigated by Källsner, Girhammar and Vessby [20] (among others), who conducted a study comparing experimental tests with different analytical and numerical models of shear walls anchored to transverse walls. Their aim was to investigate different methods of taking influence of transverse walls into account in simple hand calculations and found significant advantages from utilising transverse walls in very simplified shear wall models.

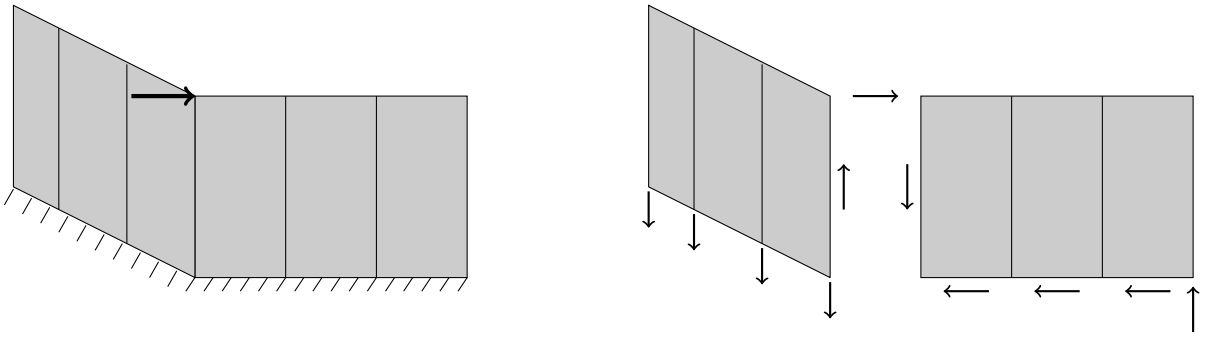

Figure 3.3: Illustration of load transfer between a transverse wall and shear wall subjected to a lateral load. Source: Adaption from [20].

Phillips, Itani and McLean [21] studied the load-distribution in a small rectangular timber-framed house with a size and structure similar to a TVE (4.88×9.75 meters). The shear walls consisted of timber frames with gypsum or plywood boards, and the ceiling consisted of a timber frame with gypsum sheathing on the inside [21]. They found the transverse walls in their model to share 8-25 % of the lateral loads with the shear walls, and the percentage decreased with increasing load applied [21]. However, the transverse walls did not seem to actually transfer any loads between the shear walls [21].

Paevere, Foliente and Kasal [22] also studied load-sharing between parallel shear walls and transverse walls in a full-scale model of an unsymmetrical, one-storey timber house. The house was loaded asymmetrically, one shear wall at a time, for both low-level forces and forces up to maximum load capacity [22]. Just as Phillips, Itani and McLean [21], they concluded that transverse walls stabilised the house and shared lateral loads with the shear walls. However, the out-of-plane reactions from the parallel walls were small, indicating lateral forces were distributed between parallel shear walls through the ceiling and not the transverse walls [22]. They also concluded that close to the maximum load,

during inelastic response from the shear walls, the load-sharing from transverse walls increased (though still small compared to forces transferred in the ceiling) [22].

3.2.2 Horizontal diaphragms

The behaviours of floors and ceilings are important for obtaining an accurate numerical model, since wind loads are mainly distributed to the shear walls through the horizontal diaphragms (as concluded in the section above). The models for the floor and ceiling therefore determine the level of load-sharing between parallel walls. Horizontal diaphragms are in design commonly assumed to be either flexible or rigid. For flexible diaphragms, the walls are assumed to function independently and the loads are distributed to the walls based on tributary areas. For rigid diaphragms, the load is distributed to the parallel shear walls in proportion to the walls' relative stiffness.

Paevere, Foliente and Kasal [22] found that for low-level forces, about 19-78 % of the applied lateral load to a shear wall in their model was shared with other parallel walls through the ceiling. For forces close to the maximum load capacity, there was a significant load-sharing between parallel walls and the ceiling showed a more flexible behaviour [22]. The ceiling had in-plane shear distortions resulting in a rigid-body rotation of the house, though the distortion in the ceiling was still small compared to the displacements in the shear walls [22]. However, the authors commented that the applied asymmetrical load (one wall at a time) is not very likely for environmental conditions, since wind pressures are generally more symmetrically distributed to structures [22].

Phillips, Itani and McLean [21] found the ceiling in their full-scale test house to function much closer to a model with a rigid diaphragm than a model with a flexible diaphragm. Kasal and Leichti [23] came to the same conclusion when studying load distribution for flexible and rigid ceilings. They found that whilst assumed rigid diaphragms overestimates reaction forces in the internal walls and underestimates stiffness in external walls, it still provides sufficiently accurate results if the load-displacement behaviour for the shear walls is known [23].

3.2.3 Intercomponent connections

Experimental tests on light frame timber houses often focus on connections within shear walls, and fewer studies have been conducted on intercomponent connections. Intercomponent connections refer to the connections between floors, ceilings and walls. The importance of these connections are often neglected, resulting in over designing or under designing buildings [24]. For TVE buildings in particular, the intercomponent connections enables the TVE to obtain its characteristic box behaviour and enables load transfer between TVEs (both vertically and horizontally). There are some differences between connections within and between diaphragms. Structural components in floors, ceilings and shears walls are usually connected with simple screwed or nailed connections. Intercomponent connections are often more complex, consisting of hold-downs, brackets, contact surfaces and friction behaviour.

Hold-downs and brackets

Groom [24] conducted a study on four different types of intercomponent connections in a light frame timber building: wall to foundation, exterior wall to exterior wall, interior wall to exterior wall and ceiling to wall. He performed several small specimen tests on each connection to attain load-slip behaviours for nailed and screwed connections [24]. The test results were validated with small scale finite element models for each connection [24]. He concluded that the separation between components can be modelled using nonlinear load-displacement behaviours if single nails or screws are used in the connections [24]. For shear tests on connections consisting of steel plates attached to the timber members with multiple screws, such as hold-downs and brackets, the stiffness for the individual screws was determined by dividing the applied load with the number of screws or nails [24]. The opposite should therefore be applicable when determining the total stiffness for a connection with multiple fasteners, i.e. the individual connectors' stiffness can be added together to attain the total stiffness of the connection [24].

Grooms [24] load-displacement relationships were used by Collins et al. [18] [19] when modelling intercomponent connections in their finite element model of an entire house. They also used nonlinear springs to model all connections, but found the influence of rotational stiffness concluded by Groom [24] negligible in a large scale model. Groom [24] also suggested disregarding the rotational stiffness in the springs, and instead increasing the sheathing stiffness to account for the rotation behaviour.

Hummel [25] created numerical models of prefabricated multi-storey timber buildings with two, four and eight storeys for studying seismic behaviour. The buildings consisted of prefabricated cross laminated timber elements (CLT), but some of the modelling techniques are also applicable for other types of prefabricated timber buildings and for static analyses. Small specimen tests were conducted on intercomponent connections such as hold-downs and angle brackets connecting the CLT walls and floors. He found a significant difference between the primary and secondary load bearing directions for the hold-downs, hence the resistance to tension forces in the direction parallel with its length (primary direction) was significantly higher than the other directions. Angle brackets had considerable capacity in all directions, resisting both shear forces (primary direction) and tension forces (secondary direction) [25]. The shear behaviour for the angle brackets were modelled with linear elastic spring models, see illustration a) in Figure 3.4. The nonlinear tension behaviour for the brackets and hold-downs was modelled using a nonlinear spring with a high compression stiffness (accounting for the timber-to-timber contact) and a low tension stiffness (accounting for the tension stiffness), see illustration b) in Figure 3.4.

Contact and friction behaviour

Simple surface-to-surface contact between components, for example between walls and floors, has been modelled by Hummel [25] among others. He used nonlinear springs with zero tension stiffness and a high compression stiffness to attain a realistic behaviour, see illustration c) in Figure 3.4 [25]. Hummel [25] also modelled friction between timber walls (CLT) and sylodyns (elastomers) by incorporating friction behaviour in nonlinear spring models. The friction force, F_μ, can be expressed as

$$F_\mu = F_N \mu \tag{3.2}$$

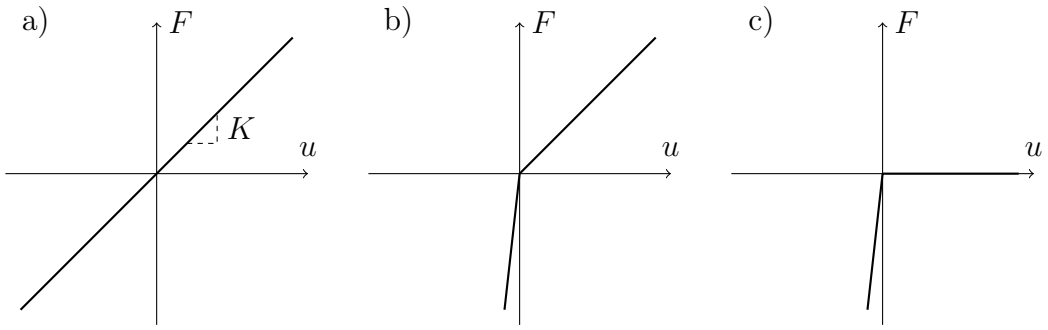

Figure 3.4: Illustration of different spring model behaviours for a) linear elastic nail slip or shear in angle bracket, b) nonlinear elastic tension and compression in hold-down and c) nonlinear elastic for surface-to-surface contact.

where F_N is the force normal to the contact area. The friction coefficient, μ, for the contact surface between timber members and sylodyns was set by Hummel [25] to be constant. He tried different values for the constant, assuming the same properties as between two timber members (a coefficient somewhere between 0.2 and 0.4) [25]. He found the load-bearing capacity to be significantly underestimated without friction and a friction coefficient of 0.38 gave the best agreement to his experimental tests [25].

Chapter 4

Analyses methods

The chapter describes the numerical methods used in the analyses. It also presents the different loads applied to the numerical models, and the load cases covered in the analyses.

4.1 The finite element method

Differential equations used for describing physical problems in engineering mechanics are often too complex to be solved using exact analytical methods. Hence, differential equations are commonly approximated using numerical methods. The finite element method is the numerical approach most commonly used in the industry. Instead of seeking an approximation for an entire region, the finite element method divides the region into smaller parts called finite elements and an approximation is carried out over each element [26]. This collection of elements is called a finite element mesh [26]. The smaller the mesh, the closer the result will be to the exact analytical solution. The approximation is usually a polynomial that describes the changes of a variable over the element, e.g. the elastic behaviour of a body. The variable is assumed to be known at certain points called nodal points. Between the nodal points, the variable is assumed to vary according to the approximation.

4.1.1 Nonlinear static analysis

The finite element analyses are performed using static analysis according to the first order theory. The assembled TVE configuration contains several surface contact connections and other compression supports, allowing parts to make or break contact with the ground or adjacent parts. Hence, a nonlinear analysis is required for accurately depicting the structural behaviour. Using the finite element method, a nonlinear static system can be expressed as

$$\mathbf{K}(\mathbf{u})\ \Delta\mathbf{u} = \Delta\mathbf{f} \tag{4.1}$$

where $\mathbf{K(u)}$ is the global stiffness matrix for the structure as a function of the global displacement vector $\mathbf{u}$. The stiffness matrix describes how the body deforms when external

forces are applied. $\Delta\mathbf{u}$ is the global incremental displacement vector and $\Delta\mathbf{f}$ is the global incremental force vector. The nonlinear analysis in FEM Design determines a solution by an iteration approach [2]. For example, in the first iteration for a compression only support FEM Design checks if tension appears in any support [2]. If so, further iterations are performed with the tension stiffness set to a very low value [2]. The iterations are repeated until no tension occurs in the support [2].

4.2 Verification of static equilibrium

As concluded in the literature study, the magnitudes of the applied loads have a significant influence on structural behaviour, especially load-sharing (between both parallel shear walls and between shear walls and transverse walls). To obtain realistic values for applied loads that enables a comparison with the analytical calculation results, calculations are performed according to load combination EQU, equation 6.10 in EKS [27]. The limit state for a system in regards to static equilibrium is verified according to equation 6.7 in Eurocode [28]:

$$E_{d,dst} \leq E_{d,stb} \tag{4.2}$$

where $E_{d,dst}$ is the design value of the effect of destabilising actions and $E_{d,stb}$ is the design value of the effect of stabilising actions. In this case, the design value of the effect of destabilising actions, $E_{d,dst}$, is the wind load actions. The wind load actions are determined according to

$$E_{d,dst} = \gamma_d \gamma_{kj} Q_{k,1} \tag{4.3}$$

where $Q_{k,1}$ is the characteristic wind pressure load. Factor γ_{kj} is set to 1.5 according to EKS [27]. For consequence class CC3, the partial coefficient γ_d is set to 1.0 [27]. The design value of the effect of stabilising actions, $E_{d,stb}$, is the combined load actions from structural dead loads. The load actions from structural dead loads are determined according to

$$E_{d,stb} = \gamma_d \gamma_{Gj} G_{kj} \tag{4.4}$$

where γ_{Gj} is set to 0.9 for the favourable load case and 1.1 for the unfavourable load case [27]. All other possible stabilising actions come from vertical loads, such as snow loads and imposed loads, and are hence disregarded in the calculations since they would result in more favourable load cases in regards to stability. Wind load actions are therefore the only and leading variable loads.

The FEM Design manual advice against using values for displacements obtained from its ULS calculations, hence a separate load case in serviceability limit state has to be used for a realistic comparison of displacements. In the SLS load case, the characteristic combination of actions is used, which considers irreversible limit states corresponding to permanent damage. Calculations in ULS only determine maximum support reactions and connection forces.

4.2.1 Wind pressure loads

The load cases resulting in the ”worst” case according to analytical calculations are also used in the numerical analyses. Hence, for wind loads towards the long side of the building,

the balcony side is set as the windward side and the corridor side as the leeward side. Wind direction has no influence on calculated wind pressure loads towards the short side (however wind direction will effect internal forces within modules as En is the outermost module at one side and B3 on the other side).

Wind loads for the analyses are determined using a basic wind velocity (v_b) of 26 m/s and terrain category I, resulting in a basic velocity pressure (q_p) of 1.165 kN/m^2. For walls, the external pressure factors for the windward side ($c_{pe,D}$) and the leeward side ($c_{pe,E}$) are calculated according to Table 7.1 in [29]. The width of the house is approximately 34 meters and the depth is approximately 9 meters. The concluded characteristic wind loads for the windward and leeward sides are presented in Table 4.1. Reduction due to correlation is not regarded, hence wind load magnitudes are slightly over-estimated for wind pressure loads towards the long side.

Table 4.1: Characteristic wind pressure loads on the windward ($q_{p,w}$) and leeward ($q_{p,l}$) sides for wind loads against the short and long sides of the building.

Wind pressure loads towards long side					
h [m]	3	6	9	12	14
d [m]	9	9	9	9	9
h/d	0.33	0.67	1.0	1.33	1.56
$c_{pe,D}$	0.71	0.76	0.8	0.8	0.8
$q_{p,w}$ [kN/m^2]	0.83	0.88	0.93	0.93	0.93
$c_{pe,E}$	-0.32	-0.41	-0.50	-0.52	-0.53
$q_{p,l}$ [kN/m^2]	-0.37	-0.48	-0.58	-0.60	-0.62
Wind pressure loads towards short side					
h [m]	3	6	9	12	14
d [m]	34	34	34	34	34
h/d	0.09	0.18	0.26	0.35	0.41
$c_{pe,D}$	0.7	0.7	0.7	0.71	0.78
$q_{p,w}$ [kN/m^2]	0.82	0.82	0.82	0.83	0.91
$c_{pe,E}$	-0.3	-0.3	-0.3	-0.33	-0.45
$q_{p,l}$ [kN/m^2]	-0.35	-0.35	-0.35	-0.38	-0.53

There are three separate load cases for wind pressure loads towards the roof, $\theta = 0$ (corridor long side), $\theta = 180$ (balcony long side) and $\theta = 90$ (short side). External pressure factors for the mono-pitch roof are determined through interpolation, using Tables 7.3a and 7.3b in [29]. The inclination for the mono-pitch roof is approximately 7°. Table 4.2 presents external pressure factors and total wind pressure loads concluded. The maximum uplifting force on the roof is 1.36 kN/m^2 for wind loads towards the balcony side of the building. For wind loads against the short side of the building, an uplifting force of about 0.67 kN/m^2 is generated.

Figure 2.8 presents an illustration of how wind pressure loads were applied to the long side of the building, but the same approach was used for the short side. Wind loads were applied as line loads along the outermost beams in the floor and ceiling diaphragms, on both windward and leeward sides. For the roof, wind loads were applied as surface loads to the wood panelling and the windbreak plates.

Table 4.2: External pressure factors and characteristic wind loads for $\theta = 90$ and $\theta = 180$.

θ	Zone	F_{up}	F_{low}	G	H	I	Q_{roof} $[kN]$
90	Area	2.025	2.025	4.05	32.4	256.5	-210
	Factor	-2.16	-2	-1.82	-0.64	-0.54	
180	Area	28.9		57.8	-	190.4	-427
	Factors	-2.34		-1.3	-0.82	-	

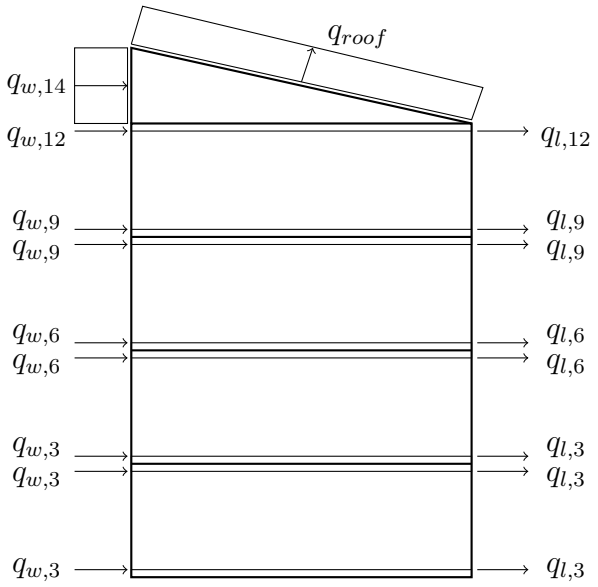

Figure 4.1: Illustration of positions for wind pressure loads.

Chapter 5

Numerical modelling

The chapter presents the process of developing the numerical models. The focal point is the different modelling choices made during the process.

5.1 Pre-study

A pre-study was performed in Abaqus to try different modelling techniques. The focal point is the conclusions drawn regarding the modelling techniques and how the knowledge can be used for developing the model in FEM Design.

5.1.1 Modelling methods

A number of different methods from the literature study was tested to attain realistic and calculation efficient models. Efforts were made to model an elastic medium between the framing members and the gypsum boards, as described by Vessby [13]. In the end, using individual connector elements, known as fasteners in Abaqus, proved to be the most accurate and time-saving approach. These are defined by giving their position in a number of rows and columns in a plane. Figure 5.1 shows a close up of the connections between the framing members and between the frame and the board (top left corner of the shear wall). Fasteners are marked with an X.

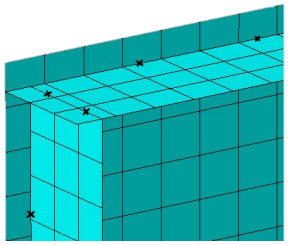

Figure 5.1: Illustration of the fasteners connecting the boards and the timber frame.

The downside with using fasteners is the small element size required (35 mm) for the components to be connected properly, as well as that fasteners are only applicable for

connecting shell elements (the timber frames could not be simplified with beam elements to reduce calculation time). Fasteners require at least one element between the elements which fasteners are connected to for creating individual connection points, hence the small mesh size. The mesh size did not have a noticeable impact on the calculation time for the shear wall models, but proved to be a problem when larger structures were assembled. A static linear calculation for the smallest TVE (B3) required a minimum of one hour, and the largest TVE (K3) required an hour and a half. Considering the final TVE configuration contains 40 TVEs, simplifications were essential for achieving a usable model.

5.1.2 Substructuring

To reduce calculation time, an approach similar to Kasal and Lechti [17] was tested. But instead of only substructuring shear walls, the entire TVEs were simplified into equivalent structures. Abaqus has a built-in substructure function applicable for static stress analysis. A substructure is a collection of elements for which the internal degrees of freedom have been eliminated for the analysis [1]. A reduced stiffness matrix is created, resulting in an easier model definition and a faster analysis [1]. The substructure is connected to the rest of the model with its retained degrees of freedom [1]. There is still a possibility to obtain a detailed result for internal degrees of freedom within the substructures by defining a recovery matrix. The original idea was to create recovery matrices for each of the four different TVEs, and to perform detailed analyses using the recovery matrices for a select number of TVEs in the configuration. The approach would enable comparisons of internal forces and connection forces within one TVE to a TVE located in another position in the building.

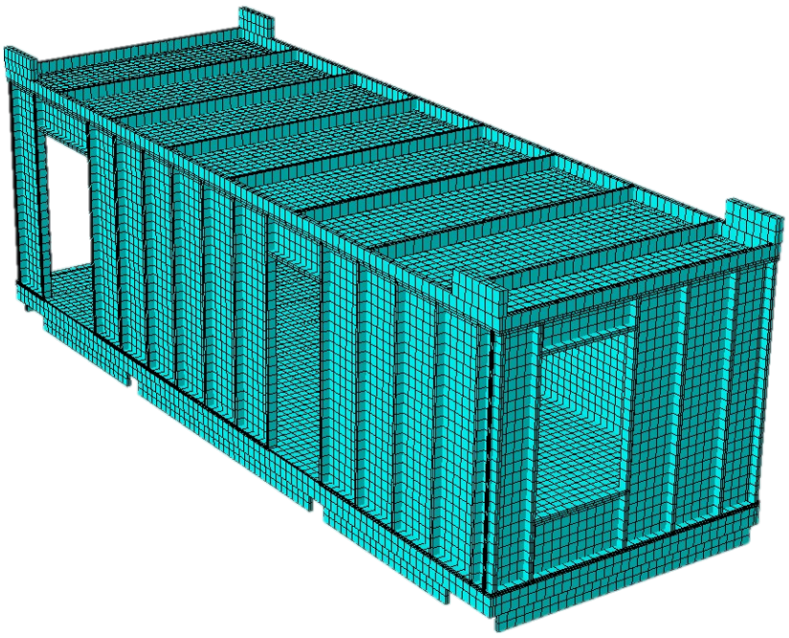

Figure 5.2: Illustration of a TVE model in Abaqus.

Important degrees of freedom within the TVEs were identified, e.g. points for connections to other TVEs and for applying loads, and substructures were generated. Figure 5.2

illustrates a detailed TVE model. The thousands of nodes in the detailed model could be simplified into just 350 in the substructure, reducing calculation time from an hour to less than a minute. Using substructures, the TVE configuration could be assembled and analysed. However, problems arose when generating recovery matrices for the substructures.

The recovery matrix file for one TVE was larger than the memory on the computer, and a computer with a larger memory would have to be used to continue with the original approach. Using the detailed models would therefore not be an option either. An alternative could be to use smaller substructures, each one only depicting a smaller region of the TVE (e.g. one wall), as originally suggested by Kasal and Leichti [17]. Another possible approach would be trying a different modelling technique altogether. Regardless of modelling alternative chosen, continuing with the Abaqus model would be very time consuming. Since the model was only a pre-study and not the finished product, it was therefore decided to continue with the calculations in FEM Design.

5.1.3 Remarks

Despite not finishing the analyses, conclusions can still be drawn regarding the modelling techniques. The substructure technique would have been a possible solution for creating a usable full building model, if the connections in the TVEs had not required such a high level of detailing. The ability to first calculate reaction forces and forces between TVEs, without having to calculate forces within the TVEs, proved to be very calculation efficient. The calculation time for half of the TVE building (5 TVEs wide and 4 TVEs tall) was about one minute. For the final model in FEM Design, an approach allowing the timber frame to be simplified into beam elements is crucial for calculation efficiency. As can be seen in Figure 5.1, the timber frame adds a significant number of elements to the model. A type of ”glue-like” contact between the timber frame and the boards would likely further reduce the number of elements in the gypsum boards.

As can be seen in Figure 5.2, the glulam beams (top corners) and the bottom beams (underneath the floor structure) were also modelled with shells. This resulted in an unnecessary increase in the number of elements, since individual connection points still had to be added to produce the contact (and friction) between TVEs. A more calculation efficient approach would be to model the horizontal contact surface (elastomers and bottom beam) between the TVEs only using one or several connection elements, e.g. springs. The horizontal "stop" provided by the contact between the glulam beam and the bottom beam can also be modelled with a spring. The actual stiffness for these connections are still unknown (theoretical values using Eurocode are used), but could easily be added to the model when obtained.

5.2 Finite element models

The finite element models in FEM Design were developed using results from the pre-study in Abaqus. Stiffness for connections within the shear walls were calibrated using results from experimental tests on actual shear walls from the TVE developers factory.

All other connection stiffnesses were calibrated using Eurocode, and detailed calculations are presented in Appendix A.

5.2.1 Shear wall stiffness calibration

The shear wall models in FEM Design were calibrated with results from experimental tests on actual shear walls from the TVE developers factory. Two separate wall models were used, one for the walls separating modules and one for the exterior walls.

Experimental validation set-up

The experimental tests used for verifying the stiffness for the stud walls in the building system were carried out in accordance with [3], and characteristic values obtained were validated according to section D7.2 in [28]. Figure 5.3 illustrates the prescribed set-up for the stud wall tests according to [30]. The load, $F_{i,v,Ek}$, was applied to the top rail. The outermost stud (on the side where the load was applied) was connected to the test rig with a bracket to create a rigid support. The other studs were screwed to the rig through the bottom rail to create pinned supports. Out-of-plane displacements were prevented with two horizontal, pinned supports in the top rail.

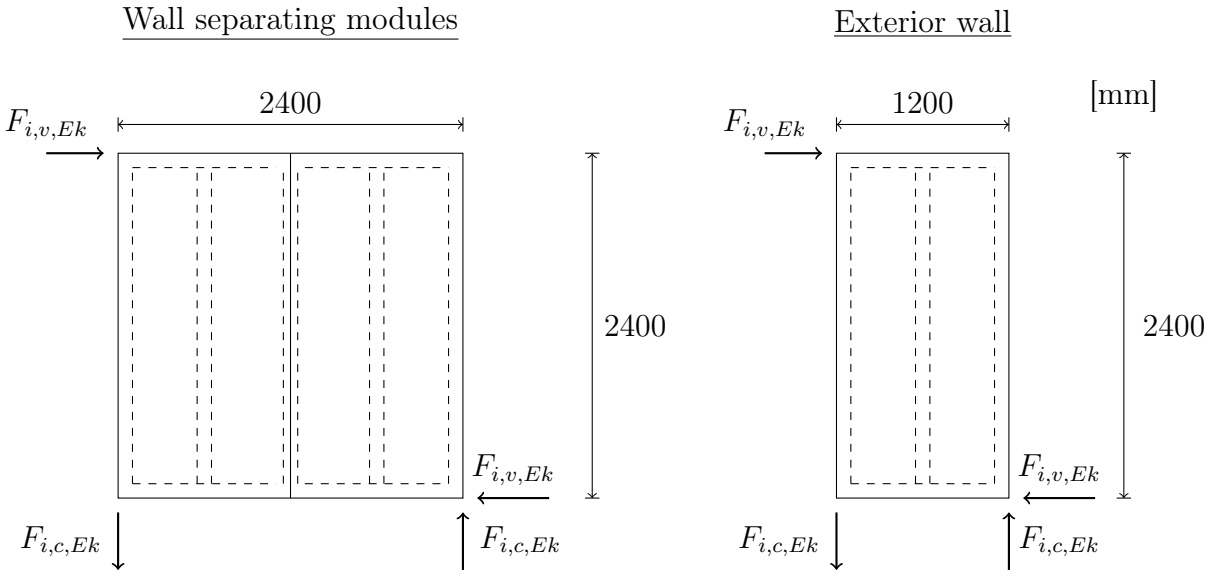

Figure 5.3: A sketch of the set-up for the stud wall tests according to [30].

The wall separating modules consisted of a timber frame with studs and rails measuring 45×95 mm of strength class C14. Two gypsum boards were attached to one side of the frame. The inner Knauf Normal gypsum board, was nailed to the frame (spacing 200 mm), and the outer Knauf Secura gypsum board was screwed on top (spacing 100 mm). The exterior wall consisted of two timber frames. On the inside, a frame with studs and rails measuring 145×145 mm of strength class C18. On the outside, a frame with studs and rails measuring 45×45 mm, also of strength class C18. The separate frames were joined with a nail plate. A Knauf Secura board was screwed to the inner frame (spaced 100mm), and a Knauf humidboard was nailed onto the outer frame (spaced 100 mm).

Displacements in the walls were measured in several different points during the tests. Figure 5.4 shows a sketch of the different measuring points for the two different set-ups. In the wall separating modules, points D2, D3, D4 and D5 measured the vertical displacements in the studs. Points D6, D7 and D8 measured the horizontal displacements in the top rail, outermost stud and bottom rail. For the exterior wall, D2 measured the horizontal displacement in the top rail, D3 the horizontal displacement in the Secura board and D4 the horizontal displacement in the Humidboard. D6 and D7 measured the vertical displacements in the studs. The load-displacement behaviour was approximately linear up to the maximum load in all measuring points for both tests.

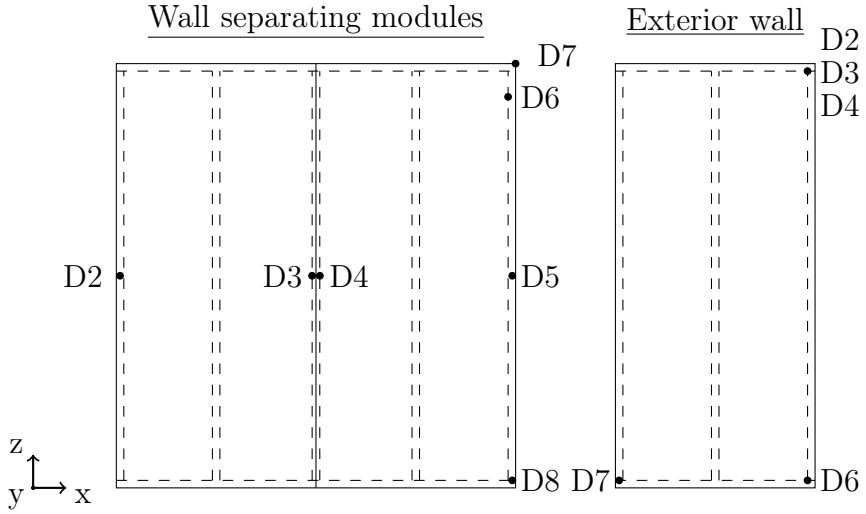

Figure 5.4: Set-up sketches with measuring positions for displacements.

Modelling techniques

Three-dimensional Timoshenko beams were used for the timber frame, and two-dimensional fictitious shells with linear elements were used for the boards. The smallest element size available for the shells in FEM Design, 100 mm, is required for obtaining only square elements. Increasing the element size creates a mix of square and triangular elements, resulting in a poorer depiction of the shear wall behaviour and its stiffness.

The components in the timber frame were connected using point-point connections, i.e. nonlinear elastic springs with six degrees of freedom. The three translation degrees of freedom are denoted K'_x, K'_y and K'_z and the three rotational degrees of freedom are denoted C'_x, C'_y and C'_z. K'_x and K'_y represent the shear behaviour of the nails (horizontal components), and K'_z represent the compression and tension behaviour (vertical component). The timber frame is connected to the gypsum boards with line-line connections. A line-line connection generates nonlinear elastic springs along a connecting line between two elements. Just as a point-point connection, the line-line connection has six degrees of freedom (K'_x, K'_y, K'_z, C'_x, C'_y and C'_z). Local directions for the point-point and line-line connections are presented in Figure 5.5. The translation degrees of freedom are assumed to be linear elastic, with the same properties in all directions. The interface position, r, is placed along the board edge. The rotational degrees of freedom are set as "Free", meaning zero rotational stiffness, for both line-line and point-point connections. For further information about the theory, see the FEM Design manual [2].

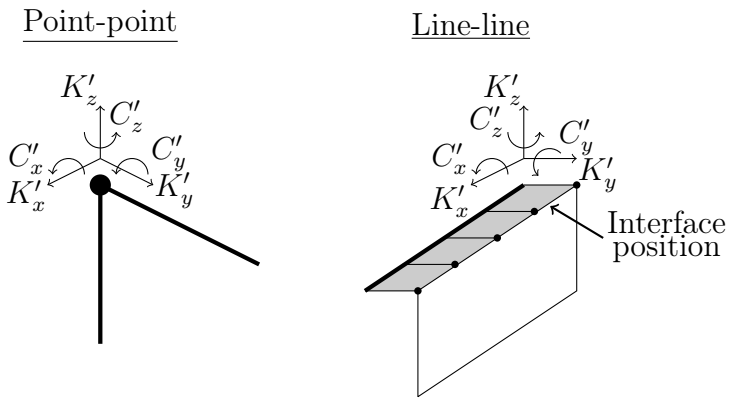

Figure 5.5: Illustration of local directions for a point-point connection between two beams, and a line-line connection between a beam and a shell.

Wall separating modules

The model of the wall separating modules consists of timber frames with beam elements 45×95 mm, given properties of structural timber C14. The two different types of gypsum boards in the frame (Normal gypsum board and Secura board) were simplified into one board. The properties for the fictitious shells modelling the gypsum boards were defined by three matrices, presented in equation A.8 in section A.3, Appendix A. The properties for the timber is presented in section A.2, Appendix A. Figure 5.6 illustrate the components in the wall. The stiffness for the line-line connection was calculated using 15 fasteners per meter, i.e. the inner and the outer board combined. Stiffness for the connections was first set according to Andreassons [15] small specimen tests (see Table 3.1), and increased until the same displacements were obtained as in the experimental validations.

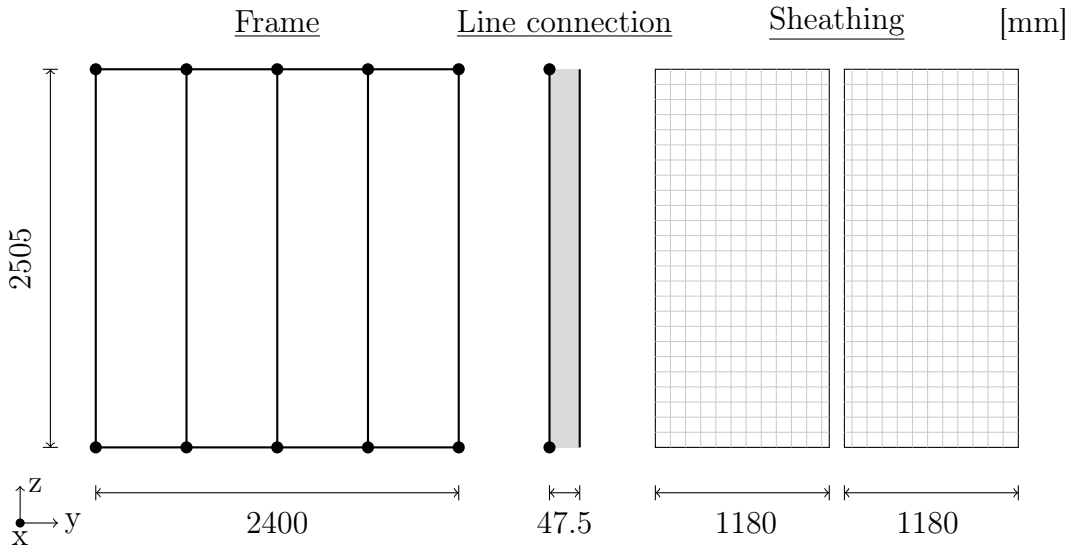

Figure 5.6: Illustration of parts included in the wall separating modules.

The width of the gypsum boards had to be reduced to enable separate connecting lines for each board, since the line-line connections do not allow two or more connecting lines to coincide. The impact from the loss of the edge to edge contact between boards in a stud wall model has been studied by Vessby [13]. He concluded that whilst there are

forces transferred between the boards, the forces have a negligible effect on the load-displacement behaviour and the load-carrying capacity. Without an edge to edge contact, forces between boards are instead transferred in the board to frame connections [13]. Mainly along the top rail, but also along the top part of the stud connected to both boards [13]. Reducing the boards in the FE model will therefore likely not have any significant impact on the shear wall behaviour, apart from an increased stiffness required for the line-line connection. The displacement shape for the wall with reduced boards was still identical to the deformed shear wall in Figure 3.1 despite removing the contact.

Table 5.1: Connection stiffness validation for walls separating modules, before and after calibrations.

	Point-point [kN/m]				Line-line [kN/m/m]	
	$K'_x = K'_y$		K'_z		$K'_x = K'_y = K'_z$	
	C	T	C	T	C	T
Before	740	740	9090	133	1350	1350
After	1221	1221	14999	220	2228	2228

The results from the calibration is presented in Table 5.1. T stands for tension and C for compression in the table. A 65 % stiffness increase was required to obtain the same displacements as in the tests. The required stiffness increase is likely due to differences between the screws used in the experimental validations and those used by Andreasson [15]. In Andreassons tests, the stiffnesses also account for timber and board properties whilst the FE model connections only account for the actual nail or screw properties. Another explanation to the stiffness increase is of course also the missing contact between the gypsum boards in the model. The simplification of the two separate boards into one board likely also impacted the results compared to the experimental test result. Section 9.2.4.2 (7) in [3] prescribes separate boards are directly additive if they are of same type and the same type of connections are used. The same type of board is used in the tests (both gypsum), but the inner board is nailed and the outer one screwed. Thus, the properties might not be directly additive and reduce stiffness compared to tests.

Table 5.2: Comparison with validation in Abaqus.

	Point-point [kN/m]				Line-line [kN/m/m]	
	$K'_x = K'_y$		K'_z		$K'_x = K'_y = K'_z$	
	C	T	C	T	C	T
Before	740	740	9090	133	900	900
After	1480	1480	18180	266	9000	9000

A comparison with results from the more detailed Abaqus model with individual connection points was also conducted. Unlike the FEM Design model, the Abaqus model included the actual edge to edge contact between the gypsum boards. The results are presented in Table 5.2, where the spacing between springs are set to the same as in Abaqus, i.e 10 fasteners per meter (resulting in a lower initial stiffness for the line-line connection). The same displacements as in the experimental tests are attained when the stiffness for the springs are increased with 130 %. In Abaqus, an 80 % increase was required. The higher stiffness required in FEM Design is likely explained by the missing edge-edge contact between the boards, resulting in larger forces transferred in the line connection between the boards and the beams.

Exterior wall

The two separate frames in the exterior wall was simplified into one frame with beam elements 45×220 mm, given properties of structural timber C18. The two gypsum boards were modelled with separate shells. The shell matrices for the inner board, a Knauf Secura board, is presented in equation A.10 and the matrices for the outer board, a Knauf Humidboard, is presented in equation A.9 in Appendix A. The width of the boards were reduced to enable connections to adjacent boards in the TVE models (as concluded in the calibration of the wall separating modules). A sketch of the components in the exterior wall model is presented in Figure 5.7. The stiffness for the line-line connection was calculated assuming a 100 mm spacing between fasteners for both boards.

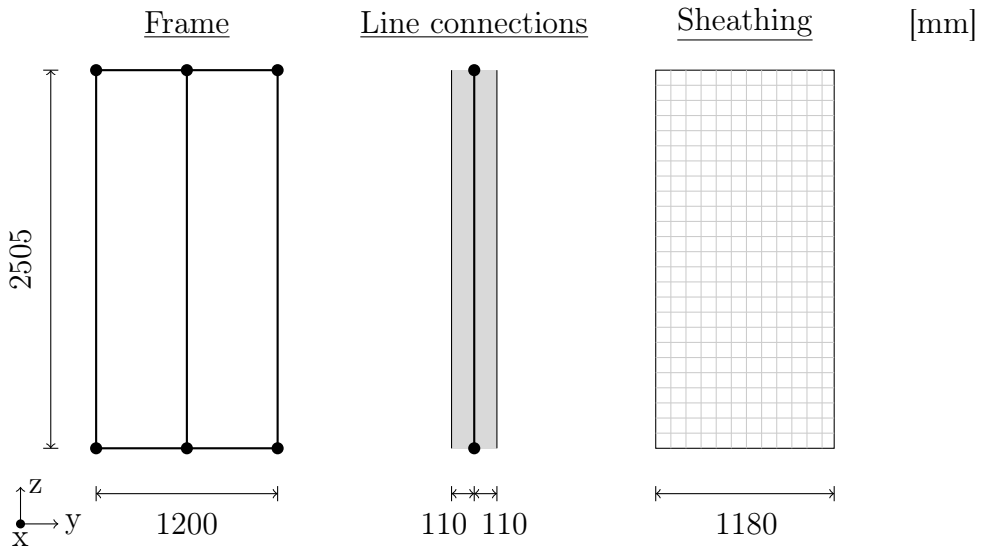

Figure 5.7: Illustration of the parts included in the exterior walls.

Table 5.3: Connection stiffness validation for exterior walls, before and after calibration.

	Point-point [kN/m]				Line-line [kN/m/m]		D2 [mm]
	$K'_x = K'_y$		K'_z		$K'_x = K'_y = K'_z$		
	C	T	C	T	C	T	
Before	740	740	9090	133	900	900	74
After	851	851	10454	153	1035	1035	67

The results from the calibration is presented in Table 5.3. About a 15 % stiffness increase was required to obtain the same displacement as the test. As for the wall separating modules, the increase is likely due to differences in properties for the screws and nails, as well as the model not accounting for timber or board properties. The reason for the lower stiffness increase compared to the wall separating modules is likely due to simplifying the two separate frames into one frame, which significantly increase stiffness.

5.2.2 Timber volume elements

Four different TVE models are used, one for each of the different types included in the configuration presented in Figure 2.2. Apart from differences in geometry, properties for the connections between components in some cases differs depending on the modules' position in the configuration.

Walls

The modelling techniques and properties from the shear wall calibrations above was used for creating the walls in the TVE models. Figure 5.8 presents an illustration of the exterior walls and the walls separating modules. The walls separating modules all have the same length, but for the exterior walls the length is different for different modules. Values for the exterior wall widths, b_1, are presented in Table 5.4. Size and positioning of openings also vary between modules. Apart from all board edges (continuous lines), beams are attached to the boards along line positions coinciding with the position of the beams (dotted lines). Since the analyses only consider stiffness and not load-bearing capacity, no reduction has been implemented on cut boards (i.e. without full height or width).

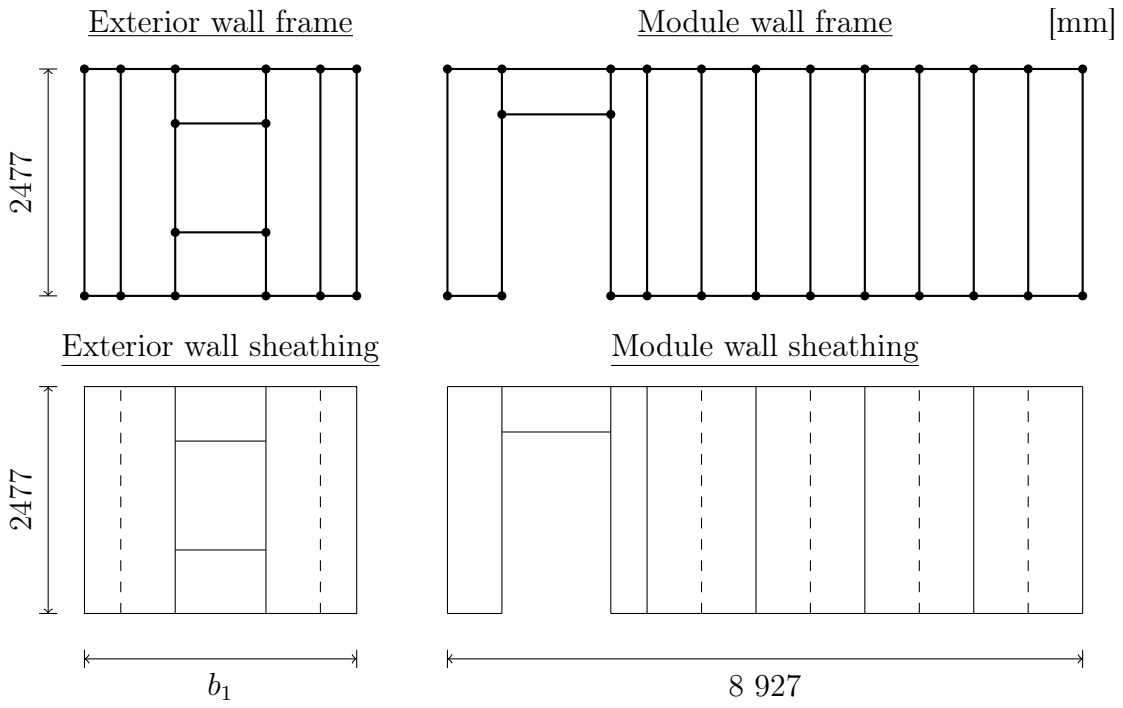

Figure 5.8: Calculation models for the exterior walls and the walls between modules.

A simple convergence study on the walls was also conducted to determine the number of elements required per beam to attain sufficiently accurate shear wall behaviours. The StruSoft FEM Design manual recommends using 4-6 elements per beam, but state up to 20 elements can be required depending on the type of analysis [2]. Walls with 1, 5, 10, 15 and 20 elements were tested by applying a 10 mm point motion support in the corner of the top beam. The reaction force from the wall was compared. The differences between the number of elements per beam was found to be negligible. The difference in reaction

force between using 1 and 20 elements was at most 2 %. No noticeable difference was found between 5 and 20 elements. Hence, influence of number of elements per beam seems negligible for the shear walls. In accordance to the FEM Design manual recommendations, the number of elements per beam is set to 5.

Floors

Timber frames in floors and ceilings were modelled using beam elements and boards were modelled using shell elements (sized 100 mm). The beam elements were connected with point-point connections, and the beams and shells were connected with line-line connections. An approach similar to Andreasson [15] was used, who based his FE model of a multi-storey timber building on the results from Phillips, Itani and McLean [21]. To achieve load-sharing between parallel walls in the model, Andreasson [15] created rigid ceiling diaphragms from simplifying the individual boards in the ceiling into one large board [15]. This enabled the ceiling on each floor to distribute loads to shear walls in relation to stiffness. For the floor and ceiling models in the TVEs, adjacent boards were attached along the same line to the beams to create stiffer connections, enabling the individual boards to function as one board.

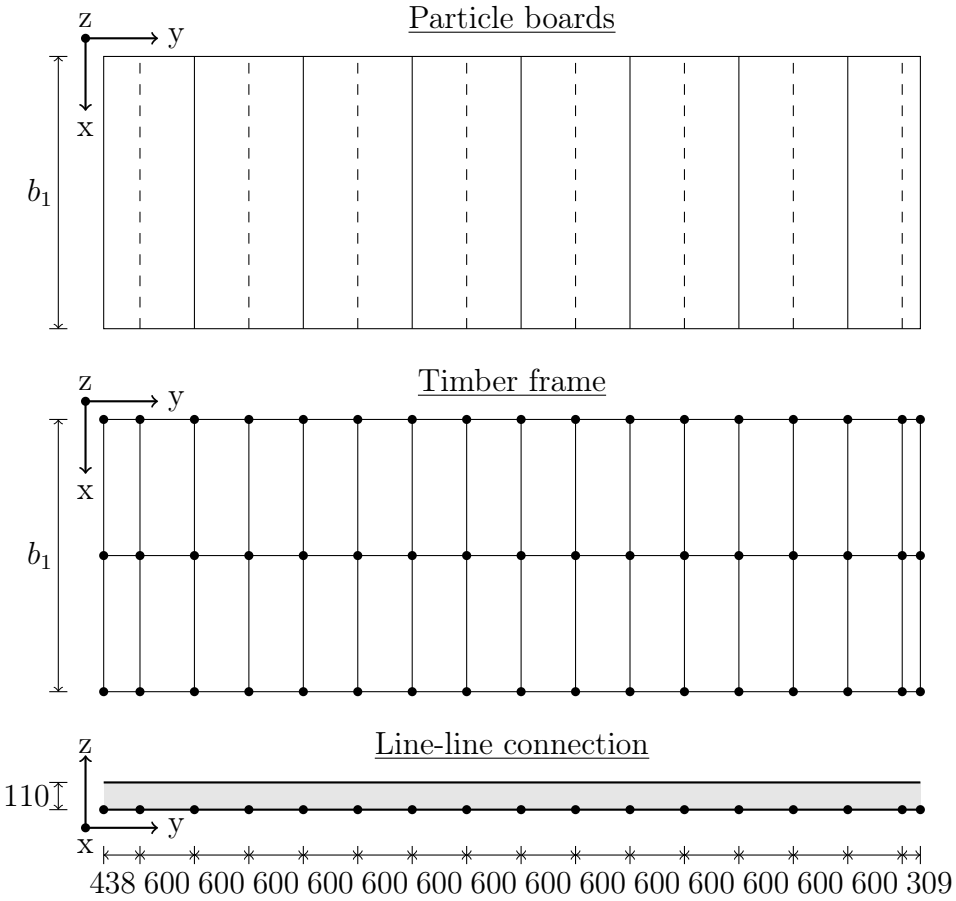

Figure 5.9: Calculation model for the floors.

The floor models consisted of Kerto-S beams, 63×220 mm, along the long side of the frame. Timber beams 45×220, structural timber C24, were placed between the Kerto

beams and connected with point-point connectors. The three screws in the connection were set to have a combined stiffness of 5625 kN/m ($K'_x = K'_y = K'_z$), see calculations Table A.1 in Appendix A. Figure 5.9 illustrates the calculation models used for the components in the floor. The timber beams are attached to a particle board with line-line connections along the edges (continuous lines in Figure 5.9) and the centre (dashed lines) of the boards.

The stiffness for the line-line connectors are different for different modules, since the spacing between screws depend on the modules' position in the configuration. For the modules placed on the gables, En and B3, screws along the edges are spaced 80 mm and the screws along the centre are spaced 160 mm. For the modules placed in the centre of the configuration, K1 and K3, screw spacing is 200 mm along both edge and centre. Table 5.4 presents stiffnesses used for the models, according to calculations in Appendix A. The rotational stiffness is set to zero for both point-point and line-line connections. Each connection is given a local coordinate system with axes parallel to the global coordinate system.

Table 5.4: Widths b_1 and b_2, and stiffness for the connections between the floor beams and the floor boards.

Module	b_1 [m]	b_2 [m]	$K'_x = K'_y = K'_z$, Edge [kN/m/m]	$K'_x = K'_y = K'_z$, Centre [kN/m/m]
En	3.215	3.120	20 625	10 312
K1	3.215	3.120	8250	8250
K3	3.815	3.720	8250	8250
B3	2.783	2.688	20 625	10 312

Ceilings

The ceilings consisted of Kerto-S beams, 145×45, placed along the long sides of the diaphragm and connected to timber beams 145×45, structural timber C24, with point-point connectors. The three screws in the connection were simplified into one point-point connector with stiffness 5193 kN/m ($K'_x = K'_y = K'_z$), see Table A.1 in Appendix A. The rotational stiffness was set to zero. A local coordinate system was created for each connector point and connector line. Figure 5.10 illustrates the calculation model for the ceiling.

The timber beams in the ceiling were only connected to the long sides of the ceiling boards (dotted lines in Figure 5.10) using line-line connections. In reality, the ceiling boards are screwed to a timber panelling. The timber panelling is connected to the ceiling truss with staples. In the model, the timber panelling and the ceiling board were simplified into one structural element modelled as a shell (Secura board, see equation A.10 in Appendix A). The five staples in each panelling to beam connection were simplified into one connection with stiffness 426 kN/m (see Table A.1 in Appendix A), and the spacing between connectors was set to the same as the spacing between the panelling, i.e. 300 mm. This gave a total stiffness of 7100 kN/m/m for the line-line connection (the same for all modules). Each connection was given a local coordinate system with axes parallel to the global coordinate system.

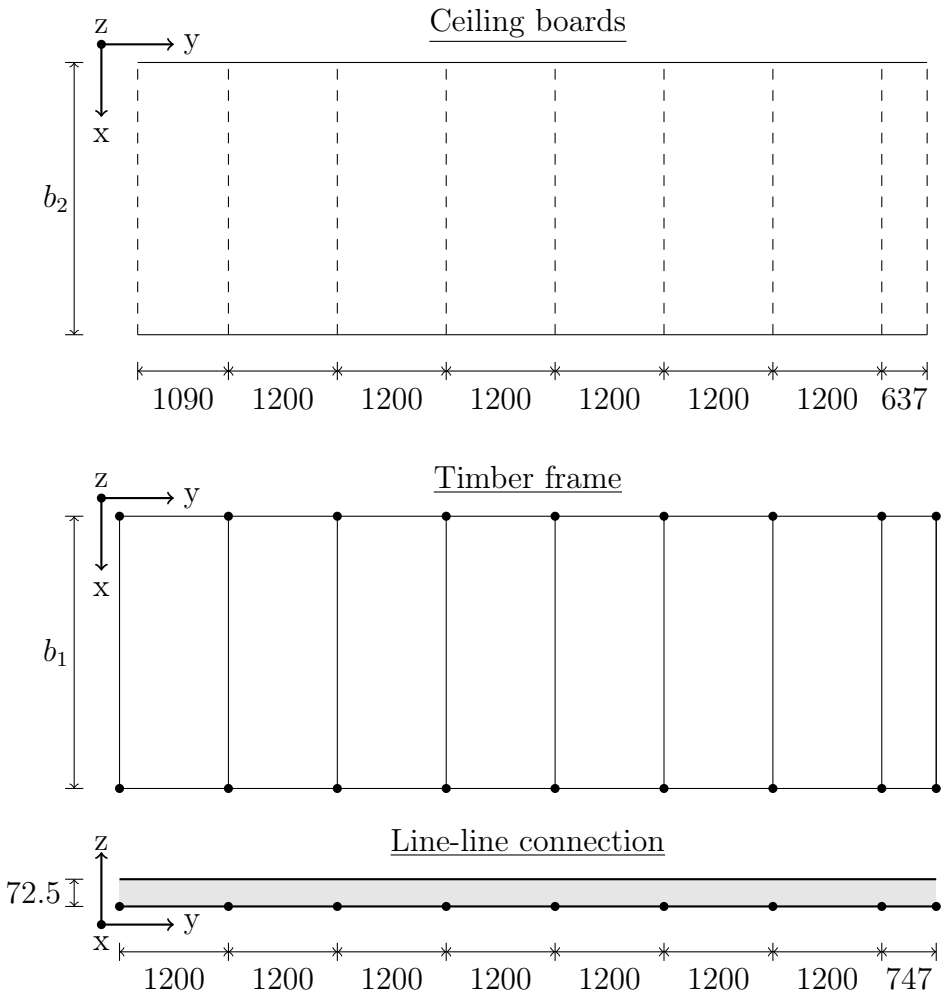

Figure 5.10: Calculation model for the ceiling truss.

Intercomponent connections

The stiffnesses for intercomponent connections were calculated according to Eurocode 5, see Table A.2 in Appendix A. Figure 2.3 in chapter 2 presents illustrations of the connections. Intercomponent connections 1 to 5 were modelled using line-line connections, and connections 6 and 7 were modelled using point-point connections. The calculated stiffness for each connection is presented in Tables 5.5 and 5.6. For the line-line connectors, the rotational stiffness was set to rigid (standard value 174 500 kN/m/° in FEM Design) to obtain a more realistic connection behaviour. The compression stiffness for the hold-downs is set to 0, thus compression forces between wall and floor is assumed to be taken by the line-line connections between the walls and floors or roofs (connections 3 and 4). Each connection was given a local coordinate system with axes parallel to the global coordinate system.

The calculated stiffness according to Eurocode only consider timber density and screw or nail diameter for each connection. Hence, theoretically calculated stiffnesses can be considered a mean value of tension, shear and compression stiffness. This likely results in a overestimation of the tension and shear stiffness, and an underestimation of the compression stiffness. The assumption seems accurate when comparing the theoretical stiffness

Table 5.5: Stiffness for the line-line connections between components within the TVEs.

	d [mm]	Spacing [mm]	$K'_x = K'_y = K'_z$ [kN/m/m]	$C'_x = C'_y = C'_z$ [kN/m/°]
1. Ceiling structure/Exterior wall	6.0	250	5552	174 500
2. Floor structure/Exterior wall	6.5	500	3008	174 500
3. Ceiling structure/Module wall	6.0	250	6040	174 500
4. Floor structure/Module wall	6.0	250	6040	174 500
5. Wall/Wall	8.0	300	5380	174 500

Table 5.6: Stiffness for the hold-downs (point-point connections), connecting the vertical beams to the Kerto beams around openings on the long side of the modules.

	$K'_x = K'_y$ [kN/m]	$K'_{z,T}$ [kN/m]	$K'_{z,C}$ [kN/m]	$C'_x = C'_y = C'_z$ [kN/°]
6. Top hold-down	0	2554	0	0
7. Bottom hold-down	0	7662	0	0

calculations in Table A.1 with the calibration using experimental test results for the stud walls in Tables 5.1 and 5.3. The stiffness calculated for framing joints in the wall separating modules, 1138 kN/m, is significantly lower than the mean value of the experimentally calibrated, 5480 kN/m. Similarly, the theoretically calculated stiffness for the framing joint in the exterior wall is 1288 kN/m compared to a mean value of 3819 kN/m for the experimentally calibrated wall. The calculation results seem therefore sufficient for giving an approximation of the overall behaviour of the TVEs, but further experimental tests are required for calibrating more accurate tension, shear and compression behaviours in the intercomponent connections. Figure 5.11 illustrate an assembled numerical TVE model in FEM Design.

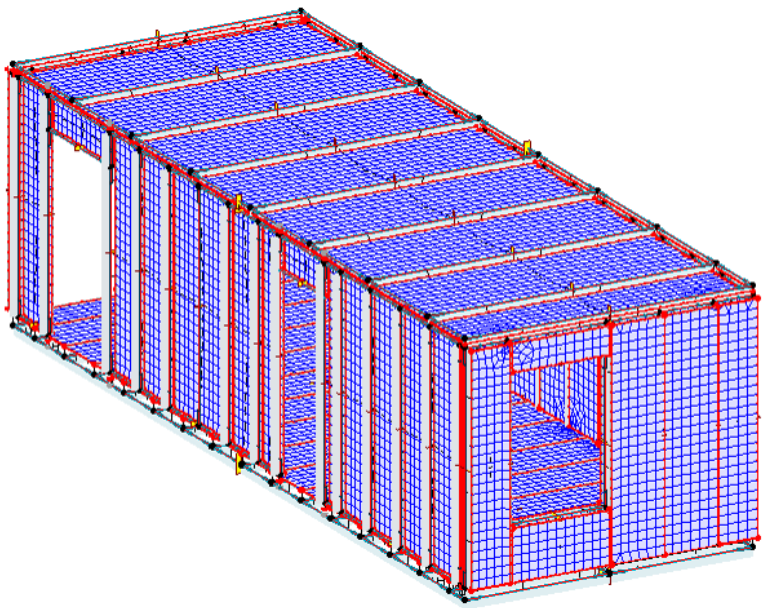

Figure 5.11: Illustration of a TVE model in FEM Design.

Structural dead loads

Simplifying the TVEs to form the FE models reduced their mass compared to the actual TVEs, but the calculations in regards to lateral stability are greatly affected by the mass since it counteracts the uplifting forces from wind loads. The dead loads were therefore multiplied with a factor to compensate for the missing components. This achieved an evenly distributed structural dead load, as in the actual TVEs.

Table 5.7: Structural dead loads for the different TVEs.

Module	TVE weight [Tons]	Model weight [Tons]	Factor
En	7.3	2.7	2.7
K1	7.3	2.7	2.7
K3	8.2	2.9	2.8
B3	6.6	2.5	2.6

The factor was calculated using results from previous estimations in analytical calculations. The ceiling is set to weigh 0.65 kN/m^2, the floor 0.75 kN/m^2, the exterior walls 0.70 kN/m^2 and the walls separating modules 0.4 kN/m^2. A comparison between the actual weights and the model weights are presented in Table 5.7. The factor was calculated by dividing the actual weight with the model weight.

The factor was set to 2.7. To achieve the actual TVE weights for K3 and B3, the weight of the floor and ceiling shells in the models were altered. The shell weights for K3 were increased about 20 % and for B3 reduced about 20 %. The roof was set to weigh approximately 0.3 kN/m^2 in the analytical calculations, which corresponded sufficiently well to the model weights. To avoid overestimating the roof weight when adding the factor, the weight for the weatherproofing boards and the wood panelling was reduced to 0.01 kg/m^3.

5.2.3 Roof

Three different types of roof models were created, one for each of the different TVE widths. The length was the same for all (9 147 mm), and the width was set according to b_1 in Table 5.4. The timber trusses were modelled with bar elements, pinned together with point-point connections ($K'_x = K'_y = K'_z = 10^{10}$ kN/m). The width was the same for all bars, 45 mm, but the height varied between 95 and 145 mm. Timber strength class C24 was used for truss members with height 145 mm, and strength class C18 was used for truss members with height 95 mm. The maximum spacing for the trusses was 1200 mm on centre, resulting in four trusses for roof models En, K1 and B3. Roof model K3 required 5 trusses. The trusses were placed with equal spacing in the individual models (distances between 953 mm and 1071 mm). Figure 2.5 illustrates a roof model.

At first, a detailed model was analysed. The trusses were connected to a wood panelling simplified into a shell in the model (shell matrices for the wood panelling are presented in equation A.12 in Appendix A) on the top. The windbreak plate boards connecting the trusses on the short sides were also modelled as shells (same properties as for the Secura board are assumed, see equation A.10 in Appendix A). Shells were connected to the bars with line-line connections with the same translation stiffness in all directions ($K'_x = K'_y = K'_z = 3243$ kN/m/m). The rotation stiffness was set to rigid.

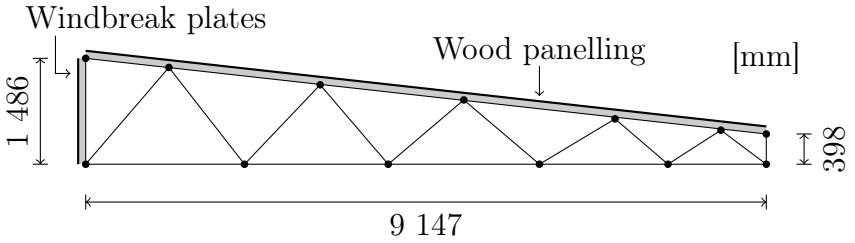

Figure 5.12: Illustration of roof models with windbreak plates and wood panelling.

Secondly, a simplified model was created with bar elements representing the boards as well as the panelling. The purpose was to study if it would have any impact on the number of iterations required to find equilibrium or the total calculation time. The purpose of adding the roof to this model was to transfer lateral loads between adjacent modules and to see if it might contribute to load-sharing between parallel shear walls in different TVEs. The simplified model was also capable of this thanks to the added bars between the trusses. The difference between the models was negligible. The detailed model added no extra iterations and a few extra seconds to the total time. The detailed model was therefore used in the following analyses.

5.2.4 Connections between TVEs

The connections between TVEs are divided into steel connections (hold-downs, plates and brackets), and diffrent types of contact connections (stops and friction).

Hold-downs, plates and brackets

The stiffness for the connections between TVEs were also determined using Eurocode, see Table A.2 in section A. Table 5.8 presents the stiffnesses used in different directions for the hold-downs (connection 8 in Figure 2.4), the steel plate (connection 9 in Figure 2.4), and the angle brackets in the roof (connection 10 in Figure 2.6). The rotational stiffness was assumed rigid for steel plates and roof truss brackets, but zero for the hold-downs (thus only resist tension forces). The connection between the roof modules (connection 11 in Figure 2.6) was modelled with a line-line connection between adjacent trusses, and the rotational stiffness is set to rigid. A local coordinate system was created for each connection, with local axes parallel to the global coordinate system.

Stops

Stops refer to the vertical contact surfaces between the glulam beam and the bottom beam preventing lateral movements between TVEs. The pre-study concluded that a calculation efficient approach would be to exclude the actual beams from the model and instead use springs to model their behaviour. The TVE models were therefore connected using point connections. The translation stiffness in the x-direction was set to rigid in compression whilst all other translation degrees of freedom were set to have zero stiffness. Figure 5.13

Table 5.8: Stiffness (C for compression and T for tension) for connections between TVEs.

	K'_x [kN/m]		K'_y [kN/m]		K'_z [kN/m]		$C'_x = C'_y = C'_z$ [kN/°]
Point-point connections	C	T	C	T	C	T	T/C
8. Hold-down	0	0	0	0	0	5693	0
9. Steel plate	3118	3118	0	0	0	0	1745 000
10. Truss/ceiling brackets	7482	7482	7482	7482	7482	7482	1745 000
Line-line connection	K'_x [kN/m/m]		K'_y [kN/m/m]		K'_z [kN/m/m]		$C'_x = C'_y = C'_z$ [kN/m/°]
11. Truss/truss sheets	3986		3986		3986		0

illustrates the actual connection, the models for the long and short sides, and the local coordinate system directions in respect to the global coordinate system.

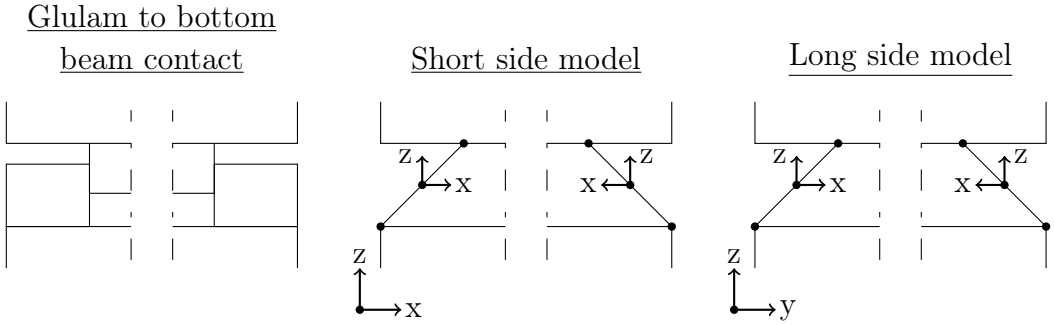

Figure 5.13: Illustration of models for vertical contact surfaces.

Horizontal contact surfaces

In the FEM Design model, nonlinear elastic springs replaced the surface-to-surface contact between the elastomers and the bottom beam. Figure 5.14 illustrates the actual elastomer connection, as well as two calculation models. In model 1, point connections represent the individual elastomers. In model 2, the individual elastomers have been simplified into a line connection assuming they are spaced close enough to distribute vertical loads evenly along the top beam. In both models, the top and bottom beams were eliminated. The floor in the top TVE was connected directly to the ceiling in the bottom TVE. For both connection models, the compression stiffness in the z-direction was set to rigid and remaining translation stiffnesses were set to zero. The rotational stiffness was set as rigid in all directions to represent contact between two planar surfaces.

Using individual connection points or one line connection was found to have a negligible impact on the vertical force distribution within the TVEs. Thus the ceiling was connected to the top beam in the wall frame with a line connection, the vertical force from the elastomers became evenly distributed to the vertical framing members regardless of model. To achieve a difference in load distribution to the vertical framing members, the ceiling to wall and the wall to floor connection would have to be modelled with individual connection points. However, this would provide an unnecessary level of detail to the model. Model 2 proved significantly faster to create, thus chosen for further analyses.

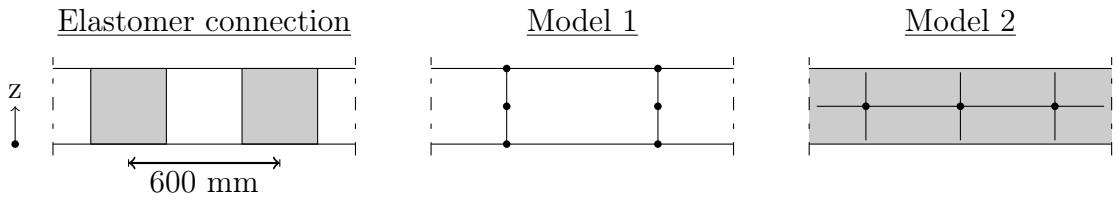

Figure 5.14: Illustration of the elastomer connection and the two different calculation models.

Friction

A alternative approach to using stops for preventing lateral movements, is assuming all lateral forces are prevented by friction between the elastomers and the bottom beam. This has been assumed in the analytical verification. To investigate the assumption, two separate calculation models were created. One assumes all lateral forces are taken by the vertical contact surfaces, thus the friction coefficient for the line connection was set to zero. The other model assumes all lateral forces are taken by friction, in which the point connections representing the glulam to bottom beam contact were removed.

5.2.5 Configurations and load cases

To evaluate how assumptions made for the TVE models affected the stability of the structural system, the TVE models were assembled into two different variations of the configuration. One complete model of the configuration containing 40 TVEs, and one reduced model containing 16 TVEs.

Complete configuration

The complete configuration model is illustrated in Figure 5.15. Axes along the TVE long sides were denoted with letters A to T, and axes on the short sides denoted U and V. The model is 10 TVEs wide and 4 TVEs high, which brings a total of 40 TVEs. The individual roof models were connected to adjacent modules with steel sheets, as described in section 5.2.4, resulting in the roof acting as a continuous beam. Thus, the roof enables all TVEs to function as one structure for wind loads towards both long and short sides.

Reduced configuration

The reduced configuration model is illustrated in Figure 5.16 and consists of four TVE "pillars" corresponding to each of the modules. It was only used for analysing wind loads towards the long side of the building, thus each "pillar" of TVEs can be regarded to function independently. Axes along the TVE long sides were numbered 1 to 8, and axes along the short sides were numbered 9 and 10. The reduced model was more calculation efficient, but disregarded stabilising effects and load-sharing between adjacent modules.

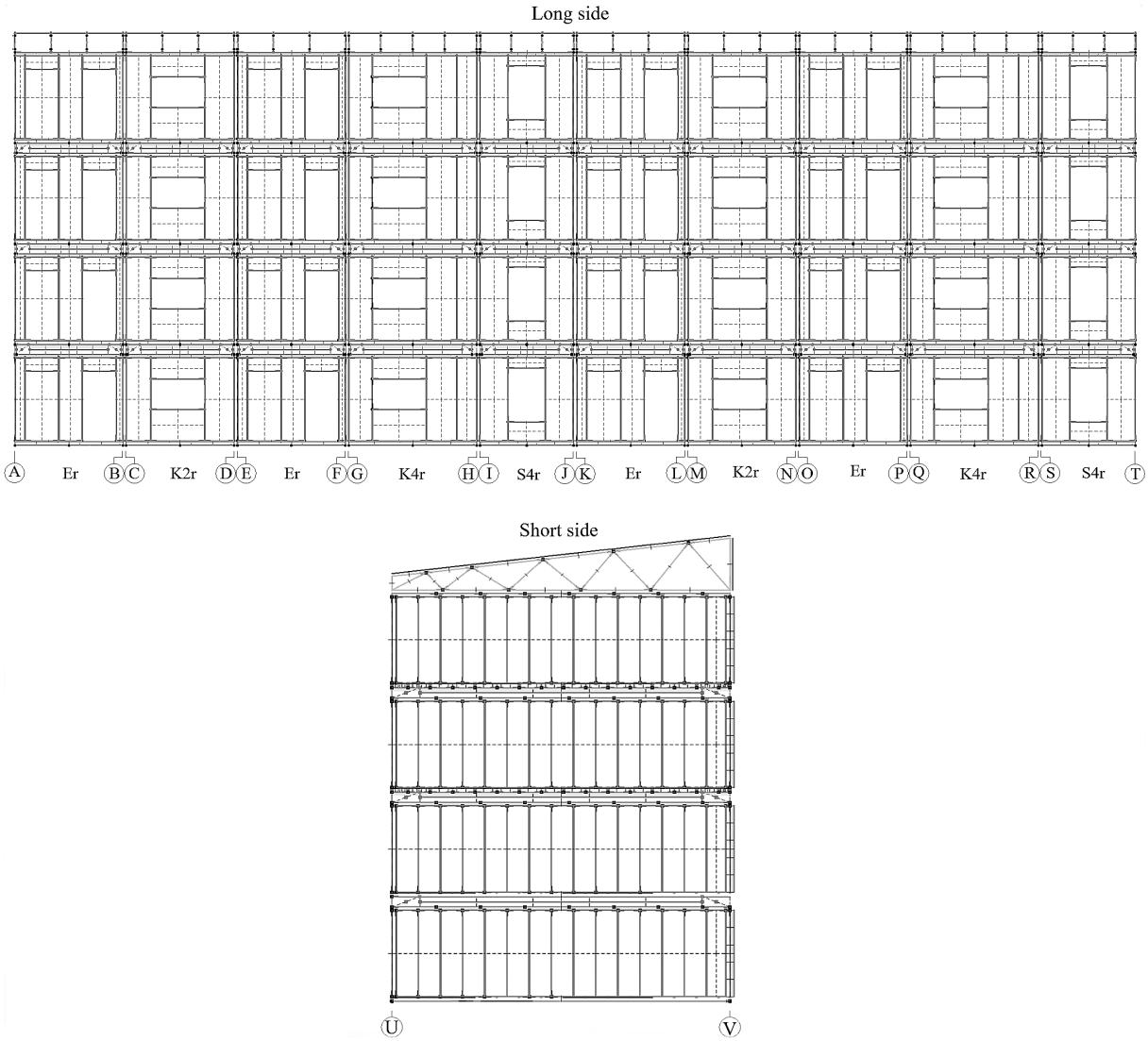

Figure 5.15: Illustration of the complete configuration model.

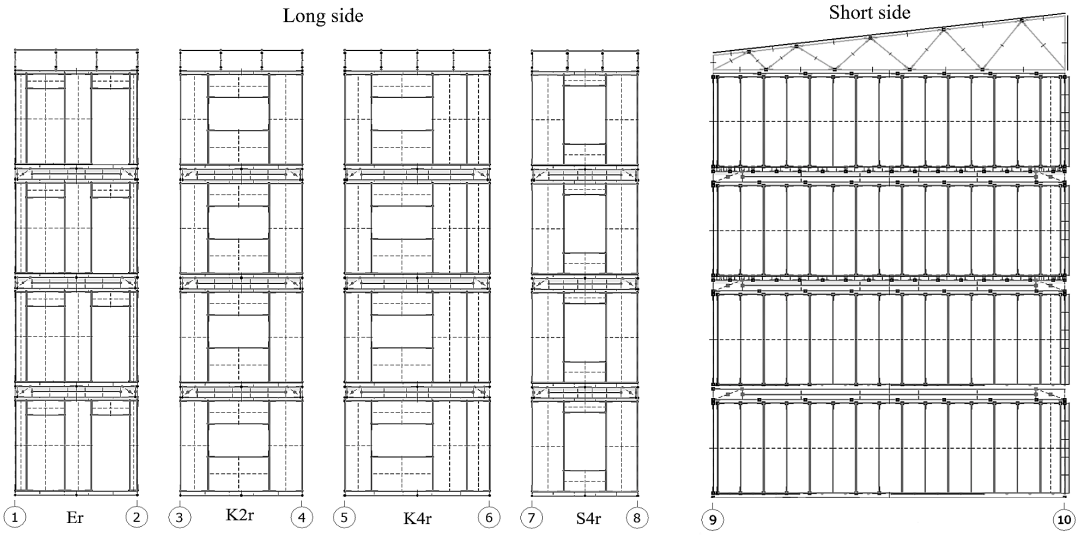

Figure 5.16: Illustration of the reduced configuration model.

Load cases

Two different load cases were evaluated, wind loads towards the long side and wind loads towards the short side. Apart from the two load cases and the two different configurations, some changes where made in the TVE models and the connections between them to investigate the influence of transverse walls and some of the intercomponent connections. The different changes are listed below.

Wind loads towards the long side of the building:

1. **Complete configuration model**
2. **Reduced configuration model**
3. **Reduced configuration model, only shear walls**
   The transverse walls, i.e. the walls on the long side of the building, are removed.
4. **Reduced configuration model, friction**
   The stops connecting the corners of the TVEs vertically on the long side are removed and replaced with friction in the line-line connections. The different values tested for the friction coefficient are presented in chapter 6.

Wind loads towards the short side of the building:

5. **Complete configuration model**
6. **Complete configuration model, only shear walls**
   The transverse walls, i.e. the walls on the short side of the building, are removed.

Chapter 6

Numerical analyses

The chapter presents the numerical analyses regarding lateral stability for the individual TVE models and the different analyses on the assembled structural system.

6.1 Visualisation of increased stiffness

The individual TVE models can be used for determining how the geometry and the different connection properties within the TVEs impact its stability. To illustrate the increase in stiffness obtained from the three-dimensional models, a comparison between five different stages of assembly was carried out with module En. A 10 mm point motion support load was applied to the top rail in one of the short side walls. The end columns in each of the short sides were pinned, but otherwise no other supports were added. Figure 6.1 illustrate the different stages of assembly and the position of the motion support load.

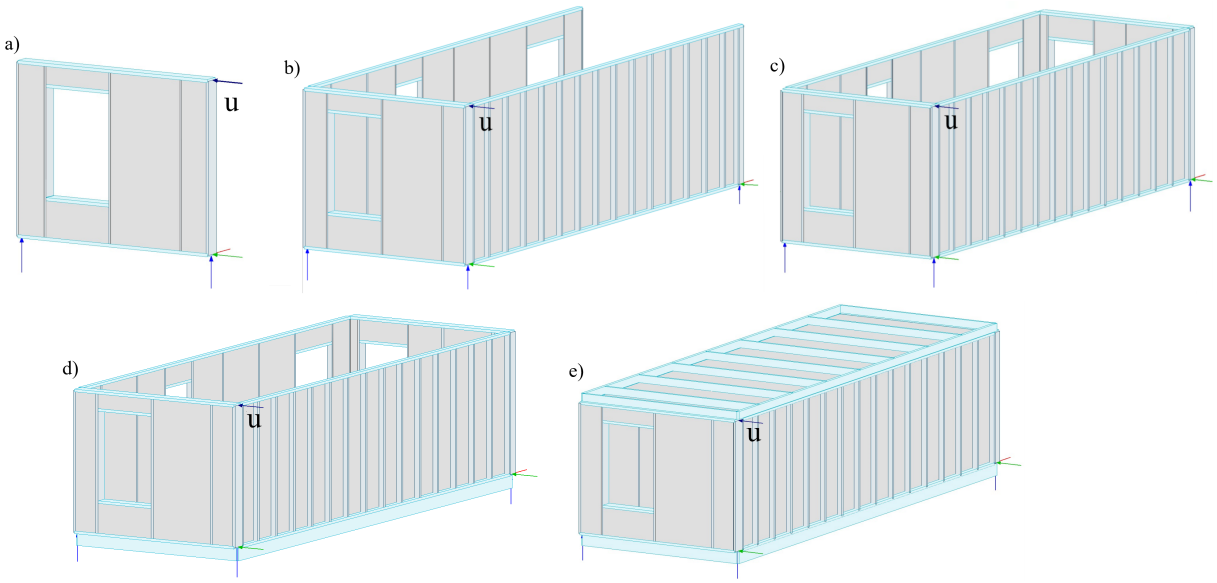

Figure 6.1: Illustration of different stages of assembly and position of motion support loads (u).

The reaction forces obtained from each stage are presented in Figure 6.2. Attaching the transverse walls (stage a to stage b) increased the reaction force from 1.3 kN to 1.8 kN, corresponding to a stiffness increase of almost 40 %. The transverse walls prevent out-of-plane displacements for the short side wall and increase rotational stiffness. Attaching the second short side wall (stage c) had negligible impact.

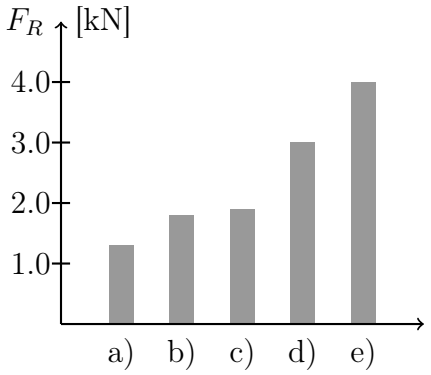

Figure 6.2: Support reaction forces for stages a to e.

The major stiffness increase seem to come from attaching the floor (stage d) and the ceiling (stage e). The floor prevents uplifting forces in the transverse walls, resulting in a drastically higher reaction force. Stage d gave a 3.0 kN reaction force, a more than doubled stiffness compared to the single shear wall. A three times higher stiffness came from attaching the ceiling, with a 4.0 kN reaction force. The ceiling distributes forces from the point support motion load to both short side walls, utilising the whole structure in preventing displacements and rotations. The results agree well with previous studies, for example Paevere, Foliente and Kasal [22] who also concluded the ceiling in their FE models and full-scale test models to contribute more to load-sharing between parallel walls compared to the transverse walls.

Several studies have been conducted on how to incorporate three-dimensional structural behaviours in simple hand calculations, most notably by Källsner, Girhammar and Vessby [8] [20]. Their analytical methods focusing on prevention of uplift in shear walls by anchorage to transverse walls and to floors have been proven successful in estimating stiffnesses and capacities compared to experimental shear wall tests. However, none of the current methods have the ability to utilise load-sharing between parallel shear walls through the ceiling. Since the most significant stiffness increase in the TVE analysis above was concluded to come from such load-sharing, the full three-dimensional effects therefore seem to currently not be efficiently utilised in simple analytical hand calculations. The numerical models contribute with about a 30 % increase in stiffness compared with analytical methods.

6.2 Wind load cases analyses

The models of the configurations are to be used for determining how connections between TVEs and between structural elements within TVEs, as well as the number of modules vertically and horizontally, affect the overall stability of the building. In the analyses

conducted for this report, comparisons are made using connection forces between structural elements within the TVEs, connection forces between TVEs, overall displacements and support reaction forces in the foundation. The number of equations and iterations required, and the corresponding approximate calculation times, for the different configurations and load cases are presented in Table 6.1.

Table 6.1: Number of equations, iterations and calculation time for the analyses.

Load case	Configuration	Equations	Iterations	Approximate time
Long side	1. Complete	7 308 000	16	13 h 36 min
	2. Reduced	1 827 096	8	1 h 22 min
	3. Reduced, shear walls	1 499 700	9	1 h 6 min
	4. Reduced, friction	1 820 616	8	2 h 26 min
Short side	5. Complete	7 308 000	6	5 h 33 min
	6. Complete, shear walls	4 743 006	11	3 h 48 min

Compared to calculations in Abaqus with substructured TVE models, the calculations in FEM Design are considerably more time consuming. To check overall stability (e.g. displacements and reaction forces) as quickly as in Abaqus, an alternative is using substructure-like TVE models in FEM Design as well. The diaphragms with beams and boards can easily be simplified with plates, walls or shells to decrease the number of nodes and hence also equations. However, the current approach provides the high level of detail necessary to study different connections within the modules.

Analyses of the individual TVEs in section 6.1 resulted in a major stiffness increase for the TVEs when attaching the ceiling and floor. Hence, an objective with using TVE models without transverse walls was to create simpler and faster calculation models for the complete configurations. However, as can be seen in Table 6.1, removing the transverse walls actually resulted in an increase in the number of iterations required to find equilibrium, and not as significant time savings as anticipated. The reduced configurations were instead only used for representing two-dimensional behaviours. Previous studies investigating the impact of transverse walls on structures have all focused on one-storey houses. The reduced configurations provide an opportunity to study the impact on a multi-storey building.

6.2.1 Data selection

Complete results from the analyses are presented in Appendices B and C. The data acquired from the complete configuration, presented in Figure 5.15, for wind loads towards the long side of the building is too extensive to be presented in the report (four storeys along 20 axis), and hence results from a select number of axes are presented here. Modules En and B3 can be placed in both the centre and at the gable of a building, and therefore results from two ”pillars” of these models was chosen. For En, axis A and B represent the behaviour of modules placed along the gable and axis K and L represent the behaviour of modules placed in centre. Results from both of the B3 modules are presented (axis I, J, S and T). Modules K1 and K3 can only be placed in centre, hence results from only one ”pillar” of each is presented. Axis C and D represent module K1, and axis Q and R represent module K3.

6.2.2 Support reaction forces distributions

The support reaction forces are used for a general comparison between the FE models and the analytical calculations. In analytical calculations, the maximum support reaction force was approximately 25 kN both horizontally and vertically.

Long side analyses

The maximum vertical reaction forces occur along axis 6, underneath the heaviest module (K3). Figure 6.3 presents a comparison between vertical and horizontal reaction forces along axis 6 for the complete analysis (configuration 1, see Figure 5.15 where axis 6 corresponds to axis R), the reduced analysis (configuration 2, see Figure 5.16) and the reduced analysis with only shear walls (configuration 3, see Figure 5.16). Wind loads are applied at the right-hand side in the illustration. As expected, the model with only shear walls produced values closest to the analytical. According to the reduced configuration with only shear walls, the maximum vertical reaction force is slightly higher, 27.3 kN, and the horizontal reaction force is lower, 18.3 kN. In the reduced analysis (configuration 2), the vertical reaction force is 20.8 kN and the horizontal 17.8 kN. The complete configuration produces a vertical reaction force of 21.3 kN and a horizontal force of 16.4 kN. Compared with the analytical calculation results, the complete configuration reduces the horizontal force with 18 % and the vertical with almost 50 %.

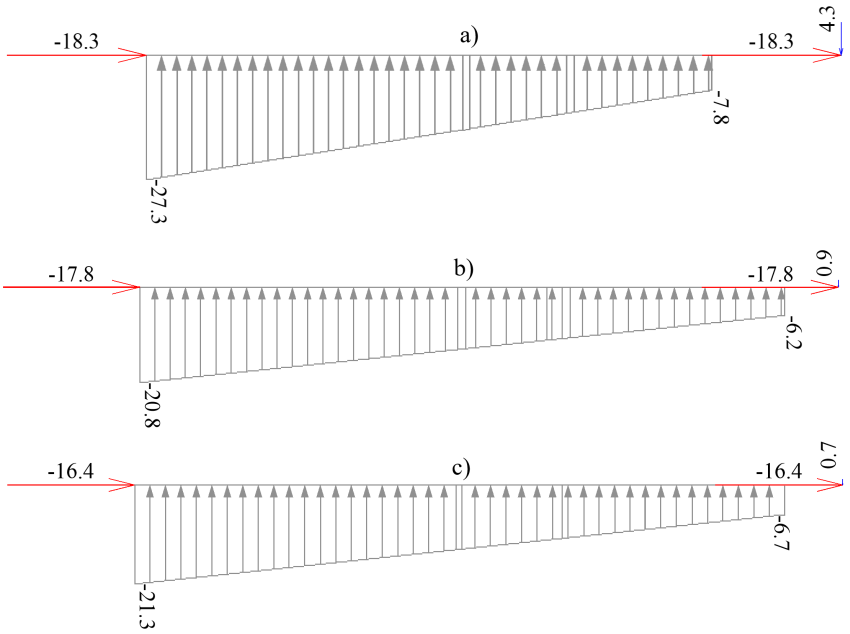

Figure 6.3: Reaction forces along axis 6 for the reduced configuration with only shear walls (a), the reduced configuration (b) and the complete configuration (c).

The risk of uplift has not been investigated in any detail analytically. However, all FE models produce some tension forces in the bed plate on the windward side of the building, indicating this behaviour should be taken into account. As would be expected the reduced model with only shear walls has the highest uplift, approximately 4.4 kN (axis 5, see Figures B.6 and B.7). All uplifting forces on the windward side are still significantly

smaller than the 15 kN tension force permitted for the concrete foundation. However, not all load cases have been investigated and further analyses are required to for a complete design of the connection between the TVEs and the foundation.

Short side analyses

Reaction forces for the short side analyses are presented in Figures C.1 to C.4. For the complete configuration (configuration 5), the largest vertical reaction force, 14.1 kN, occurs under module K3 along axis U and the largest horizontal reaction force, 7.7 kN, occurs at the windward side of module En. The complete configuration with only shear walls (configuration 6) produces significantly larger vertical reaction forces, with a maximum of 49.6 kN. No noticeable uplift was obtained from any of the models.

The dramatic increase in reaction forces when removing the transverse walls is likely due the redistribution of dead loads. The dead load factor was increased to make up for the missing walls, hence the vertical forces were distributed on a smaller area. The reaction forces in the model without transverse walls is therefore a very large overestimation, almost 25 % higher than the capacity of the foundation, and probably nowhere close to the actual vertical force distribution in the foundation.

6.2.3 Two- and three-dimensional modelling

Comparisons between the models with transverse walls (configurations 2 and 5) and the models with only shear walls (configurations 3 and 6) indicate significant differences between regarding the TVEs as two-dimensional or three-dimensional structures. The effect from the transverse walls on the structure is most clearly visible for wind loads towards the short side of the building.

Horizontal displacements

The difference in horizontal displacements before and after attaching the transverse walls for the analyses of wind loads towards the long side of the building (configurations 2 and 3) is presented in Tables B.2 and B.3 in Appendix B. The largest horizontal displacements occur along axes 5 and 6 (module K3), as this wall has the largest percentage of openings in relation to its total area. Figure 6.4 illustrates the displacements along the axes for both models, with scale factor 2 to more clearly present the results. The displacement in the top ceiling diaphragm in the reduced model with only shear walls is 151 mm along axis 5, which is reduced to 99 mm when adding transverse walls. The analyses on wind loads towards the short side of the building (configurations 5 and 6) resulted in the same behaviour though with even larger differences, see Table C.1 in Appendix C. The complete configuration with transverse walls had a 63 mm maximum displacement in the top ceiling diaphragm, whilst the one with only shear walls had a 216 mm displacement.

The results seem to agree with Andreassons [15] conclusions from studying interactions between shear walls and transverse walls for multi-storey buildings. He also found it more effective to counteract uplifting forces at the shear wall ends by applying vertical dead loads to the transverse wall compared to applying vertical dead loads on the shear

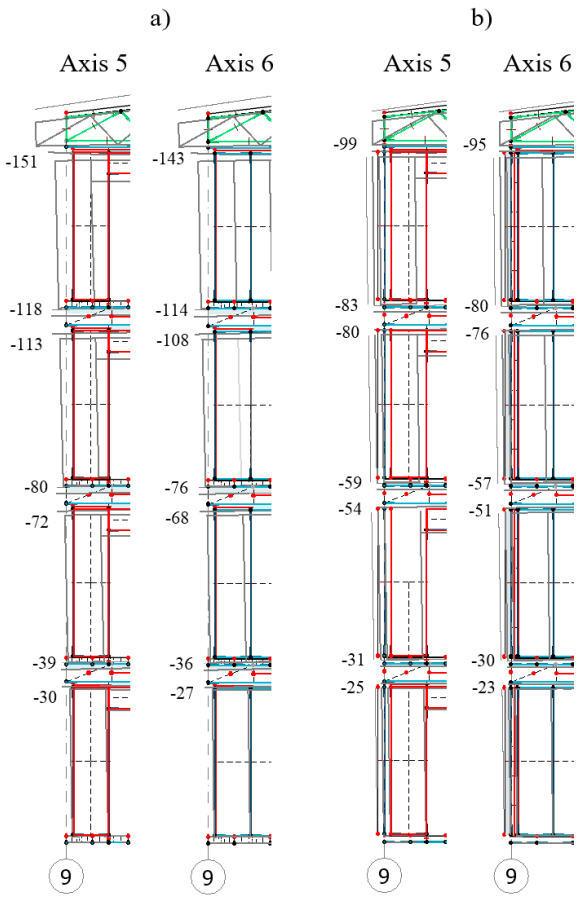

Figure 6.4: Horizontal displacements [mm] along axis 5 and 6 for the reduced configuration with only shear walls (a) and the reduced configuration (b). Scale factor 2.

wall [15]. When dead loads were applied to the transverse wall, a larger percentage of the wall length was utilised to counteract shear forces [15]. The models with only shear walls therefore represent the worst case possible in terms of uplift, as no transverse walls can counteract uplift and in-plane horizontal displacements. Furthermore, no vertical dead loads are applied at the shear wall corners which would also counteract uplift. Hence, the models without transverse walls are likely not sufficiently detailed to accurately predict uplift and horizontal displacements as it produces unrealistically large displacements. The models with transverse walls provided a more efficient utilisation of the three-dimensional behaviour of the TVEs.

The models without transverse walls aside, both complete configuration analyses with full three-dimensional structures (configurations 1 and 5) also resulted in large horizontal displacements. A probable explanation is an underestimation of the ceiling to shear wall and the floor to shear wall connection stiffnesses due to using theoretical calculations. As previously concluded from comparing the experimentally calibrated stiffnesses for the shear walls (Tables 5.1 and 5.2) with those theoretically calculated (Table A.1 in Appendix A), the calculated stiffnesses were lower than the mean value of the experimental. This might explain the significantly large displacements for wind loads towards the short side (model 5), as the stiffness calculations do not take material and fastener orientation into account. The exterior wall to floor connection (connection 2 in Figure 2.3) is designed as a stiffer connection compared to the module wall to floor connection (connection 4 in Figure 2.3)

to prevent uplift, though calculations resulted in the opposite (see Table 5.5).

Another explanation for the large displacements in the short side analysis, despite loads distributed between all adjacent shear walls, is that door and window openings make up a significant percentage of the wall area. For the long side walls, openings make up 20 % of the wall area at most (axis 2, 3 and 5). However, the short side has a total of 40 % openings. The reduction of shear stiffness due to openings is likely also enhanced by the many identical storeys with openings aligned vertically.

The issue has been investigated by Andreasson [15] who studied how positioning of openings in a model of a four storey building effected the shear wall stiffness. He found a conventional layout with openings aligned vertically (as in the TVE building) to have a significantly lower stiffness compared to a staggered layout. In the staggered layout, openings on alternate storeys were mirrored to avoid vertical alignments, resulting in displacements being reduced up to 20 %. Changing the configuration to a staggered layout is currently not possible for the building system, but vertical alignments of openings may explain the large displacements.

Torsional effects

Out-of-plane displacements (perpendicular to the shear wall plane) are also significantly larger for the models without transverse walls. An example is module K1, which has one shear wall with a high stiffness (axis 4, no openings) and one shear wall with a low stiffness (axis 3, large openings). The horizontal displacement at axis 3 perpendicular to the wind load direction is 4-5 mm for the reduced model, and 6-11 mm for the reduced model without shear walls. This corresponds to approximately 9 % and 16 % at most, respectively, compared to in-plane displacement.

Despite having the same layout (though mirrored), module En shows little torsion. A probable explanation is the stiffer board to beam connection in the floor (see Table 5.4), creating an almost completely rigid diaphragm. The torsion in the TVE ”pillars” are likely a result of both differences in stiffness between different walls and a low stiffness in the timber frame to board connections. In the actual configuration, modules K1 and K3 will never be placed at gables. Hence, rotations will always be prevented by the stiffer modules En and B3, as is proven by the analyses on the complete configuration (model 1). Table B.1 presents the negligible out-of-plane displacements when modules are placed in the actual configuration. The more calculation efficient reduced model should not necessarily be disregarded, thus displacements are still small. Paevere, Foliente and Kasal [22] found the out-of-plane displacements in their model of a one-storey building to be up 16 % when asymetrically loaded, which is double the torsion in the four-storey K1 ”pillar”.

Transverse walls seem to have an even greater influence on rotational stiffness for wind loads towards the short side (configurations 5 and 6). The out-of-plane displacements in the top ceiling diaphragm for configuration 6 corresponds to 40-54 % of the in-plane displacements. For the configuration with transverse walls, configuration 5, out-of-plane displacements correspond to about 8-9 %. With a reduction of rotations as significant as this, the entire structural behaviour seem to alter as the short side shear walls are attached. However, as previously concluded, the reason is the lower percentage of openings enabling

longer effective lengths and more effective use of dead loads to counteract uplift and shear forces.

A significant increase in load-sharing between parallel walls, including an increase in rotational stiffness, is observed when the full three-dimensional behaviour of the TVE structure is considered. Hence, load-sharing seems to not only occur through the roof, but the transverse walls as well. The result is different from conclusions drawn by Phillips, Itani and McLean [21], who found no load-sharing through transverse walls. However, their analyses only included a small one-storey house. Torsion likely has a greater effect on multi-storey buildings, thus the out-of-plane displacements are negligible for the bottom storey in most of the analyses. Paevere, Foliente and Kasals [22] found the transverse walls to contribute about 4 % of the load-sharing between parallel walls in their analysis of an asymmetrical house.

Vertical connection force distributions

The effects of load-sharing between parallel shear walls within the same module are also visible from comparing vertical connection forces. Tables B.5 to B.17 in Appendix B present line connection force distributions for all floors along all axes. Figures B.12 to B.19 illustrate the position of line connections and hold-downs along each axis. Line connection forces have been linearized to enable a simpler overview of the result. Uplifting forces in hold-downs and around openings generally decrease in all models as the transverse walls are attached, whilst the connection forces in the stiffer walls (without openings) increase. Module En (axis 1 and 2) is a typical example. Figure 6.5 illustrates the forces for the reduced model with only shear walls and the reduced model.

The vertical connection forces in hold-downs at the bottom of openings are largest for the bottom storey and smallest for the top storey, as the largest shear forces occur in the bottom storey. This agrees with Andreassons [15] conclusions, who also found that each storey functions as a separate shear wall [15]. Dead loads from upper storeys cannot effectively be utilised to prevent uplift, as the uplift forces in the bottom storeys increase as the number of storeys increase [15]. The only top hold-downs around openings that seem to be carrying any loads are the hold-downs in the top storey for modules En (both configurations) and K3 (only reduced configuration without shear walls). In the remaining cases, vertical uplifting forces may be small enough to be taken by the wall to ceiling connections or may not occur at all.

Uplift does not only occur at the windward side of the walls, but tension forces also appear in hold-downs placed on the leeward side (where there should be compression). The reason might be the effective length of the shear wall, i.e. the part of the wall resisting shear forces, corresponding to the entire length of the wall. The effective length is affected by the racking load, i.e. the vertical dead load applied at the top of the shear wall. Since the dead loads are significantly larger for module K3, there might not appear any tension forces in hold-downs along axis 5 despite having the same percentage of openings as axis 2 in module En.

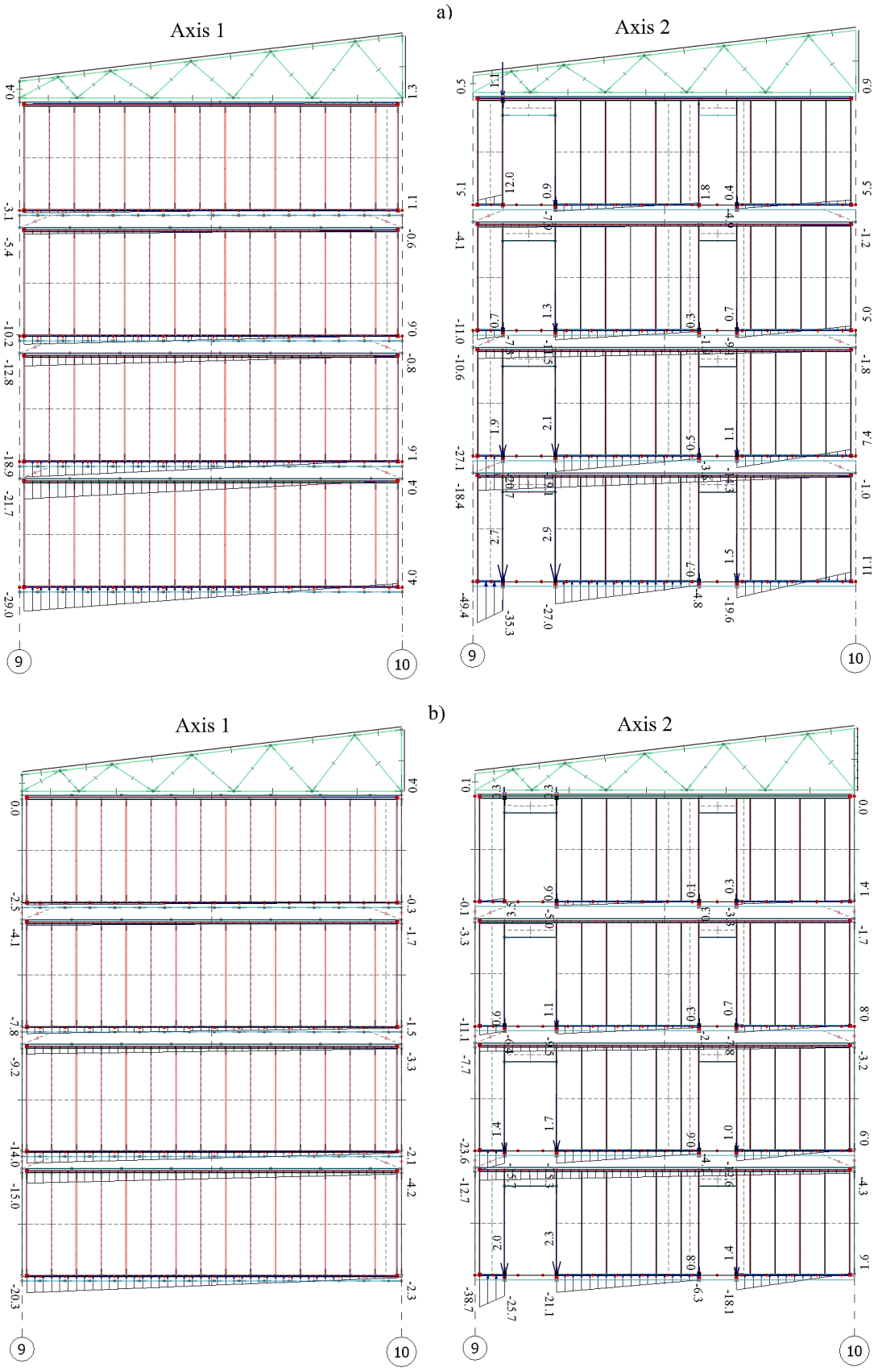

Figure 6.5: Vertical line connection forces [kN/m] and tension forces in hold-downs [kN] along axis 1 and 2 for the reduced configuration with only shear walls (a) and the reduced configuration (b).

Horizontal shear force distribution

Force distributions in the shear walls for the numerical models can be compared to those concluded in analytical calculations using the wall to ceiling connection. The wall to ceiling connection distributes wind loads from the horizontal diaphragms to the shear walls. The FE analyses results for the horizontal connection force distribution is presented in Table B.19 for the reduced configuration analyses (configurations 1 and 2). The distribution has been linearized to enable a simpler comparison with the analytical results. The largest horizontal connection forces occur at the bottom storey along axis 6 in module K3, see illustration in Figure 6.6. A 2.4-3.9 kN/m horizontal force was concluded for the reduced model and a 2.8-4.7 kN/m horizontal force was concluded for the reduced model with only shear walls.

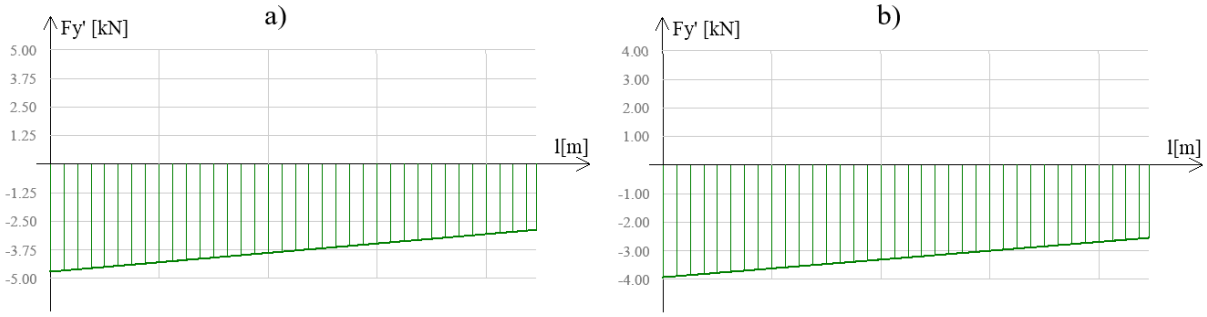

Figure 6.6: Horizontal shear force distribution [kN/m] along axis 6 for the reduced configuration with only shear walls (a) and the reduced configuration (b). Note the different scales.

Both analyses resulted in lower horizontal forces compared to the analytical calculations, in which an approximate 7 kN/m horizontal force was estimated for the bottom storey (however this regards the total force subjected to the shear wall). The transverse walls seem to share 17-26 % of the wind load with the shear walls. The results are very similar to the conclusions from Phillips, Itani and McLean [21], who found the transverse wall in their small one-storey building to carry 8-25 % of the applied load depending on the magnitude of the load. The transverse walls carried the highest percentage of loads close to the maximum shear wall capacity, also agreeing well with the TVE analysis which was conducted in ultimate limit state.

According to analytical calculations, the horizontal force distributions in the shear walls should be approximately equal for both long and short sides. In the complete analysis on the short side (configuration 5), the horizontal force distributions in the shear wall to ceiling connection is up to 3.4 kN/m for the bottom TVEs, see Table C.6. For the analysis without transverse walls (configuration 6), the force distribution is up to 4.8 kN/m, see Table C.7. The magnitude of the loads are in the same range as for the analysis on the long side, though load-sharing with transverse walls is significantly higher.

The attached transverse walls shared up to 40 % of the applied load, further proving how significant three-dimensional modelling is for the structural behaviour. The higher increase in stiffness from the transverse wall in the short side analyses compared to the long side analysis is likely due to smaller sized openings, longer uninterrupted wall lengths and a more efficient utilisation of dead loads (as was discussed above).

6.2.4 Load-sharing between adjacent modules

Load-sharing between adjacent modules was studied for wind loads towards the long side of the building. In the complete configuration (configuration 1), the TVE "pillars" were connected with a rigid roof model. The roof acted as a continuous beam, allowing all modules to function as one structure with load-sharing between all parallel shear walls within the building. For the reduced configuration (configuration 2), a simplified modelling approach with each "pillar" acting independently was analysed.

Horizontal displacements and torsional effects

The effects from load-sharing between adjacent modules becomes evident when comparing differences in horizontal displacements, see Tables B.1 and B.2. The reduced analysis (configuration 2) had horizontal displacements in the load direction between 99 mm (axis 5) and 63 mm (axis 8). A significant reduction was achieved from the complete analysis (configuration 1), with horizontal displacements between 70 mm (axis T) and 76 mm (axis Q). As previously concluded, the complete model also had significantly smaller out-of-plane displacements in shear walls compared to the reduced models. Out-of-plane displacements were reduced from 11 mm in configuration 3 to only 4 mm for configuration 1. This corresponds to approximately 7 % of the in-plane displacement at most, and occurs at the TVE located at the gables. For the TVEs placed in centre, out-of-plane displacements seem negligible (only 1-2 mm).

Connection forces distributions

No significant differences in load-distributions can be observed for connections within the TVEs. Table B.18 shows the horizontal force distributions in the ceiling to shear wall connections, which approximately varies in the same way as for the reduced models. The vertical force distributions in connections between horizontal diaphragms and walls, as well as in hold-downs, is also approximately the same as for the reduced analyses, see Tables B.5-B.17. The positioning of the modules in the configuration has no noticeable effect, hence analyses on central and gable placed En and B3 generally result in similar force magnitudes and distributions.

However, some differences can be observed when comparing horizontal connection forces between TVEs placed in centre and at the gables, presented in Table B.20 and visualised in Figure B.21. One example is illustrated in Figure 6.7. The moments along axis A (modules En) are approximately the same as along axis T (module B3), i.e. the both TVEs placed at the gables. The same module types and shear walls appear along axis J and K, though with noticeably different moment distributions. The moments decrease along axis J (B3), but increase along axis K (En). The heavier module En seems to prevent rotations in the lighter module B3 through load-sharing.

Idealised roof model

Despite advantages from utilising the complete analysis, especially when analysing displacements, there is a very high risk of overestimating load-sharing due to the rigid roof

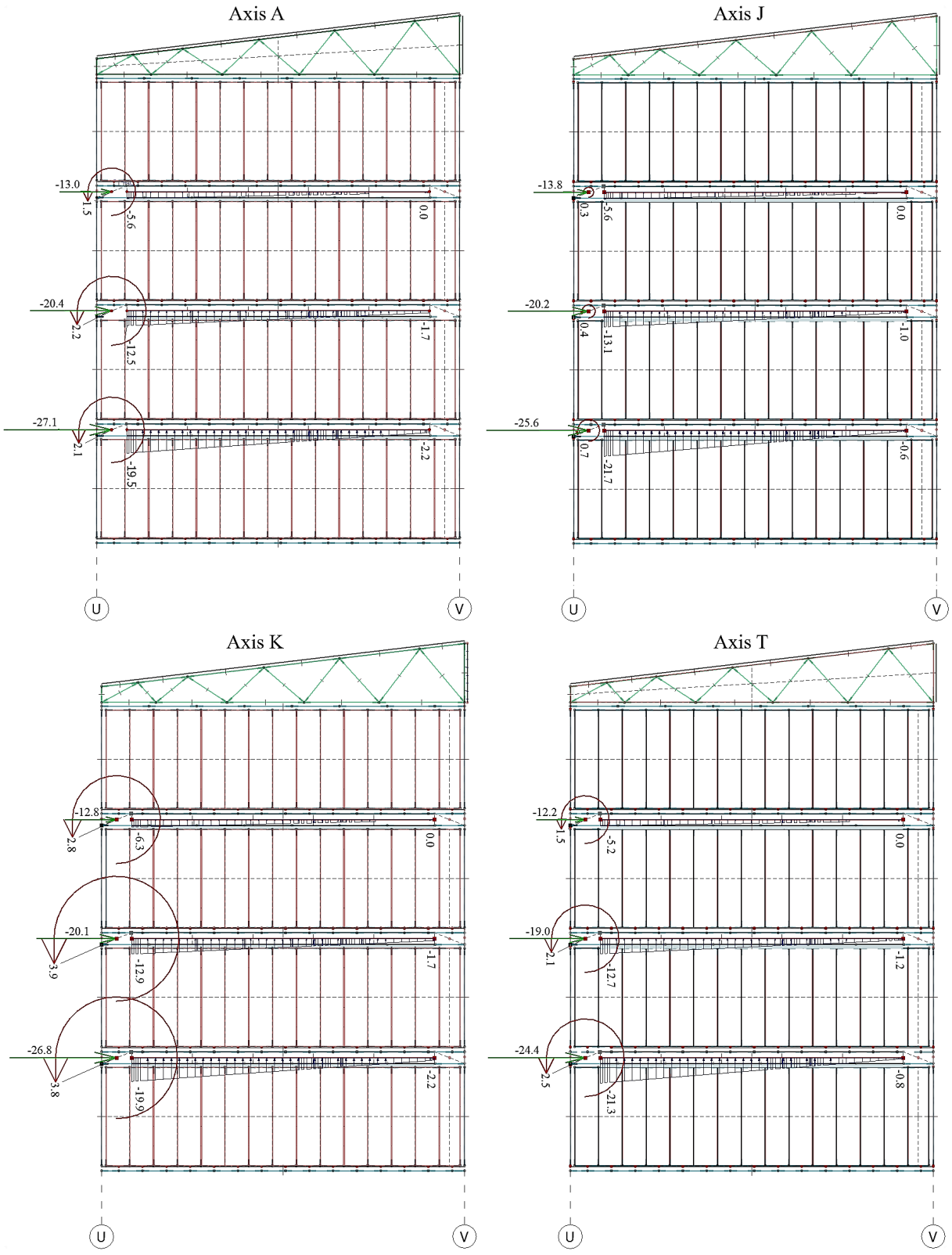

Figure 6.7: Point forces [kN], moments [kNm] and line forces [kN/m] along axes A, J, K and T.

model. The roof represents an idealised model, with rigid rotational degrees of freedom between TVE "pillars". In reality, the steel sheets connecting adjacent trusses have only been designed to distribute wind loads towards the short side of the building. These connections will not have sufficient rotational stiffness to prevent movements between long side walls in adjacent modules. In reality, rotations and displacements will occur in the roof, resulting in larger differences in displacements and in horizontal force distributions between "pillars" of modules. Some advantages of load-sharing between adjacent modules could well be accounted for, but it is unrealistic to expect the whole building to function as one continuous beam. The actual structural behaviour of the roof is somewhere in between completely free (configuration 2) and completely rigid (configuration 1).

6.2.5 Load transfer between adjacent shear walls

For wind loads towards the short side of the TVE building, the number of adjacent modules have been adapted to enable sufficient redistribution of lateral loads between shear walls. Due to the large percentage of openings on the short side of the TVEs, analytical calculations resulted in a minimum of 10 adjacent modules. However, a more effective use of shear walls might be possible from the three-dimensional model. As proven by the comparisons between the two- and three-dimensional analyses (configurations 5 and 6) above, attaching the transverse wall had a great impact on structural behaviours.

Steel plate connection

As concluded when analysing horizontal shear force distributions between the ceiling and the shear walls (section 6.2.3), shear walls in all modules seemed to carry loads. The force distribution between adjacent shear walls is also visible in the horizontal connection forces in steel plate connection, see Tables C.8 to C.8 and illustration in Figure C.9. All but one horizontal connection (between axis N and O in storey 2) is in either tension or compression. No tension forces could be detected in the hold-downs connecting vertical beams in the short side walls, indicating that no uplift occurs at all. The reason is probably vertical displacements, as for the analyses on hold-downs within modules. The analyses on wind loads towards the short side resulted in 3-4 mm vertical deformations per storey, but might not be realistic as some structural elements in the walls have been removed in the FE models. For a better depiction of forces in hold-downs, further knowledge about vertical deformations are required.

Force distributions in stops

Forces distributed in the corners between modules are, however, significantly lower than observed in the models with wind loads towards the short side. Results are presented in Tables C.10 and C.11, and linearized distributions are illustrated in Figure C.10. The reduced analysis (configuration 2) had moments between 1.1 and 2.7 kNm, and horizontal forces between 20 and 28.8 kN, in the stops between modules. In the complete model subjected to wind loads towards the short side (configuration 5), the largest moment is 2.5 kNm and the maximum horizontal force is 12.4 kN. Hence, a more efficient utilisation might be possible.

6.2.6 Friction model

Previous analyses assumed all lateral movements between TVEs were prevented by the stops. Analytically, a calculation model using only friction to prevent movements has successfully been used. To investigate the friction method, stops on the long sides of the TVEs are removed and replaced by friction coefficients in the vertical line connections between modules in configuration 4.

Friction coefficient for elastomer to timber contact surface

The friction coefficient for the surface between the elastomers and the bottom beam was assumed 0.4 in the analytical calculations, which is very close to the experimentally validated value, 0.38, concluded by Hummel [25]. Since the actual coefficient for this connection is unknown, different values were investigated. According to Hummel [25], the friction coefficient for an elastomer to timber surface is similar to a timber to timber surface. Hence, friction coefficients 0.2, 0.3 and 0.4 were tested. All friction models were concluded to be in static equilibrium. The result was surprising, as reducing the coefficient was presumed to give an estimation of the minimum friction coefficient required to obtain static equilibrium. A possible explanation could be that dead loads have been over-estimated. The estimations were based on values from analytical calculations to enable comparisons, but required significant increases of the model weights (factor 2.7). Results from the analysis with friction coefficient 0.4 is used in following comparisons, hence previously used in analytical calculations and also close to the experimentally validated by Hummel [25].

Horizontal displacements

Using friction instead of stops had a significant impact on overall in-plane horizontal displacements, see Table B.4. Compared to the reduced analysis with stops (configuration 2), the maximum horizontal displacement along each axis was approximately reduced with 20-15 mm. Displacements between TVEs changed from 3-7 mm in the model with stops to 0-1 mm in the friction model. A utilisation of the entire elastomer to bottom beam surface is probably more realistic, as the stops in the corners are not utilised until lateral movements have already been initiated. The friction model seems to distribute the lateral loads more evenly across the shear walls, allowing shear walls to prevent in-plane displacements more efficiently than the models with stops. Comparing vertical load distributions for the connection between TVEs, Tables B.20 to B.23, the friction model produces lower maximum vertical loads at the leeward sides (positions L_1, L_3 and L_5). This corresponds well with Hummels [25] study, which also concluded connections stiffnesses to be significantly underestimated without taking friction into account.

Connection force distributions

The vertical connection forces between walls and horizontal diaphragms (presented in Tables B.5 to B.17 in Appendix B) are approximately the same compared to the other

reduced configuration. The same applies for the horizontal force distribution in the connection between the shear walls and the ceiling. Comparing connection forces between TVEs (Tables B.21 and B.23), the friction model seems to produce larger uplifting forces since there are no stops in the corners of the TVE models to prevent rotations. Therefore, the stops with rigid rotations may underestimate tension forces in hold-downs between TVEs. However, there are still no differences in hold-down forces (at either long or short sides of the building) between the friction model and the reduced models. This may be a result of overestimated vertical displacements.

Comparisons between methods for preventing lateral movements

Comparisons between the configurations with stops and the configuration with friction showed no significant differences in connection force magnitudes or load distributions. The friction model seems to distribute horizontal forces more evenly along the shear walls, resulting in reduced horizontal displacements. A more efficient utilisation of the shear walls counteracted the lateral loads. All models, regardless of method for preventing lateral movements, were in static equilibrium. Not even significantly lowering the friction coefficient below the experimentally validated value resulted in any change in the load distribution. Hence, the connection between TVEs is over-designed, and either one of the methods would probably be sufficient on its own. For wind loads towards the long side of the building, where there is a gap between the glulam beam and the bottom beam, the stops will not actually be utilised until movements have already been initiated. Further investigations regarding the stops and the friction coefficient for the horizontal surface-to-surface contact are required to predict the prevention of lateral movements more accurately.

Chapter 7

Concluding remarks

The chapter presents a summary and discussions regarding the main conclusions drawn from the analyses. Suggestions for further research to enable an even more accurate depiction of the structural system are also presented.

7.1 Summary of results

- Compared to analytical methods, the additional stability from the numerical TVE models mainly comes from load-sharing between parallel shear walls. Load-sharing is enabled by the ceilings, which function almost as rigid diaphragms distributing loads in relation to shear wall stiffness. Investigations of the three-dimensional behaviour for an individual TVE concluded an approximate 30 % stiffness increase compared to analytical methods.

- The transverse walls were found to have a significant impact on stabilisation for the complete four-storey structural system. Noticeable load-sharing between parallel shear walls through the transverse walls was observed, along with a more effective use of dead loads. In-plane and out-of-plane displacements were reduced with 17-26 % for wind loads towards the long side, and with up to 40 % for the short side, when attaching the transverse walls.

- Assumptions made in the analytical calculations regarding friction seem correct according to the numerical analyses. Static equilibrium was obtained for the structural system when friction prevented all lateral movements between modules.

- The connections between TVEs, preventing lateral movements, were found to be over-designed. Using only stops or only friction is sufficient for attaining static equilibrium.

- Incorporating friction in the contact surface between TVEs increased the overall stiffness of the structural system. Reduced in-plane displacements in walls was observed, as well as reduced displacements in the surface connection between TVEs.

7.2 Discussion

Very detailed models of the TVEs were used in the analyses, thus the TVE developer intends to use them for product development purposes. This resulted in accurate depictions of shear wall behaviours, but also significant calculation times. If the developer decides to use the models more often, e.g in every project and not only for changes in the structural system, the substructure approach used in Abaqus is recommended. The diaphragms can easily be modelled with shell, wall or plate elements which would significantly reduce the number of elements required and thus also calculation time. This technique would not provide sufficient detail to design components within modules, but could be used for estimating approximate horizontal displacements, support reaction forces and connection forces between modules and between diaphragms.

The increase in stiffness from the three-dimensional model compared to simple analytical calculations was clearly observed in the analysis of a single TVE. The ceiling contributed greatly to load-sharing, a three-dimensional effect that cannot be utilised in simple hand calculations. For the multi-storey building, the transverse walls were found to also contribute to load-sharing by reducing rotations due to out-of-plane displacements. Differences in size and position of openings between shear walls in the same module contributed to out-of-plane displacements, and the increased load-sharing from transverse walls distributed horizontal loads more evenly to both shear walls.

The stiffness of the structural system was also affected by how efficient dead loads could be used for counteracting lateral loads. Attaching the transverse walls to the multi-storey models, as well using friction in the horizontal contact surfaces between TVEs, resulted in more evenly distributed dead loads and more efficient counteraction of uplifting forces. How much of the dead loads that can be used in analyses depend on load combination according to Eurocode, hence the only load combination used in the analysis (EQU) is not sufficient for a complete design of the structural system. Values for dead loads obtained from estimation in analytical calculations also seemed overestimated in comparison with the model weights (required model weights to be multiplied with a factor 2.7), thus further investigations are recommended.

The connections between the floors and ceilings to the stud walls was found to be very important, as the ceiling to wall connection governs the load-distribution to the shear walls and the floor to wall connection prevents uplift. Only using theoretically calculated values likely resulted in underestimating stiffnesses. Thus, calibration of the connections within the shear walls resulted in more than doubled stiffnesses compared to theoretical values. The effects of underestimated connection stiffnesses on the complete structural system was most clearly observed in the floor to exterior wall connection, as significant horizontal displacements occurred between diaphragms for the analysis on wind loads towards the short side of the building. Unlike the connections within modules, the connections between modules preventing lateral movements were concluded to be over-designed. Each method, the friction method and the stop method, was investigated separately and found to be sufficient for obtaining static equilibrium.

The numerical model provided sufficiently accurate depictions of connection force distributions though further experimental calibrations are required to take full advantage of the three-dimensional structural behaviour. The forces in hold-downs were very difficult to predict as actual vertical deformations are unknown and might contribute to underesti-

mating or overestimating hold-down forces in the current model, e.g. hold-downs between TVEs have no forces regardless of configuration or load direction. A possible explanation may be that vertical deformations distribute loads in a way which is not intended in the numerical model, and further investigations are therefore recommended to attain more accurate results.

7.3 Suggestions for further research

- The two different methods used for preventing lateral movements between modules, stops and friction, were investigated separately and each method was found to be sufficient on its own. In the actual building system however, these methods are combined. Knowledge about the actual friction coefficient for the surfaces, and if the stops come to use for wind loads towards the long side at all, would make calculations more accurate.
- The stiffness for connections between exterior walls and horizontal diaphragms impacted the stability of the structural system greatly. Underestimating the stiffness using theoretical calculations resulted in large horizontal displacements. For a more accurate model, the actual stiffness of the configuration ought to be investigated.
- Vertical deformations had a greater impact on lateral stability than first anticipated, and should be investigated further to get a sense of the forces in hold-downs and brackets. The current approach may underestimate or overestimate uplift and vertical deformations.

Bibliography

[1] Dassault Systèmes. *Abaqus/CAE User's Manual.* Dassault Systèmes Simulia Corp. Providence, Rhode Island, USA, 2012.

[2] StruSoft. *FEM Design User Manual.* 2010.

[3] Swedish Standards Institute. SS-EN 1995-1-1. *Design of timber structures.* European committee for standardisation, 2005.

[4] P. Vollaard. Model House. *Mark.* 2016; (64): 54-57.

[5] Boverket. *Bostäder byggda med volymelement. En fallstudie av svenska bostadsprojekt – verklighet och vision.* Växjö: Allkopia i Växjö AB, 2006.

[6] Boverket. Beräkning av behovet av nya bostäder till 2025. Boverket, Report 2017:17.

[7] L. Stehn, L.O. Rask, I. Nygren & B. Östman. *Byggandet av flervåningshus i trä. Erfarenheter efter tre års observation av träbyggandets utveckling.* Luleå University of Technology, Luleå, 2017.

[8] B. Källsner & U.A. Girhammar. *Horisontalstabilisering av träregelstommar. Plastisk dimensionering av väggar med träbaserade skivor.* SP Sveriges Tekniska Forskningsinstitut, 2008.

[9] J.D. Dolan. *The dynamic response of timber shear walls.* The University of British Columbia, Vancouver, 1989.

[10] M.W. White & J.D. Dolan. Nonlinear Shear-Wall Analysis. *Journal of Structural Engineering* 1995; 121(11): 1629-1635.

[11] K. Ajaya, A.K. Gupta & G.P. Kuo. Behaviour of Wood-framed Shear Walls. *Journal of Structural Engineering* 1985; 111(8): 1722-1733.

[12] K. Ajaya, A.K. Gupta & G.P. Kuo. Modelling of a Wood-framed House. *Journal of Structural Engineering* 1987; 113(2): 260-278.

[13] J. Vessby. *Analysis of Shear Walls for Multi-Storey Timber Buildings.* Diss. Växjö: Linnaeus University, 2011.

[14] J. Vessby, B. Källsner & U.A. Girhammar. Influence of contact stress between sheets on strength and stiffness of timber frame shear walls. In: *Proceedings of the 11th World Conference on Timber Engineering.* (2): 2283-2288. Riva del Garda, Italy, 2010.

[15] S. Andreasson. *Three-Dimensional Interaction in Stabilisation of Multi-Storey Timber Frame Building Systems.* Division of Structural Engineering, Lund Institute of Technology, Lund University, Report: TVBK-1017, 2000.

[16] J. Vessby, E. Serrano & A. Olsson. Coupled and uncoupled nonlinear elastic finite element models for monotonically loaded sheating-to-framing joints in timber based shear walls. *Engineering Structures* 2010; 32 (11): 3433-3442.

[17] B. Kasal & R.J. Leichti. Nonlinear Finite-Element Model for Light-frame Stud Walls. *Journal of Structural Engineering.* 1992; 118 (11) ss. 3122-3135.

[18] M. Collins, B. Kasal, P. Paevere & G.C. Foliente. Three-Dimensional Model of Light Frame Wood Buildings. I: Model Description. *Journal of Structural Engineering.* 2005; 131 (4): 676-683.

[19] M. Collins, B. Kasal, P. Paevere & G.C. Foliente. Three-Dimensional Model of Light Frame Wood Buildings. II: Experimental Investigation and Validation of Analytical Model.

[20] B. Källsner, U.A. Girhammar and J. Vessby. Some design aspects on anchoring timber frame shear walls by transverse walls. *Proceedings of the 11th World Conference on Timber Engineering,* (2): 3412-3419. Riva del Garda, Italy, 2010.

[21] T.L. Phillips, R.Y. Itani & D.I. McLean. Lateral Load Sharing by Diaphragms in Wood-framed Buildings. *Journal of Structural Engineering.* 1993; 119(5): 1556-1571.

[22] P.J. Paevere, G.C. Foliente & B. Kasal. Loaad-sharing and Redistribution in a One-Story Woodframe Building. *Journal of Structural Engineering.* 2003; 129 (9): 1275-1284. *Journal of Structural Engineering.* 2005; 131 (4): 684-692.

[23] B. Kasal & R.J. Leichti. Incorporating Load Sharing in Shear Wall Design of Light-Frame Structures. *Journal of Structural Engineering.* 1992; 118(12): 1629-1635.

[24] K. Groom. *Nonlinear Finite-Element Modeling of Intercomponent Connections in Light-Frame Wood Structures.* Oregon State University, 1992.

[25] J. Hummel. *Displacement-based seismic design for multi-storey cross laminated timber buildings.* Kassel University, 2017.

[26] N. Ottosen & H. Petersson. *Introduction to the Finite Element Method.* New York: Prentice Hall, 1992.

[27] Boverket. *Boverkets konstruktionsregler, EKS 10.* Boverket, 2016.

[28] Swedish Standards Institute. SS-EN 1990. *Basis of structural design.* European committee for standardisation, 2010.

[29] Swedish Standards Institute. SS-EN 1990-1-4:2005. *Actions on structures - General actions - wind loads.* European committee for standardisation, 2005.

[30] Swedish Standards Institute. SS-EN 594:2011. *Timber structures - Test methods - Racking strength and stiffness of timber frame wall panels.* European committee for standardisation, 2011.

Appendix A

Connection and material properties

A.1 Connection stiffness calculations

The connector stiffnesses that cannot be calibrated with experimental data are calculated using Eurocode. The stiffness in the ultimate limit state for a connection between two timber members is calculated according to section 2.2.2 in [3]. The stiffness for a connection in N/mm is given by

$$K_u = \frac{2}{3} K_{ser} \tag{A.1}$$

where K_{ser} is the stiffness in the serviceability limit state. For a nailed or screwed connections, the stiffness in the serviceability limit state is calculated according to Table 7.1 in [3], according to

$$K_{ser} = \frac{\rho_m^{1.5} d}{23} \tag{A.2}$$

where d is the screw diameter and ρ_m is the mean density for the timber members. If the connected timber members have different densities, the mean density is calculated according to

$$\rho_m = \sqrt{\rho_{m,1}\rho_{m,2}} \tag{A.3}$$

where $\rho_{m,1}$ is the density for the first timber beam and $\rho_{m,2}$ is the density for the second timber beam. For a staple, the stiffness in the serviceability limit state is calculated according to Table 7.1 in [3], according to

$$K_{ser} = \frac{\rho_m^{1.5} d^{0.8}}{80} \tag{A.4}$$

A.1.1 Walls and horizontal diaphragms

The calculated stiffness for the screwed or nailed connections between timber members in walls, ceilings and floors are presented in Table A.1. All of the connections are of the type screwed or nailed connections, except the connection between the ceiling panels and the ceiling beams that are of the staple type.

Table A.1: Theoretically calculated stiffnesses for connections within walls, ceilings and and floors.

	d [mm]	$\rho_{m,1}$ [kg/m^3]	$\rho_{m,2}$ [kg/m^3	ρ_m [kg/m^3]	K_{ser} [kN/m]	K_u [kN/m]
Module wall frame	6.0	350	350	350	1708	1138
Exterior wall frame	6.0	380	380	380	1932	1288
Floor beam/Kerto beam	6.5	510	420	462.8	2813	1875
Particle board/Floor beam	4.2	420	770	568.6	2476	1650
Ceiling beam/Kerto beam	6.0	420	510	462.6	2597	1731
Ceiling panel/Ceiling beam	11	350	420	383.4	639	426

A.1.2 Intercomponent connections

The theoretically calculated stiffness for intercomponent connections are presented in A.2. Connections within TVEs are visualised in Figure 2.3, and connections between TVEs are visualised in Figures 2.4. For connections with multiple screws, such as hold-downs and brackets, the stiffness for the connection is the combined stiffness of the individual screws. Since these connections are also double sided, the combined stiffness is halved. The top hold-down around door openings (connection 6) has 4 screws on each side and the bottom hold-down (connection 7) has 12 screws on each side. The hold-downs between TVEs has 12 screws on each side, and the angle brackets connecting the roof to the top TVEs have 6 screws on each side.

Table A.2: Theoretically calculated stiffnesses for intercomponent connections.

Connection	d [mm]	$\rho_{m,1}$ [kg/m^3]	$\rho_{m,2}$ [kg/m^3]	ρ_m [kg/m^3]	K_{ser} [kN/m]	K_u [kN/m]
1. Ceiling/Exterior wall	6.0	420	380	399.5	2083	1388
2. Floor/Exterior wall	6.5	420	380	399.5	2256	1504
3. Ceiling/Module wall	6.0	510	350	422.5	2265	1510
4. Floor/Module wall	6.0	510	350	422.5	2265	1510
5. Wall/Wall	8.0	350	380	365.7	2422	1614
Hold-down screws	5.0	350	510	236.6	1915	1277
6. Top hold-down	-	-	-	-	-	2554
7. Bottom hold-down	-	-	-	-	-	7662
Hold-down screws	5.0	350	350	350	1423	948
8. Hold-down	-	-	-	-	-	5693
Steel plate screws	5.0	420	420	420	1871	1247
9.Steel plates	-	-	-	-	-	3118
Angle bracket screws	5.0	420	420	420	1871	1247
10. Roof truss brackets	-	-	-	-	-	3741
Roof sheet screws	4.8	420	420	420	1796	1197
Wood panelling screws	6.5	420	420	420	2432	1621

A.2 Timber properties

Young's modulus, shear modulus and density for the structural timbers used in the models are presented in Table A.3.

	Young's modulus [MPa]		Shear modulus [MPa]	Density [kg/m^3]
Timber	$E_{0,mean}$	$E_{90,mean}$	G_{mean}	ρ_{mean}
C14	7000	230	440	350
C18	9000	300	560	380
C24	11000	370	690	420
Kerto-S	11600	350	400	510

Table A.3: Properties for structural timbers included in the models.

A.3 Fictitious shell matrices

The behaviour of the fictitious shells in FEM Design are defined by three matrices: a membrane stiffness matrix (D), a flexural stiffness matrix (K) and a shear stiffness matrix (H). For an orthotropic material, the matrices are calculated according to

$$\mathbf{D} = \begin{pmatrix} \frac{E_r t}{1-\nu_{rs}\nu_{sr}} & \frac{\nu_{sr}E_r t}{1-\nu_{rs}\nu_{sr}} & 0 \\ \frac{\nu_{rs}E_s t}{1-\nu_{rs}\nu_{sr}} & \frac{E_s t}{1-\nu_{rs}\nu_{sr}} & 0 \\ 0 & 0 & G_{rs}t \end{pmatrix} \tag{A.5}$$

$$\mathbf{K} = \begin{pmatrix} \frac{E_r t^3}{12(1-\nu_{rs}\nu_{sr})} & \frac{\nu_{sr}E_r t^3}{12(1-\nu_{rs}\nu_{sr})} & 0 \\ \frac{\nu_{rs}E_s t^3}{12(1-\nu_{rs}\nu_{sr})} & \frac{E_s t^3}{12(1-\nu_{rs}\nu_{rs})} & 0 \\ 0 & 0 & \frac{G_{rs}t^3}{12} \end{pmatrix} \tag{A.6}$$

$$\mathbf{H} = \begin{pmatrix} \frac{G_{rt}t}{1.2} & 0 \\ 0 & \frac{G_{st}t}{1.2} \end{pmatrix} \tag{A.7}$$

where E is Young's modulus, t is the thickness, ν is Poisson's ratio and G is the shear modulus.

Combined normal and secura board

$E_r = E_s = 3000$ MPa
$G_{rs} = G_{st} = G_{rt} = 1250$ MPa
$t = 28$ mm
$\nu_{rs} = \nu_{sr} = 0.2$
$m = 22$ kg/m^2

$$\mathbf{D} = 10^6 \begin{pmatrix} 87.5 & 17.5 & 0 \\ 17.5 & 87.5 & 0 \\ 0 & 0 & 35 \end{pmatrix};\ \mathbf{K} = \begin{pmatrix} 5716 & 1143 & 0 \\ 1143 & 5716 & 0 \\ 0 & 0 & 2286 \end{pmatrix};\ \mathbf{H} = 10^6 \begin{pmatrix} 29.16 & 0 \\ 0 & 29.16 \end{pmatrix} \tag{A.8}$$

Humid board & Normal gypsum board

$E_r = E_s = 3000$ MPa
$G_{rs} = G_{st} = G_{rt} = 1250$ MPa
$t = 12.5$ mm
$\nu_{rs} = \nu_{sr} = 0.2$
$m = 9$ kg/m^2

$$\mathbf{D} = 10^6 \begin{pmatrix} 39.06 & 7.81 & 0 \\ 7.81 & 39.06 & 0 \\ 0 & 0 & 15.62 \end{pmatrix}; \ \mathbf{K} = \begin{pmatrix} 508 & 101 & 0 \\ 101 & 508 & 0 \\ 0 & 0 & 203 \end{pmatrix}; \ \mathbf{H} = 10^6 \begin{pmatrix} 13.02 & 0 \\ 0 & 13.02 \end{pmatrix} \tag{A.9}$$

Secura board

$E_r = E_s = 3000$ MPa
$G_{rs} = G_{st} = G_{rt} = 1250$ MPa
$t = 15.5$ mm
$\nu_{rs} = \nu_{sr} = 0.2$
$m = 13$ kg/m^2

$$\mathbf{D} = 10^6 \begin{pmatrix} 48.43 & 9.68 & 0 \\ 9.68 & 48.43 & 0 \\ 0 & 0 & 19.37 \end{pmatrix}; \ \mathbf{K} = \begin{pmatrix} 970 & 194 & 0 \\ 194 & 970 & 0 \\ 0 & 0 & 388 \end{pmatrix}; \ \mathbf{H} = 10^6 \begin{pmatrix} 16.14 & 0 \\ 0 & 16.14 \end{pmatrix} \tag{A.10}$$

Particleboard

$E_r = E_s = 2000$ MPa
$G_{rs} = G_{st} = G_{rt} = 770$ MPa
$t = 22$ mm
$\nu_{rs} = \nu_{sr} = 0.3$
$m = 12$ kg/m^2

$$\mathbf{D} = 10^6 \begin{pmatrix} 48.35 & 14.50 & 0 \\ 14.50 & 48.35 & 0 \\ 0 & 0 & 16.94 \end{pmatrix}; \ \mathbf{K} = \begin{pmatrix} 1950 & 585 & 0 \\ 585 & 1950 & 0 \\ 0 & 0 & 683 \end{pmatrix}; \ \mathbf{H} = 10^6 \begin{pmatrix} 14.11 & 0 \\ 0 & 14.11 \end{pmatrix} \tag{A.11}$$

Wood panelling

$E_r = 230$ MPa
$E_s = 7000$ MPa
$G_{rs} = 690$ MPa
$G_{st} = 690$ MPa
$G_{rt} = 69$ MPa
$t = 23$ mm

$\nu_{rs} = \nu_{sr} = 0.3$
$m = 8 \ \ \mathrm{kg/m^2}$

$$\mathbf{D} = 10^6 \begin{pmatrix} 5.81 & 1.74 & 0 \\ 53.07 & 176.92 & 0 \\ 0 & 0 & 15.87 \end{pmatrix}; \ \mathbf{K} = \begin{pmatrix} 256 & 76 & 0 \\ 2339 & 7294 & 0 \\ 0 & 0 & 699 \end{pmatrix}; \ \mathbf{H} = 10^6 \begin{pmatrix} 1.32 & 0 \\ 0 & 13.20 \end{pmatrix} \tag{A.12}$$

Appendix B

Analyses results - Wind loads towards building long side

B.1 Support reaction forces

B.1.1 Complete model

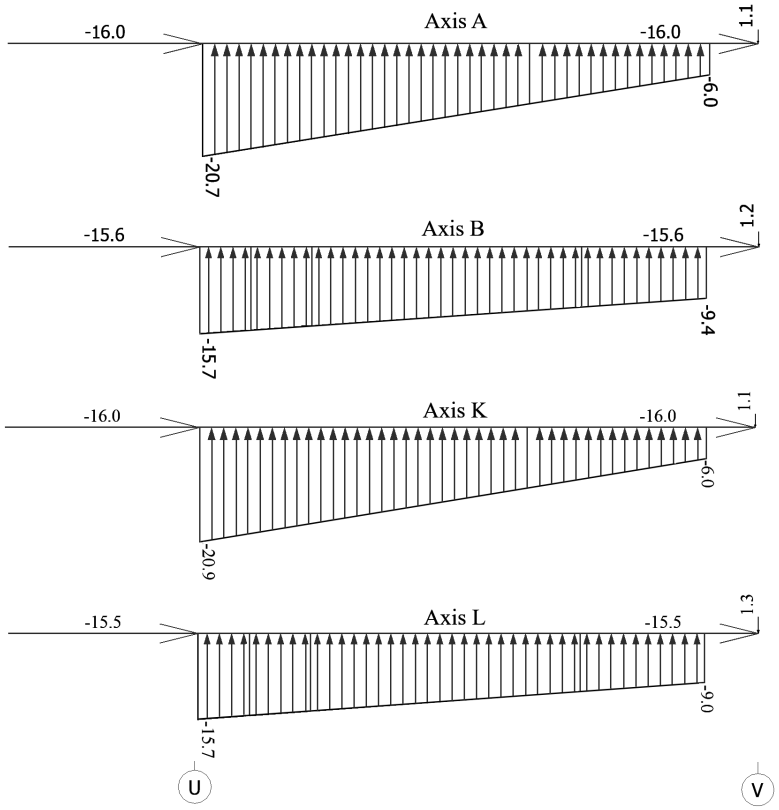

Figure B.1: Line support reaction forces [kN/m] for gable (axis A and B) and centre (K and L) placed En.

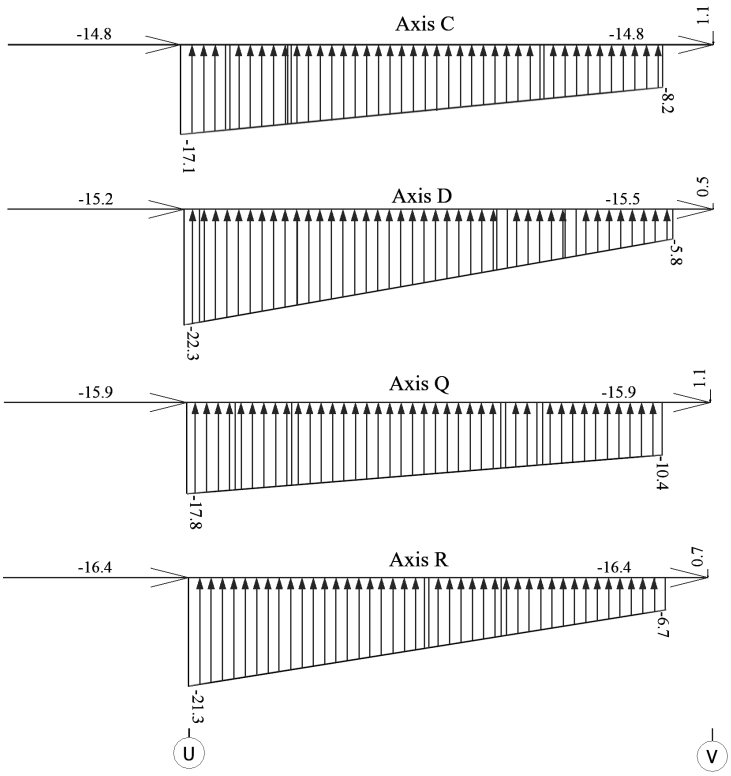

Figure B.2: Line support reaction forces [kN/m] for K1 (axis C and D) and K3 (axis Q and R).

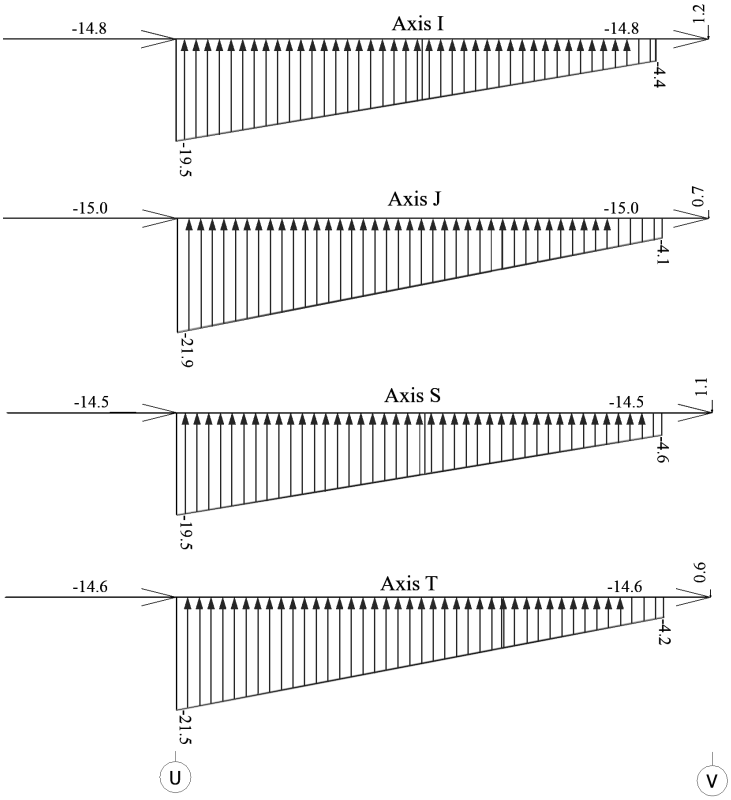

Figure B.3: Line support reaction forces [kN/m] for gable (axis S and T) and centre (I and J) placed B3.

B.1.2 Reduced model

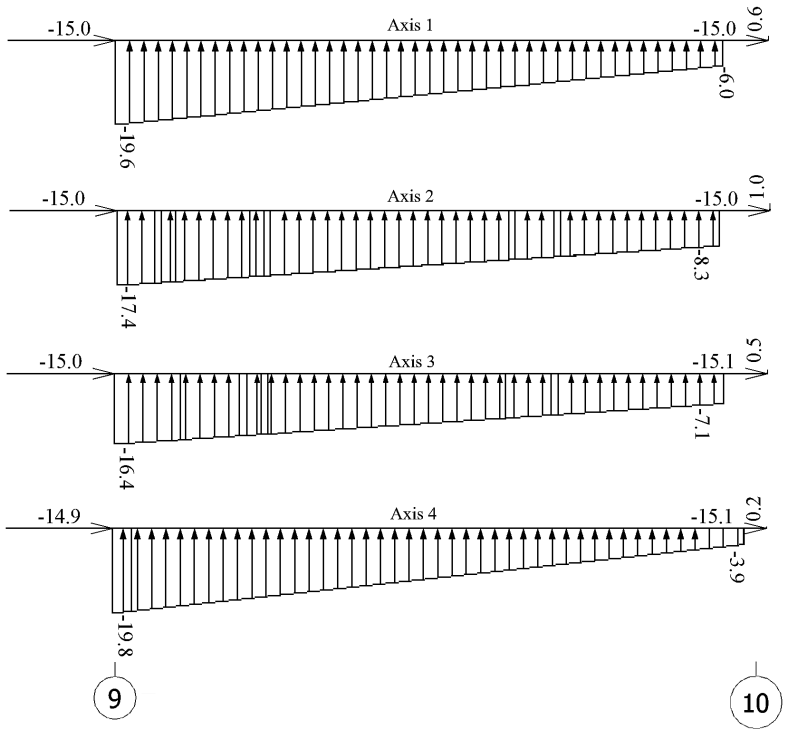

Figure B.4: Line support reaction forces [kN/m] and point support reaction forces [kN] along axes 1 to 4.

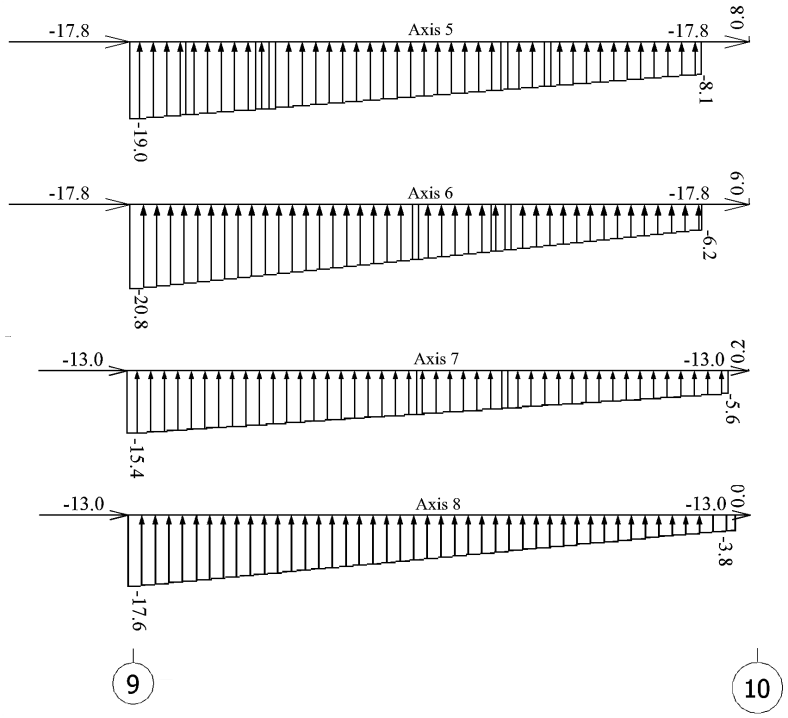

Figure B.5: Line support reaction forces [kN/m] and point support reaction forces [kN] along axes 5 to 8.

B.1.3 Reduced model with only shear walls

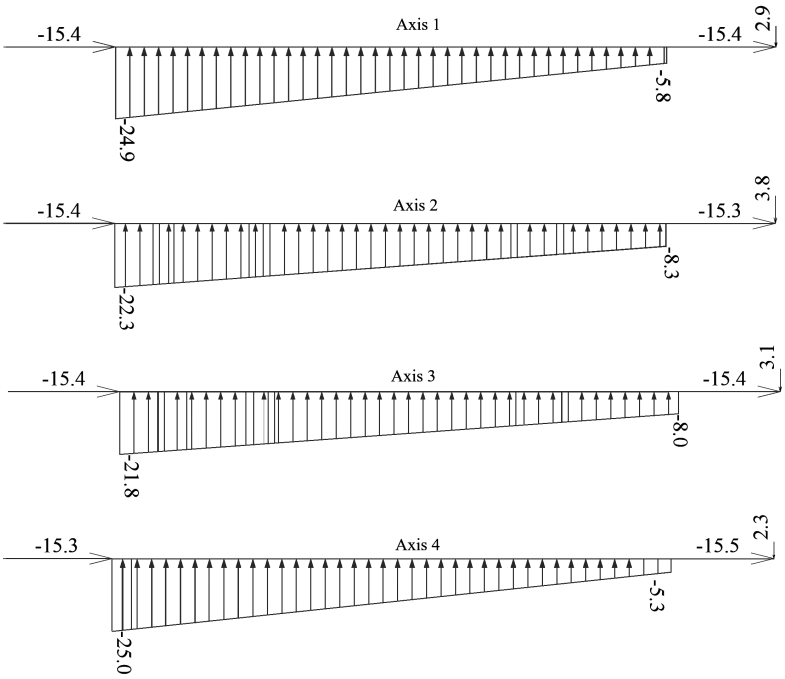

Figure B.6: Line support reaction forces [kN/m] along the long side axes 1 to 4.

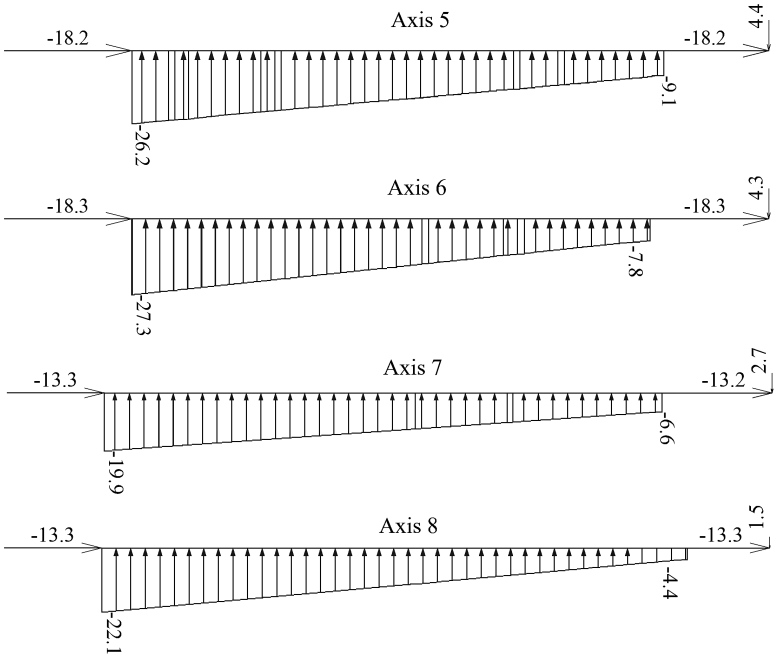

Figure B.7: Line support reaction forces [kN/m] along the long side axes 5 to 8.

B.1.4 Reduced model with friction

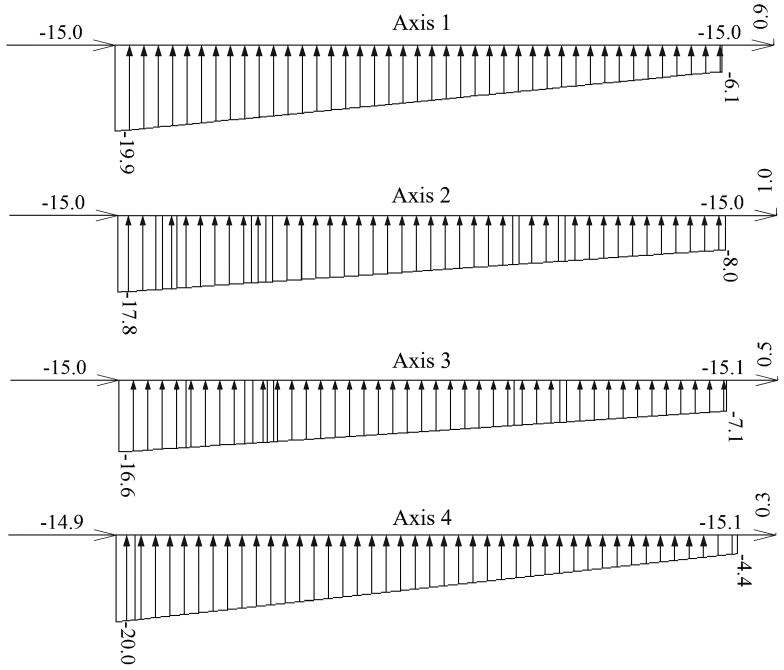

Figure B.8: Line support reaction forces [kN/m] along the long side axes 1 to 4.

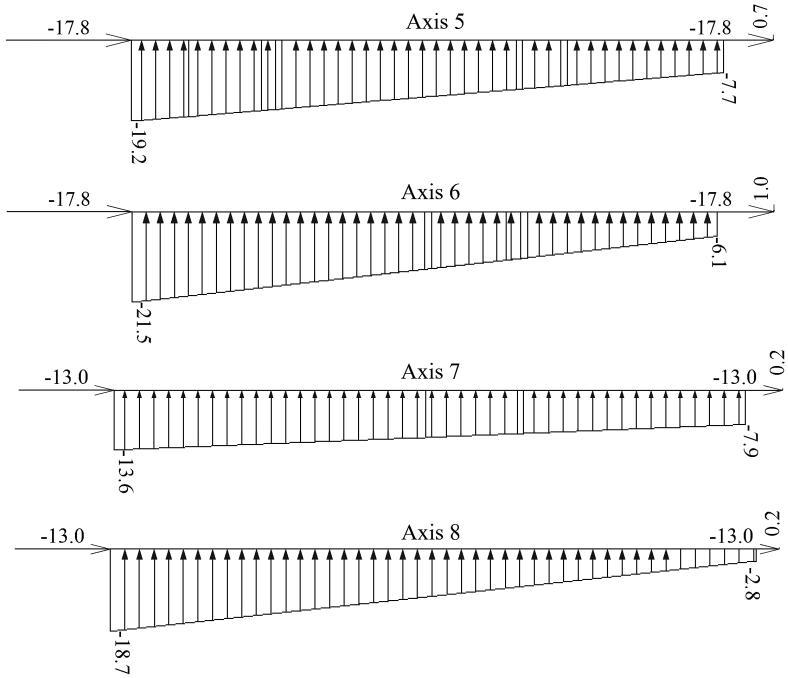

Figure B.9: Line support reaction forces [kN/m] along the long side axes 5 to 8.

B.2 Displacements

B.2.1 Complete model

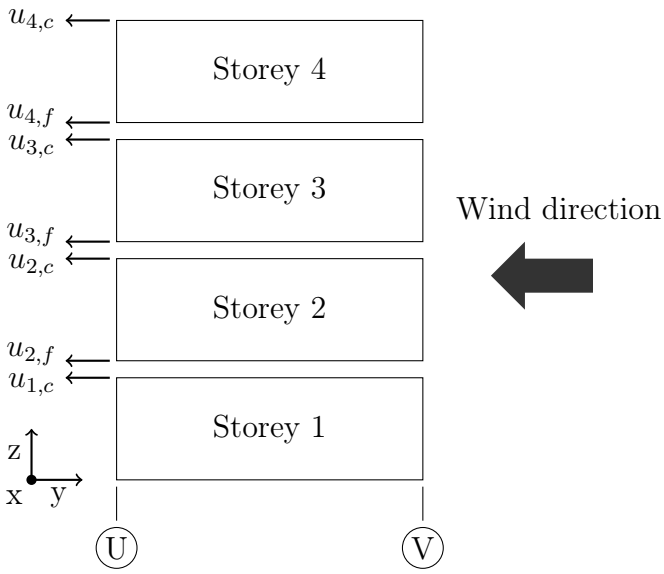

Figure B.10: Illustration of displacement measuring positions in the ceiling (u_c) and floor (u_f) for the complete analysis.

Table B.1: Horizontal displacements [mm] in the x- (u_x) and y-direction (u_y) for the complete analysis.

Module	En				K1		K3		B3			
Axis	A	B	K	L	C	D	Q	R	I	J	S	T
$u_{1,c,x}$	0	0	1	1	1	1	1	1	1	1	1	1
$u_{1,c,y}$	-17	-18	-17	-18	-18	-17	-20	-20	-16	-16	-16	-15
$u_{2,f,x}$	0	0	1	1	0	0	1	1	1	1	1	1
$u_{2,f,y}$	-24	-24	-24	-24	-24	-24	-26	-26	-22	-22	-22	-21
$u_{2,c,x}$	1	1	1	1	1	1	2	2	1	1	2	2
$u_{2,c,y}$	-39	-40	-39	-40	-40	-39	-44	-42	-37	-37	-37	-36
$u_{3,f,x}$	0	0	1	1	1	1	2	2	1	1	2	2
$u_{3,f,y}$	-45	-45	-45	-45	-45	-44	-48	-48	-43	-42	-42	-41
$u_{3,c,x}$	1	1	1	1	1	1	2	2	1	1	3	3
$u_{3,c,y}$	-58	-59	-58	-58	-59	-59	-63	-61	-57	-57	-56	-55
$u_{4,f,x}$	0	0	1	1	1	1	2	2	2	2	4	4
$u_{4,f,y}$	-62	-62	-62	-62	-62	-62	-65	-65	-61	-61	-60	-59
$u_{4,c,x}$	1	1	1	1	1	1	2	2	2	2	4	4
$u_{4,c,y}$	-72	-73	-73	-73	-74	-74	-76	-75	-74	-73	-72	-70

B.2.2 Reduced models

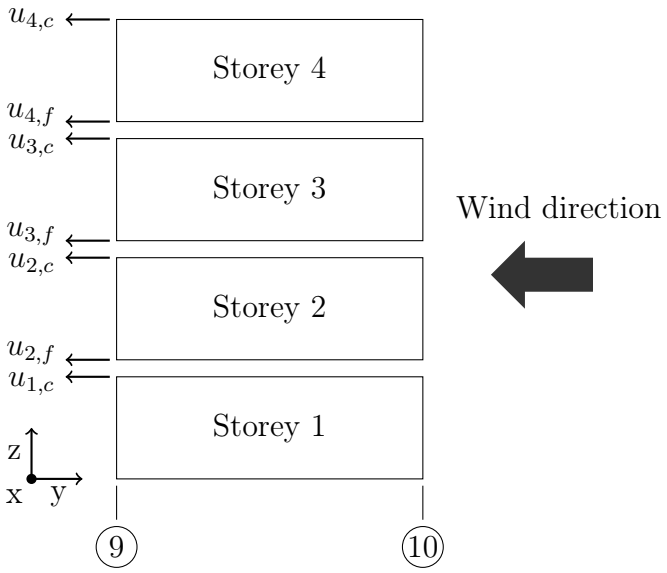

Figure B.11: Illustration of displacement measuring positions in the ceiling (u_c) and floor (u_f) for the reduced analyses.

Table B.2: Horizontal in-plane (u_y) and out-of-plane (u_x) displacements [mm] for the reduced analysis.

Module	Er		K2r		K4r		S4r	
Axis	1	2	3	4	5	6	7	8
$u_{1,c,x}$	2	-1	2	2	2	2	1	1
$u_{1,c,y}$	-20	-20	-20	-18	-25	-23	-15	-15
$u_{2,f,x}$	2	-1	2	2	1	1	3	3
$u_{2,f,y}$	-25	-25	-25	-23	-31	-30	-20	-20
$u_{2,c,x}$	4	-1	4	4	3	3	3	3
$u_{2,c,y}$	-44	-45	-44	-40	-54	-51	-35	-34
$u_{3,f,x}$	4	-1	4	4	2	2	3	3
$u_{3,f,y}$	-48	-50	-48	-45	-59	-57	-39	-38
$u_{3,c,x}$	4	0	4	4	3	3	3	3
$u_{3,c,y}$	-65	-68	-65	-60	-80	-76	-52	-50
$u_{4,f,x}$	4	0	4	4	3	3	4	4
$u_{4,f,y}$	-68	-71	-68	-63	-83	-80	-55	-53
$u_{4,c,x}$	5	0	5	5	3	3	4	4
$u_{4,c,y}$	-81	-86	-81	-75	-99	-95	-65	-63

Table B.3: Horizontal in-plane (u_y) and out-of-plane (u_x) displacements [mm] for the reduced analysis with only shear walls.

Module	En		K1		K3		B3	
Axis	1	2	3	4	5	6	7	8
$u_{1,c,x}$	-4	-4	6	6	2	2	4	8
$u_{1,c,y}$	-20	-24	-24	-20	-30	-27	-18	-16
$u_{2,f,x}$	-4	-4	6	6	2	2	4	8
$u_{2,f,y}$	-27	-31	-31	-28	-39	-36	-24	-23
$u_{2,c,x}$	-5	-5	9	9	1	1	7	8
$u_{2,c,y}$	-51	-57	-58	-52	-72	-68	-45	-42
$u_{3,f,x}$	-4	-4	9	9	1	1	8	8
$u_{3,f,y}$	-58	-63	-65	-58	-80	-76	-51	-48
$u_{3,c,x}$	-3	-3	9	9	-1	-1	10	8
$u_{3,c,y}$	-83	-90	-92	-83	-113	-108	-72	-68
$u_{4,f,x}$	-2	-2	8	9	-2	-2	10	8
$u_{4,f,y}$	-87	-94	-96	-88	-118	-114	-76	-72
$u_{4,c,x}$	-2	-2	11	10	0	0	12	8
$u_{4,c,y}$	-109	-118	-122	-111	-151	-143	-94	-90

Table B.4: Horizontal in-plane (u_y) and out-of-plane (u_x) displacements [mm] for the reduced analysis with friction.

Module	En		K1		K3		B3	
Axis	1	2	3	4	5	6	7	8
$u_{1,c,x}$	-1	-1	2	2	2	2	1	1
$u_{1,c,y}$	-17	-19	-19	-17	-24	-22	-14	-14
$u_{2,f,x}$	-2	-2	2	2	3	2	2	2
$u_{2,f,y}$	-18	-19	-19	-18	-24	-23	-15	-14
$u_{2,c,x}$	-1	-1	3	3	3	3	-1	-1
$u_{2,c,y}$	-34	-37	-37	-33	-46	-42	-29	-28
$u_{3,f,x}$	-1	-1	3	3	3	3	-1	-1
$u_{3,f,y}$	-35	-38	-37	-34	-46	-43	-30	-29
$u_{3,c,x}$	2	2	2	2	3	3	-1	-4
$u_{3,c,y}$	-51	-55	-53	-48	-65	-61	-43	-42
$u_{4,f,x}$	2	2	2	2	2	2	-4	-4
$u_{4,f,y}$	-52	-56	-53	-48	-66	-62	-43	-42
$u_{4,c,x}$	4	4	1	1	1	1	-7	-7
$u_{4,c,y}$	-65	-70	-65	-59	-81	-76	-54	-52

B.3 Connection forces

B.3.1 Vertical connection forces distributions within modules

Axis 1/A/K

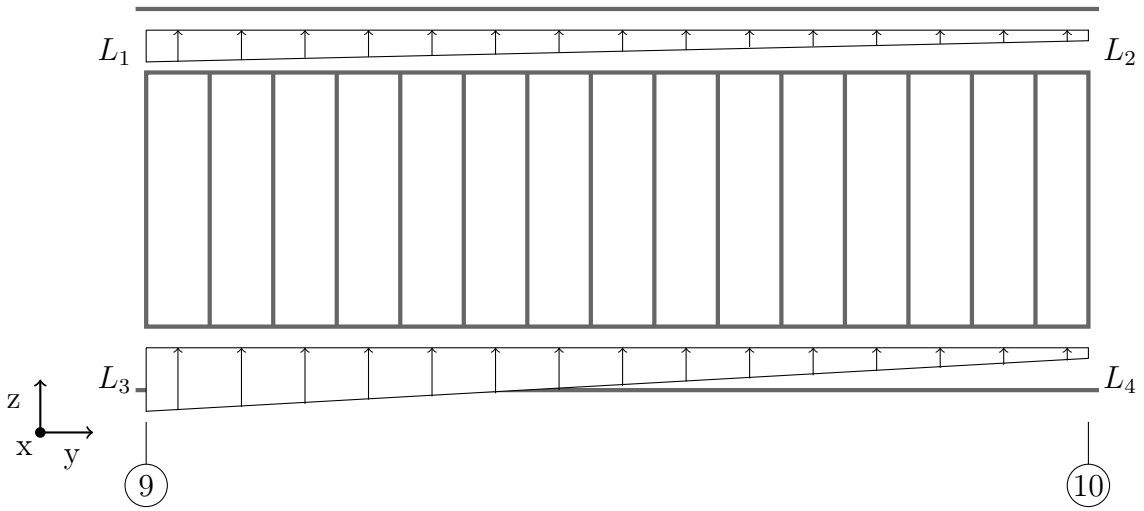

Figure B.12: Illustration of the vertical force distributions between the shear wall and the ceiling/floor along axis 1/A/K, module En.

Table B.5: Vertical connection forces [kN/m] in the line connection between shear wall and floor/ceiling along axis 1/A/K, module En.

Analysis	Axis	Storey	L_1	L_2	L_3	L_4
Complete	A	4	-0.8	1.4	-4.0	1.3
		3	-4.5	-1.0	-9.2	-2.1
		2	-10.4	-2.1	-15.9	0.1
		1	-14.1	-3.8	-21.1	-1.1
	K	4	-1.1	1.0	-4.2	0.9
		3	-4.9	-1.0	-9.5	0.2
		2	-10.6	-2.2	-16.2	0.1
		1	-14.2	-3.7	-21.3	-1.1
Reduced	2	4	0	0.4	-2.5	-0.3
		3	-4.1	-1.7	-7.8	-1.5
		2	-9.2	-3.3	-14.0	-2.1
		1	-15.0	-4.2	-20.3	-2.3
Reduced, shear walls only	2	4	0.4	1.3	-3.1	1.1
		3	-5.4	0.6	-10.2	0.6
		2	-12.8	0.8	-18.9	1.6
		1	-21.7	0.4	-29.0	4.0
Reduced, friction	2	4	0	0.4	-2.1	-0.2
		3	-4.3	-1.4	-7.6	-1.3
		2	-9.6	-2.8	-13.8	-2.0
		1	-15.7	-3.6	-20.7	-2.0

Axis 2/B/L

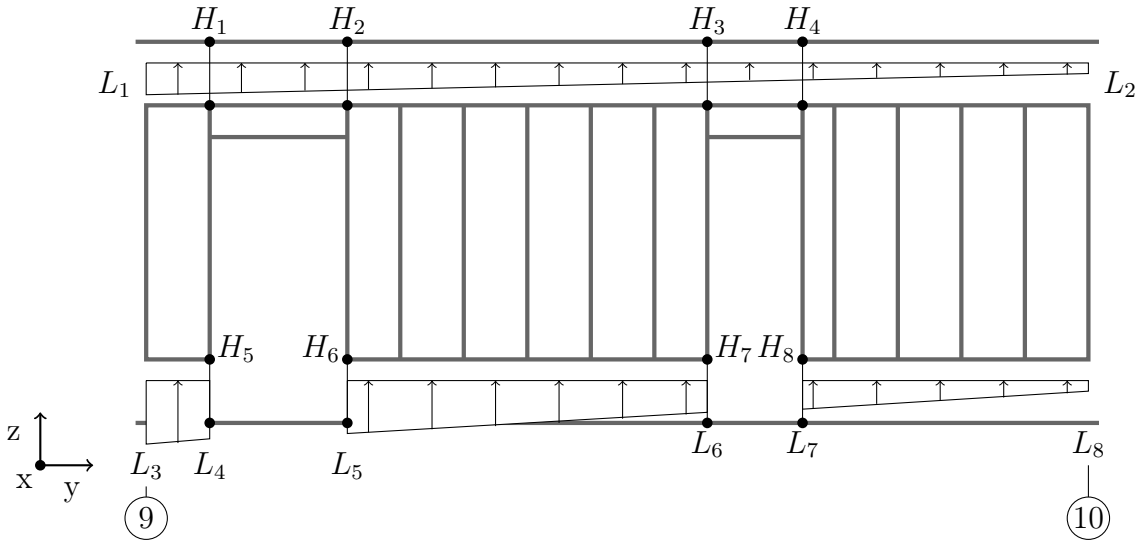

Figure B.13: Illustration of the vertical force distributions between the shear wall and the ceiling/floor along axis 2/B/L, module En. Hold-downs are numbered 1 to 8.

Table B.6: Vertical connection forces [kN/m] in the line connection between shear wall and floor/ceiling along axis 2/B/L, module En.

Analysis	Axis	Storey	L_1	L_2	L_3	L_4	L_5	L_6	L_7	L_8
Complete	B	4	-1.0	0.5	-0.7	0.1	-5.4	-0.6	-3.9	2.2
		3	-3.9	-1.7	-8.2	-5.4	-11.0	-4.1	-7.2	1.4
		2	-7.9	-3.2	-17.4	-9.6	-17.6	-6.4	-12.0	1.8
		1	-11.8	-5.3	-28.3	-17.1	-24.4	-7.3	-19.3	6.2
	L	4	-0.9	0.6	0	0.8	-5.4	-0.4	-3.8	2.4
		3	-3.8	-1.5	-8.3	-4.5	-10.8	-4.0	-7.1	1.6
		2	-7.6	-3.4	-17.3	-9.5	-17.5	-6.1	-11.9	1.9
		1	-11.7	-5.0	-28.2	-17.1	-24.2	-7.1	-18.9	6.4
Reduced	2	4	0.1	0	-0.1	3.5	-5.0	0.3	-3.3	1.4
		3	-3.3	-1.7	-11.1	-6.4	-9.5	-2.1	-7.8	0.8
		2	-7.7	-3.2	-23.6	-15.7	-15.3	-4.1	-12.6	-4.3
		1	-12.7	-4.3	-38.7	-25.7	-21.1	-6.2	-18.1	1.6
Reduced, shear walls only	2	4	0.5	0.9	5.1	12.0	-7.9	1.8	-4.9	5.5
		3	-4.1	-1.2	-11.0	-7.3	-11.5	-1.9	-9.1	5.0
		2	-10.6	-1.9	-27.1	-20.7	-19.1	-3.6	-14.3	7.4
		1	-18.4	-1.0	-49.4	-35.3	-27.0	-4.8	-19.6	11.1
Reduced, friction	2	4	0.1	0	-0.8	3.9	-5.0	0.7	-2.9	1.2
		3	-3.4	-1.5	-12.7	-6.7	-8.6	-2.0	-7.6	0.9
		2	-7.9	-2.8	-25.1	-15.9	-14.1	-4.7	-12.5	1.6
		1	-13.2	-3.7	-38.1	-25.8	-20.8	-7.2	-17.9	2.3

Table B.7: Tension in hold-downs [kN] between shear walls and floor/ceiling along axis 2/B/L, module En.

Analysis	Axis	Storey	H_1	H_2	H_3	H_4	H_5	H_6	H_7	H_8
Complete	B	4	0	0	0	0	0	0.5	0	0.3
		3	0	0	0	0	0	0.9	0.3	0.5
		2	0	0	0	0	0.8	1.5	0.5	0.8
		1	0	0	0	0	1.2	2.2	0.6	1.2
	L	1	0	0	0	0	0	0.5	0	0.3
		3	0	0	0	0	0.4	0.9	0.3	0.5
		2	0	0	0	0	0.8	1.5	0.4	0.8
		1	0	0	0	0	1.2	2.2	0.6	1.1
Reduced	2	4	0.3	0.3	0	0	0	0.6	0.1	0.3
		3	0	0	0	0	0.6	0.7	0.3	0.7
		2	0	0	0	0	1.4	1.7	0.6	1.0
		1	0	0	0	0	2.0	2.3	0.8	1.4
Reduced, shear walls only	2	4	1.1	0	0	0	0	0.9	0	0.4
		3	0	0	0	0	0.7	1.3	0.3	0.7
		2	0	0	0	0	1.9	2.1	0.5	1.1
		1	0	0	0	0	2.7	2.9	0.7	1.5
Reduced, friction	2	4	0.2	0.3	0	0	0	0.7	0.1	0.3
		3	0	0	0	0	0.6	1.2	0.4	0.8
		2	0	0	0	0	1.3	1.9	0.7	1.2
		1	0	0	0	0	2.0	2.4	0.9	1.5

Axis 3/C

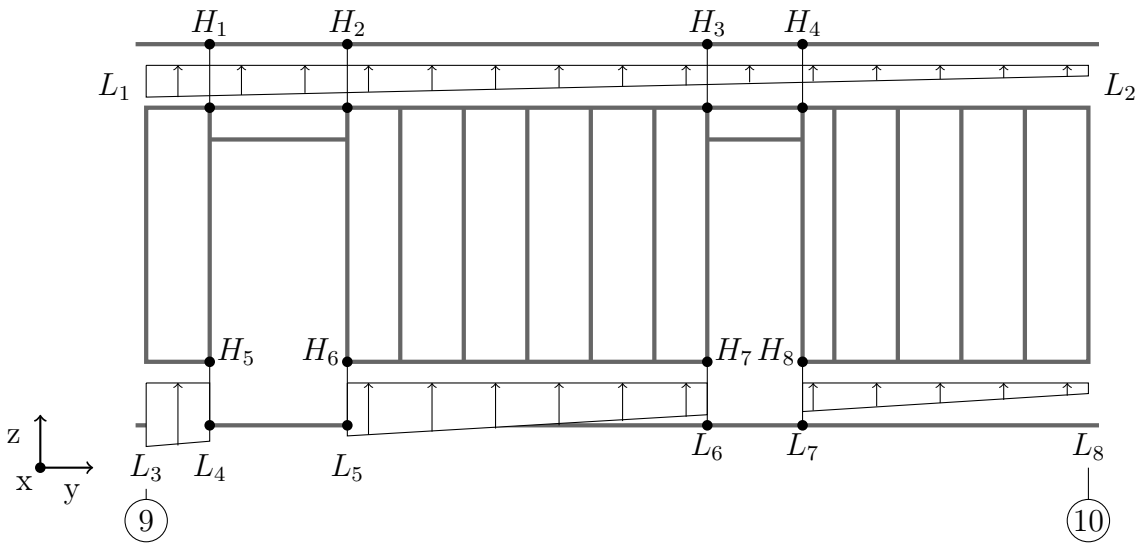

Figure B.14: Illustration of the vertical force distributions between the shear wall and the ceiling/floor along axis 3/C, module K1. Hold-downs are numbered 1 to 8.

Analysis	Axis	Storey	L_1	L_2	L_3	L_4	L_5	L_6	L_7	L_8
Complete	C	4	0.3	-0.4	-0.5	1.2	-5.1	-0.9	-3.4	1.4
		3	-3.3	-2.0	-5.4	-4.9	-10.9	-4.2	-7.6	3.2
		2	-8.4	-3.1	-13.5	-13.9	-19.4	-5.8	-12.2	4.3
		1	-13.6	-4.1	-24.5	-22.8	-27.4	-6.7	-17.8	6.0
Reduced	3	4	0.1	0.2	-1.0	2.4	-5.8	1.1	-2.6	0.9
		3	-2.9	-1.6	-8.9	-6.2	-10.2	-0.7	-6.9	0.3
		2	-6.3	-3.3	-17.9	-15.9	-15.8	-2.4	-11.4	0.4
		1	-10.1	-4.7	-27.3	-25.2	-21.4	-4.7	-17.2	2.1
Reduced, shear walls only	3	4	0.9	0.7	0.7	4.6	-8.8	2.1	-4.2	4.7
		3	-4.0	-1.3	-10.7	-10.0	-12.7	-1.2	-8.7	4.4
		2	-10.4	-1.9	-25.9	-27.7	-21.1	-2.6	-13.6	6.5
		1	-18.1	-1.2	-47.3	-45.6	-29.6	-3.8	-19.0	10.4
Reduced, friction	3	4	0.1	0.3	-1.6	2.3	-7.8	3.2	-0.2	-0.8
		3	-3.4	-0.5	-10.0	-6.9	-11.0	1.4	-6.1	-0.3
		2	-6.6	-2.5	-18.8	-16.3	-14.9	-2.4	-11.0	0.8
		1	-10.8	-3.8	-27.2	-26.0	-21.2	-5.2	-16.9	2.6

Table B.8: Vertical connection forces [kN/m] in the line connection between shear wall and floor/ceiling along axis 3/C, module K1.

Table B.9: Tension forces in hold-downs [kN] between shear walls and floor/ceiling along axis 3/C, module K1.

Analysis	Axis	Storey	H_1	H_2	H_3	H_4	H_5	H_6	H_7	H_8
Complete	C	4	0.3	0	0	0	0.9	0	0	0.3
		3	0	0	0	0	0	0	0.4	0.5
		2	0	0	0	0	0	0	0.6	0.8
		1	0	0	0	0	0	0	0.8	1.2
Reduced	3	4	0.3	0.2	0	0	1.3	0	0	0.3
		3	0	0	0	0	0	0.2	0.4	0.6
		2	0	0	0	0	0	0	0.7	1.1
		1	0	0	0	0	0	0	0.8	1.6
Reduced, shear walls only	3	4	0.8	0	0	0	3.6	0	0	0
		3	0	0	0	0	0	0	0.4	0.7
		2	0	0	0	0	0	0	0.7	1.2
		1	0	0	0	0	0	0	0.9	1.6
Reduced, friction	3	4	0.2	0.2	0	0	1.4	0	0	0
		3	0	0	0	0	0	0	0.2	0.7
		2	0	0	0	0	0	0	0.8	1.2
		1	0	0	0	0	0	0	0.9	1.6

Axis 4/D

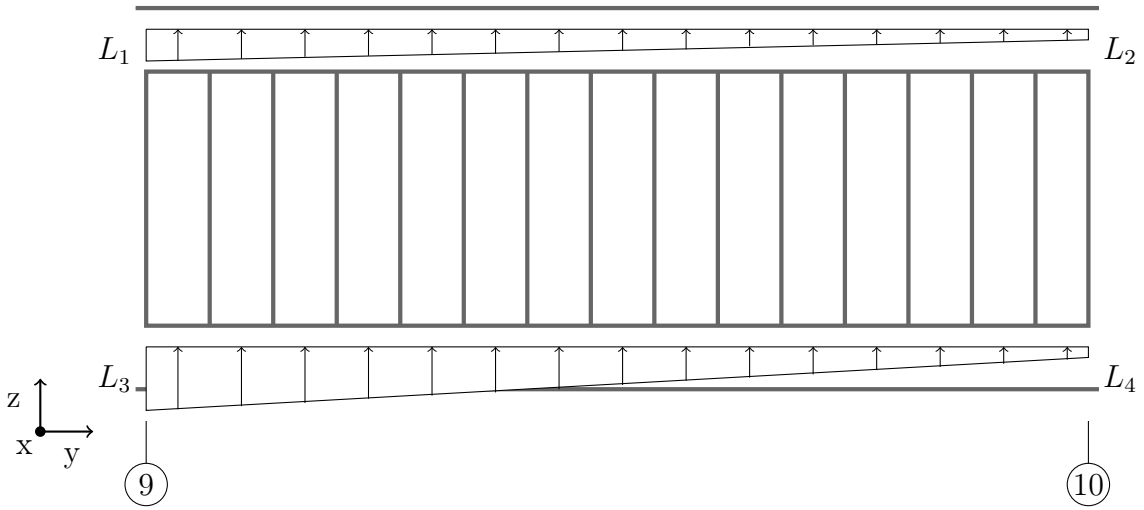

Figure B.15: Illustration of the vertical force distributions between the shear wall and the ceiling/floor along axis 4/D, module K1.

Table B.10: Vertical connection forces [kN/m] in the line connection between shear wall and floor/ceiling along axis 4/D, module K1.

Analysis	Axis	Storey	L_1	L_2	L_3	L_4
Complete	D	4	0	0	-3.2	-0.1
		3	-4.7	-1.4	-8.8	-1.0
		2	-10.8	-2.5	-16.1	-1.1
		1	-17.7	-2.8	-24.0	0.4
Reduced	4	4	-0.1	0.4	-2.4	-0.1
		3	-3.5	-1.8	-7.5	-1.3
		2	-7.5	-1.3	-13.4	-1.7
		1	-12.3	-4.7	19.7	-1.8
Reduced, shear walls only	4	4	0.3	1.3	-3.1	1.2
		3	-5.5	-0.5	-10.3	0.7
		2	-13.0	-0.7	-19.1	1.8
		1	-22.1	0.7	-29.2	4.3
Reduced, friction	4	4	-0.1	0.5	-2.3	0.0
		3	-3.8	-1.4	-7.4	-1.1
		2	-8.0	-3.1	-13.4	-1.5
		1	-13.4	-3.9	-20.2	-1.4

Axis 5/Q

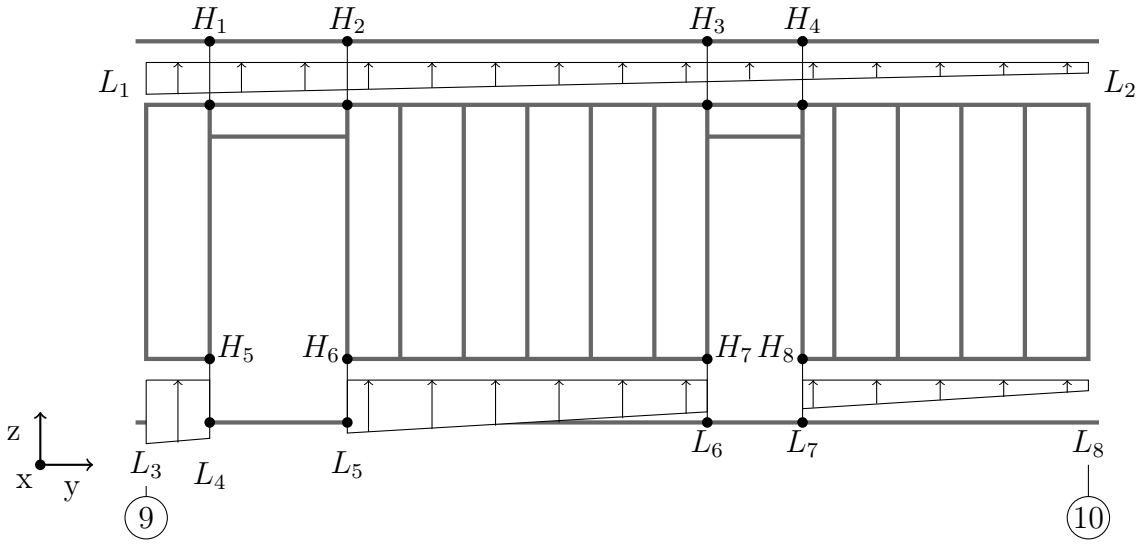

Figure B.16: Illustration of the vertical force distributions between the shear wall and the ceiling/floor along axis 5/Q, module K3. Hold-downs are numbered 1 to 8.

Table B.11: Vertical connection forces [kN/m] in the line connection between shear wall and floor/ceiling along axis 5/Q, module K3.

Configuration	Axis	Storey	L_1	L_2	L_3	L_4	L_5	L_6	L_7	L_8
Complete	Q	4	-0.1	0.1	-0.9	1.0	-5.3	-1.1	-2.8	1.2
		3	-3.6	-2.2	-6.1	-5.0	-11.3	-4.9	-8.3	3.5
		2	-8.3	-4.2	-13.7	-13.3	-19.9	-7.3	-14.4	4.5
		1	-13.7	-5.8	-25.3	-22.2	-29.2	-8.2	-22.0	6.8
Reduced	5	4	-0.2	0	-1.3	2.5	-6.9	1.6	-3.1	1.0
		3	-3.3	-1.9	-10.0	-6.3	-11.9	-0.4	-8.1	0.3
		2	-7.2	-3.4	-20.4	-17.2	-18.4	-2.2	-13.9	0.9
		1	-11.7	-4.8	-31.5	-28.2	-25.0	-4.7	-21.8	3.7
Reduced, shear walls only	5	4	0.7	1.0	0.5	5.5	-10.7	3.1	-5.3	6.8
		3	-4.9	-1.5	-12.8	-11.9	-15.1	-0.9	-11.2	6.2
		2	-12.2	-2.2	-31.0	-32.7	-25.1	-2.9	-17.5	9.0
		1	-21.8	-1.1	-56.9	-54.4	-35.4	-4.2	-24.4	14.3
Reduced, friction	5	4	-0.3	0.2	-2.2	2.5	-9.2	4.5	0	-1.3
		3	-4.0	-0.4	-11.4	-7.3	-12.6	-2.3	-7.2	-0.6
		2	-7.6	-2.5	-21.3	-17.6	-17.2	-2.2	-13.4	1.0
		1	-12.5	-3.8	-31.2	-29.0	-24.6	-5.4	-21.2	4.0

Table B.12: Tension forces in hold-downs [kN] between shear walls and floor/ceiling along axis 5/Q, module K3.

Analysis	Axis	Storey	H_1	H_2	H_3	H_4	H_5	H_6	H_7	H_8
Complete	Q	4	0.3	0	0	0	0	0	0	0
		3	0.9	0	0	0	0	0	0	0
		2	0	0	0	0	0	0	0	0
		1	0	0	0	0	0	0	0	0
Reduced	5	4	0.1	0.2	0	0	1.2	0	0	0
		3	0	0	0	0	0	0	0	0
		2	0	0	0	0	0	0	0	0
		1	0	0	0	0	0	0	0	0
Reduced, shear walls only	5	4	0.9	0	0	0	4.2	0	0	0
		3	0	0	0	0	0	0	0	0
		2	0	0	0	0	0	0	0	0
		1	0	0	0	0	0	0	0	0
Reduced, friction	5	4	0.1	0.3	0	0	1.4	0	0	0
		3	0	0	0	0	0	0	0	0
		2	0	0	0	0	0	0	0	0
		1	0	0	0	0	0	0	0	0

Axis 6/R

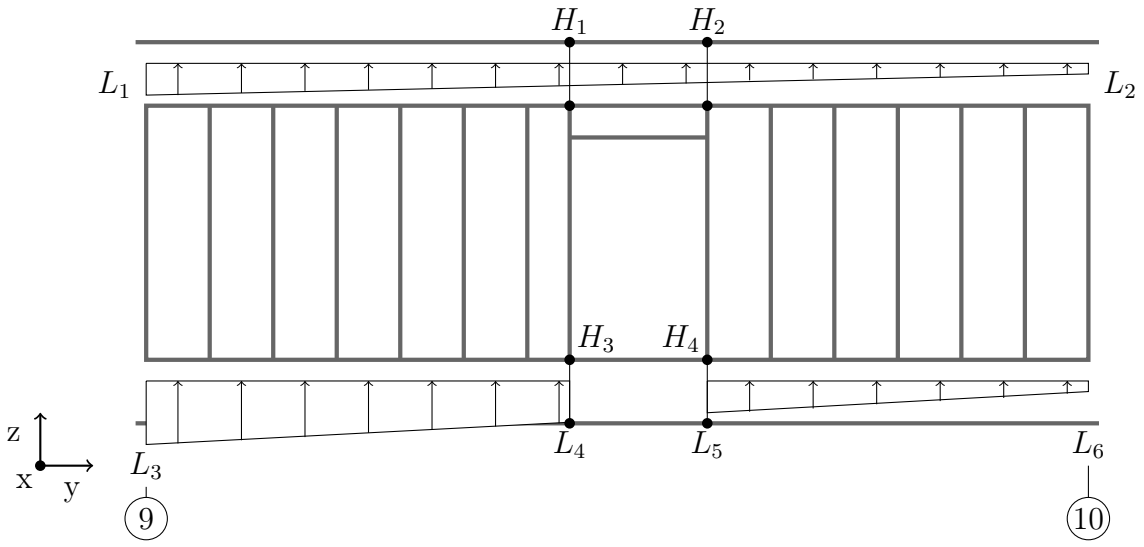

Figure B.17: Illustration of the vertical force distributions between the shear wall and the ceiling/floor along axis 6/R, module K3. Hold-downs are numbered 1 to 4.

Table B.13: Vertical connection forces [kN/m] in the line connection between shear wall and floor/ceiling along axis 6/R, module K3.

Analysis	Axis	Storey	L_1	L_2	L_3	L_4	L_5	L_6
Complete	R	4	-0.9	0.4	-3.7	-1.7	-3.4	1.2
		3	-5.7	-0.6	-9.3	-5.9	-8.4	1.1
		2	-11.0	-2.1	-16.4	-8.8	-14.4	0.8
		1	-14.6	-4.3	-25.0	-8.3	-23.2	4.9
Reduced	6	4	0	-0.5	-3.4	-0.1	-3.8	1.5
		3	-4.6	-0.9	-10.2	-2.6	-8.4	1.0
		2	-9.4	-1.8	-17.9	-5.0	-4.3	1.4
		1	-14.3	-2.9	-26.3	-6.1	-22.4	3.1
Reduced, shear walls only	6	4	0.2	1.6	-1.8	-1.7	-5.0	5.4
		3	-6.5	-0.1	-11.8	-5.5	-11.2	5.7
		2	-15.2	0.1	-23.4	-9.1	-18.2	8.7
		1	-25.5	1.9	-40.2	-8.2	-25.5	-12.5
Reduced, friction	6	4	0	-0.5	-3.2	0.2	-3.2	1.5
		3	-4.9	-0.5	-9.9	-2.7	-8.3	1.6
		2	-10.2	-0.9	-17.5	-5.6	-14.4	-1.5
		1	-15.8	-1.5	-25.8	-8.0	-22.0	4.2

Table B.14: Tension forces in hold-downs [kN] between shear walls and floor/ceiling along axis 6/R, module K3.

Analysis	Axis	Storey	H_1	H_2	H_3	H_4
Complete	R	4	0	0	0.2	0
		3	0	0	0	0
		2	0	0	0	0
		1	0	0	0	0
Reduced	6	4	0	0	0.2	0
		3	0	0	0	0
		2	0	0	0	0
		1	0	0	0	0
Reduced, shear walls only	6	4	0	0	0	0
		3	0	0	0	0
		2	0	0	0	0
		1	0	0	0	0
Reduced, friction	6	4	0	0	0	0
		3	0	0	0	0
		2	0	0	0	0
		1	0	0	0	0

Axis 7/I/S

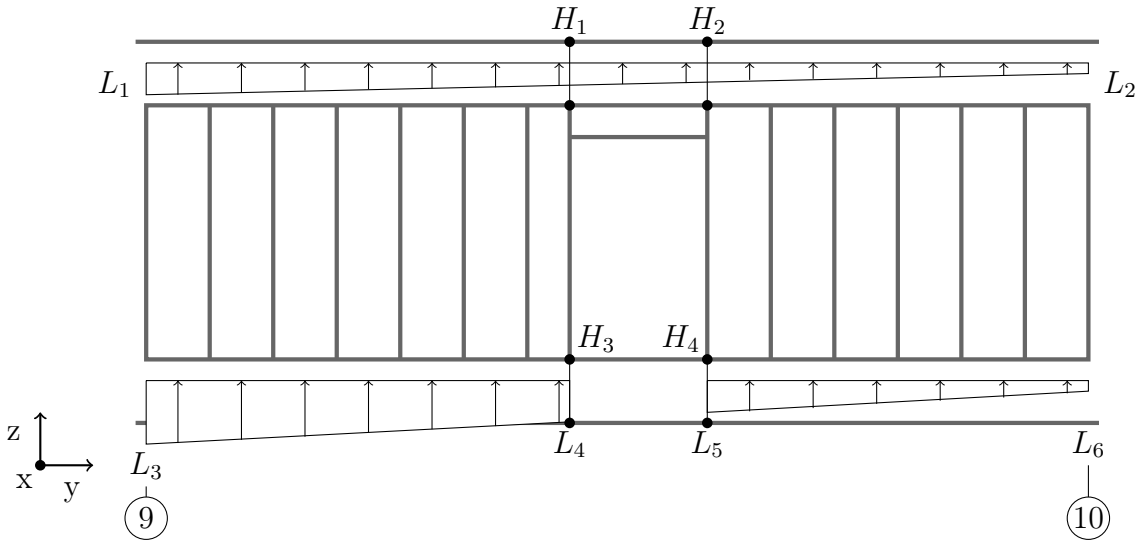

Figure B.18: Illustration of the vertical force distributions between the shear wall and the ceiling/floor along axis 7/I/S, module B3. Hold-downs are numbered 1 to 4.

Table B.15: Vertical connection forces [kN/m] in the line connection between shear wall and floor/ceiling along axis 7/I/S, module B3.

Analysis	Axis	Storey	L_1	L_2	L_3	L_4	L_5	L_6
Complete	I	4	-0.3	0.2	-3.2	-1.3	-5.6	3.1
		3	-4.7	-0.7	-7.7	-6.1	-9.1	3.6
		2	-10.1	-1.3	-15.1	-8.4	-13.4	-1.2
		1	-15.9	-1.2	-24.2	-7.7	-18.7	5.1
	S	4	-0.4	0.1	-3.2	-1.6	-5.5	2.8
		3	-4.9	-0.7	-7.7	-6.5	-9.6	3.8
		2	-10.5	-1.0	-15.2	-8.7	-13.9	4.3
		1	-15.9	-1.3	-24.1	-0.8	-18.9	4.8
Reduced	7	4	-0.1	0.3	-1.9	-1.1	-3.3	1.1
		3	-3.3	-1.0	-7.0	-3.3	-7.9	0.5
		2	-7.0	-2.1	-12.5	-5.8	-13.6	0.9
		1	-12.5	-2.6	-19.4	-6.3	-19.8	1.5
Reduced, shear walls only	7	4	0.6	0.9	-0.7	-2.2	-4.5	3.5
		3	-4.4	-0.5	-7.9	-5.0	-9.7	4.0
		2	-10.8	-0.5	-16.3	-7.7	-15.8	6.3
		1	-18.1	0.3	-28.7	-6.5	-21.9	8.8
Reduced, friction	7	4	0	0.2	-1.6	-1.1	-3.1	1.0
		3	-3.3	-0.9	-6.1	-3.5	-8.4	0.9
		2	-6.5	-2.4	-8.2	-7.9	-15.5	1.7
		1	-10.4	-4.2	-15.2	-9.2	-22.0	2.3

Table B.16: Tension forces in hold-downs [kN] between shear walls and floor/ceiling along axis 7/I/S, module B3.

Analysis	Axis	Storey	H_1	H_2	H_3	H_4
Complete	I	4	0	0	0	0
		3	0	0	0	0
		2	0	0	0	0
		1	0	0	0	0
	S	4	0	0	0	0
		3	0	0	0	0
		2	0	0	0	0
		1	0	0	0	0
Reduced	7	4	0	0	0	0
		3	0	0	0	0
		2	0	0	0	0
		1	0	0	0	0
Reduced, shear walls only	7	4	0	0	0	0
		3	0	0	0	0
		2	0	0	0	0
		1	0	0	0	0
Reduced, friction	7	4	0	0	0	0
		3	0	0	0	0
		2	0	0	0	0
		1	0	0	0	0

Axis 8/J/T

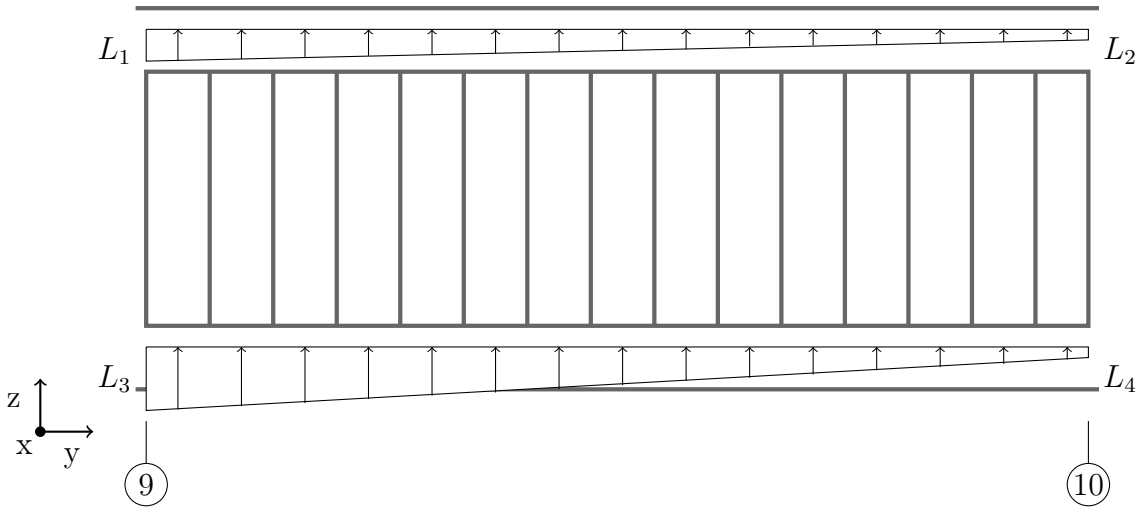

Figure B.19: Illustration of the vertical force distributions between the shear wall and the ceiling/floor along axis 8/J/T, module B3.

Table B.17: Vertical connection forces [kN/m] in the line connection between shear wall and floor/ceiling along axis 8/J/T, module B3.

Analysis	Axis	Storey	L_1	L_2	L_3	L_4
Complete	J	4	-0.2	0.4	-3.6	0.5
		3	-4.6	-1.2	-9.3	0.2
		2	-10.6	-1.8	-16.2	0.4
		1	-17.0	-1.8	-22.9	1.0
	T	4	-0.1	0.8	-3.3	0.8
		3	-4.4	-1.1	-8.9	0
		2	-10.3	-1.9	-15.7	0.2
		1	-16.6	-1.9	-22.4	0.8
Reduced	8	4	-0.2	0.6	-2.3	-0.3
		3	-3.1	-1.6	-6.8	-1.5
		2	-6.8	-3.1	-12.2	-1.9
		1	-10.9	-4.0	-17.5	-2.2
Reduced, shear walls only	8	4	0.4	1.2	-2.8	0.7
		3	-4.5	-0.8	-8.9	0
		2	-10.9	-1.2	-16.4	0.7
		1	-18.8	-0.2	-25.2	2.6
Reduced, friction	8	4	-0.3	0.7	-2.4	-0.1
		3	-3.6	-1.0	-7.0	-1.0
		2	-7.7	-2.1	-12.8	-1.0
		1	-12.6	-2.4	-18.8	-1.0

B.3.2 Horizontal force distribution in shear walls

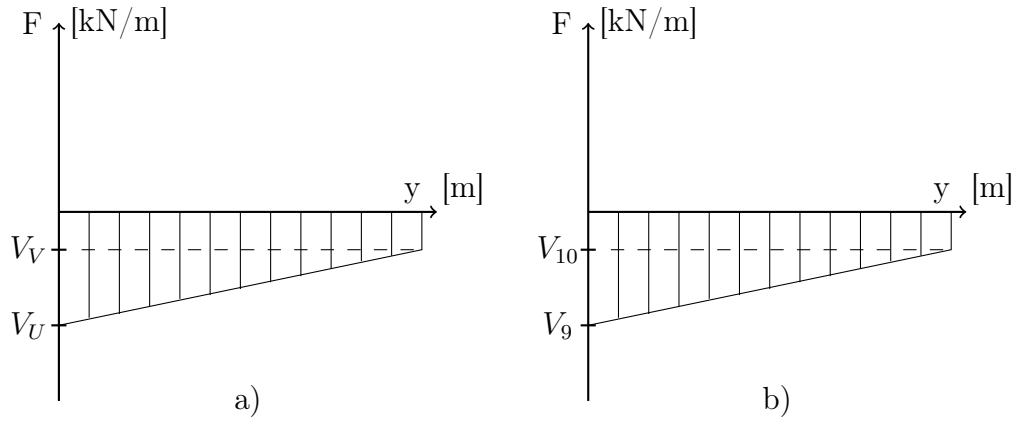

Figure B.20: Horizontal force distribution (linearized) in connections between ceilings and shear walls for the complete model (a) and the reduced models (b).

Table B.18: Horizontal connection forces [kN/m] in the line connection between shear wall and ceiling for the complete analysis.

		Axis											
Storey		A	B	C	D	I	J	K	L	Q	R	S	T
4	V_U	-1.3	-1.0	-0.9	-1.2	-0.8	-1.1	-1.3	-1.1	-1.0	-1.3	-0.9	-1.1
	V_V	-0.9	-0.5	-0.4	-0.8	-1.2	-1.2	-0.8	-0.6	-0.1	0	-1.1	-1.0
3	V_U	-2.4	-1.6	-1.5	-2.2	-1.2	-1.8	-2.3	-1.6	-1.7	-2.4	-1.3	-1.8
	V_V	-1.6	-1.3	-1.2	-1.6	-2.0	-2.1	-1.6	-1.4	-1.1	-0.9	-2.0	-1.9
2	V_U	-3.7	-2.4	-2.1	-3.0	-1.9	-2.1	-3.6	-2.4	-2.5	-3.4	-1.4	-2.1
	V_V	-1.8	-1.7	-1.6	-2.4	-2.5	-3.1	-1.9	-1.7	-1.7	-1.6	-2.8	-2.9
1	V_U	-4.5	-3.1	-2.9	-4.6	-1.5	-2.2	-4.4	-3.1	-3.4	-4.6	-1.6	-2.2
	V_V	-2.5	-2.0	-1.9	-2.4	-3.8	-4.2	-2.5	-2.0	-2.2	-2.0	-3.7	-4.0

Table B.19: Horizontal connection forces [kN/m] in the line connection between shear wall and ceiling for the reduced analyses.

			Axis							
Analysis	Storey		1	2	3	4	5	6	7	8
Reduced	4	V_9	-1.7	-1.3	-1.4	-2.0	1.7	-2.3	-1.4	-1.5
		V_{10}	-0.1	0	0	0	0	0	0	8
	3	V_9	-1.8	-1.8	-1.9	-1.6	-2.3	-2.4	-1.4	-1.4
		V_{10}	-1.5	-1.0	-0.9	-1.6	-0.1	-1.2	1.0	-1.3
	2	V_9	-2.8	-2.5	-2.4	-2.7	-3.1	-3.2	-1.5	-2.3
		V_{10}	-2.0	-1.6	-1.4	-2.0	-1.7	-1.9	-1.8	-1.7
	1	V_9	-2.7	-3.0	-3.0	-3.6	-3.7	-3.9	-1.8	-2.9
		V_{10}	-3.6	-2.0	-1.9	-2.5	-2.4	-2.5	-1.7	-2.0
Reduced, only shear walls	4	V_9	-2.6	-2.3	-2.4	-2.7	-3.0	-3.3	0	0
		V_{10}	0	0	0	0	0	0	-2.2	-2.1
	3	V_9	-1.6	-2.1	-2.1	-1.6	-2.5	-2.4	-1.3	-1.8
		V_{10}	-2.1	-1.2	-1.2	-2.2	-1.5	-1.8	-1.5	-1.3
	2	V_9	-2.1	-2.8	-2.8	-2.1	-3.5	-4.7	-1.9	-2.7
		V_{10}	-3.1	-1.9	-1.8	-3.2	-2.3	-2.9	-2.1	-1.8
	1	V_9	-2.9	-3.7	-3.6	-2.9	-4.5	-4.7	-2.1	-3.2
		V_{10}	-3.7	-2.2	-2.2	-3.7	-2.8	-2.9	-3.0	-2.5
Reduced, friction	4	V_9	-1.9	-1.4	-1.7	-2.1	-2.1	-2.5	0	0
		V_{10}	0	0	0	0	0	0	-1.4	-1.6
	3	V_9	-1.5	-1.9	-1.8	1.6	-2.2	-2.5	-1.0	-1.5
		V_{10}	-1.8	-1.0	-0.9	1.7	-1.0	-1.3	-1.4	-1.3
	2	V_9	-1.8	-2.4	-2.3	-1.9	-3.0	-3.1	-1.5	-2.6
		V_{10}	-3.0	-1.7	-1.5	-2.9	-1.8	-2.1	-1.5	-1.7
	1	V_9	-2.3	-2.7	-2.8	-2.2	-3.5	-3.7	-2.1	-3.1
		V_{10}	-4.0	-2.3	-2.1	-3.9	-2.7	-2.8	-2.6	-1.8

B.3.3 Connection forces between modules

Figure B.21: Line forces (L), point forces (F) and moments (M) in connections between TVEs for the complete analysis.

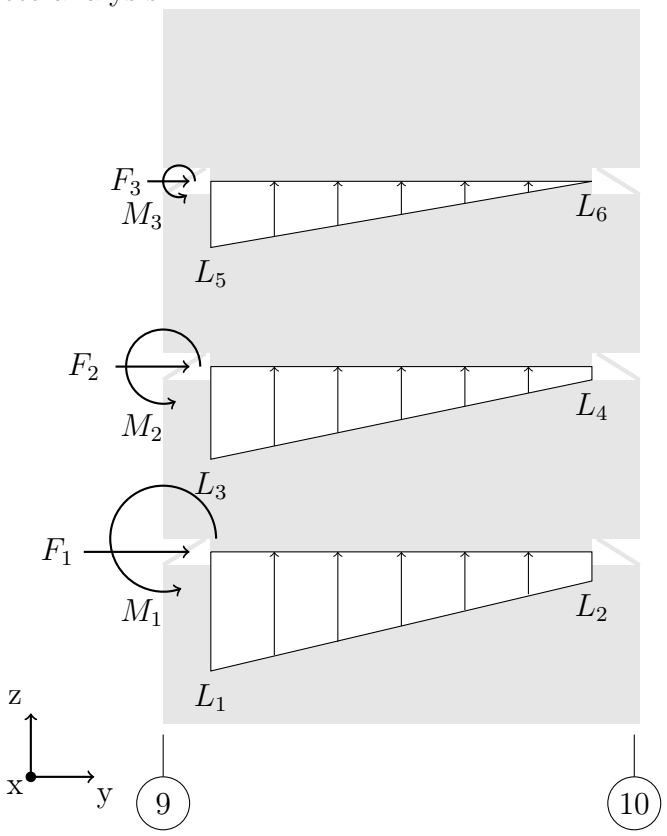

Table B.20: Line forces L [kN/m], point forces F [kN] and moments M [kNm] in connections between TVEs for the complete analysis.

Axis	A	B	C	D	I	J	K	L	Q	R	S	T
F_1	-27.1	-24.5	-23.2	-25.6	-24.0	-25.6	-26.8	-24.5	-24.8	-26.0	-23.8	-24.1
F_2	-20.4	-18.9	-17.4	-19.1	-18.7	-20.2	-20.1	-18.9	-18.0	-18.2	-18.6	-19.0
F_3	-13.0	-12.5	-10.8	-11.8	-13.2	-13.8	-12.8	-12.3	-9.8	-10.1	-13.4	-12.2
M_1	2.1	3.6	1.3	0.4	1.0	0.7	3.8	3.6	2.1	3.1	1.0	2.5
M_2	2.2	3.3	0.7	0.4	1.2	0.4	3.9	3.2	1.8	2.8	1.2	2.1
M_3	1.5	1.8	1.0	0.7	0	0.3	2.8	1.9	2.0	3.0	-0.2	1.5
L_1	-19.5	-15.5	-16.3	-22.2	-20.8	-21.7	-19.9	-15.5	-16.2	-20.5	-20.8	-21.3
L_2	-2.3	-5.2	-3.9	-2.6	-0.8	-0.6	-2.2	-4.9	-6.9	-3.4	-1.1	-0.9
L_3	-12.5	-10.0	-9.6	-13.3	-13.2	-13.1	-12.9	-9.7	-9.5	-13.9	-13.4	-12.7
L_4	-1.7	-3.7	-3.2	-2.0	-1.0	-1.0	-1.7	-3.7	-4.6	-2.2	-1.2	-1.2
L_5	-5.7	-4.0	-3.8	-5.6	-5.9	-5.6	-6.3	-4.5	-4.1	-7.5	-6.1	-5.2
L_6	0	0	0	0	0	0	0	0	0	0	0	0

Table B.21: Line forces L [kN/m], point forces F [kN] and moments M [kNm] in connections between TVEs for the reduced analysis.

Axis	1	2	3	4	5	6	7	8
F_1	-24.4	-24.1	-24.2	-24.4	-28.8	-28.8	-20.2	-21.8
F_2	-17.9	-18.2	-18.4	-17.8	-22.0	-20.9	-15.1	-16.2
F_3	-10.9	-11.6	-11.6	-10.7	-13.8	-12.7	-9.5	-9.8
M_1	2.3	2.7	1.4	1.0	1.8	1.5	1.4	0.9
M_2	1.9	2.2	1.5	1.1	1.9	1.5	1.0	1.1
M_3	1.3	1.4	1.3	1.0	1.6	1.2	0.9	0.9
L_1	-28.8	-21.8	-20.3	-27.0	-23.4	-29.2	-23.1	-24.0
L_2	-3.7	-6.8	-5.6	-3.6	-5.3	-1.1	-2.3	-3.5
L_3	-17.0	-12.8	-12.1	-16.0	-13.8	-18.1	-13.5	-14.3
L_4	-3.4	-4.8	-3.8	-3.0	-3.8	-0.7	-1.8	-3.1
L_5	-7.0	-5.8	-4.9	-6.6	-5.7	-8.0	-5.8	-5.9
L_6	-1.3	0	-1.6	-1.2	-1.8	-0.1	-0.6	-1.4

Table B.22: Line forces L [kN/m], point forces F [kN] and moments M [kNm] in connections between TVEs for the reduced analysis with only shear walls.

Axis	1	2	3	4	5	6	7	8
F_1	-25.2	-24.8	-24.7	-25.3	-29.8	-29.5	-21.2	-21.9
F_2	-19.1	-18.5	-18.7	-19.0	-22.5	-22.2	-16.0	-16.5
F_3	-11.8	-12.0	-11.9	-11.9	-14.2	-14.0	-10.2	-10.4
M_1	3.7	3.6	3.6	3.7	4.4	4.3	3.1	3.2
M_2	2.8	2.7	2.7	2.8	3.3	3.2	2.4	2.4
M_3	1.7	1.8	1.8	1.8	2.1	2.1	1.5	1.5
L_1	-39.3	-30.7	-30.2	-39.8	-36.2	-45.3	-32.4	-34.2
L_2	0	0	0	0	0	0	0	0
L_3	-22.9	-17.2	-16.8	-23.1	-20.1	-26.5	-18.9	-19.7
L_4	0	0	-1.0	0	0	0	0	0
L_5	-8.5	-6.2	-6.0	-8.8	-7.7	-10.3	-6.9	-7.5
L_6	0	0	0	0	0	0	0	0

Table B.23: Line forces L [kN/m] and point forces F [kN] in connections between TVEs for the reduced analysis with friction.

Axis	1	2	3	4	5	6	7	8
L_1	-33.2	-31.0	-29.6	-30.5	-33.7	-40.4	-27.9	-29.5
L_2	0	0	0	0	0	0	0	0
L_3	-18.9	-17.3	-17.6	-17.3	-20.0	-24.2	-23.6	-16.7
L_4	0	0	0	0	0	0	0	0
L_5	-5.7	-6.4	-8.7	-5.1	-11.0	-7.5	-3.6	-5.5
L_6	0	0	0	0	0	0	0	0

Appendix C

Analyses results - Wind loads towards building short side

C.1 Support reaction forces

C.1.1 Complete model

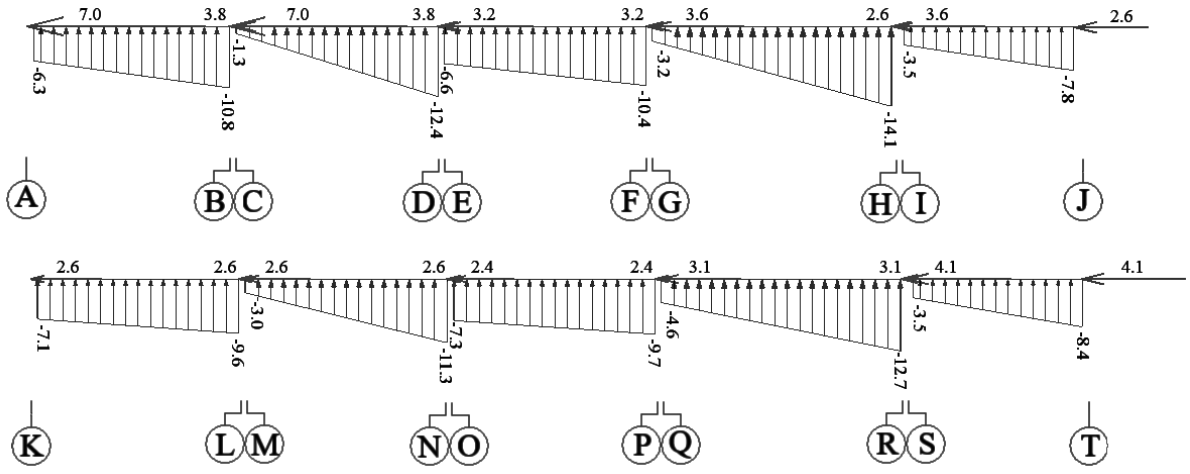

Figure C.1: Line support reaction forces [kN/m] and point support reaction forces [kN] along axis U.

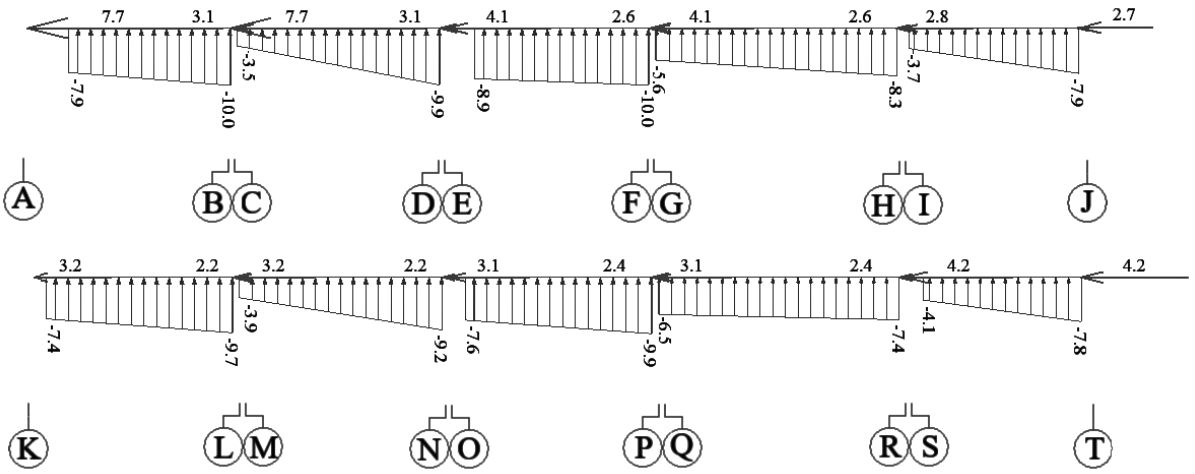

Figure C.2: Line support reaction forces [kN/m] and point support reaction forces [kN] along axis V.

C.1.2 Complete model with only shear walls

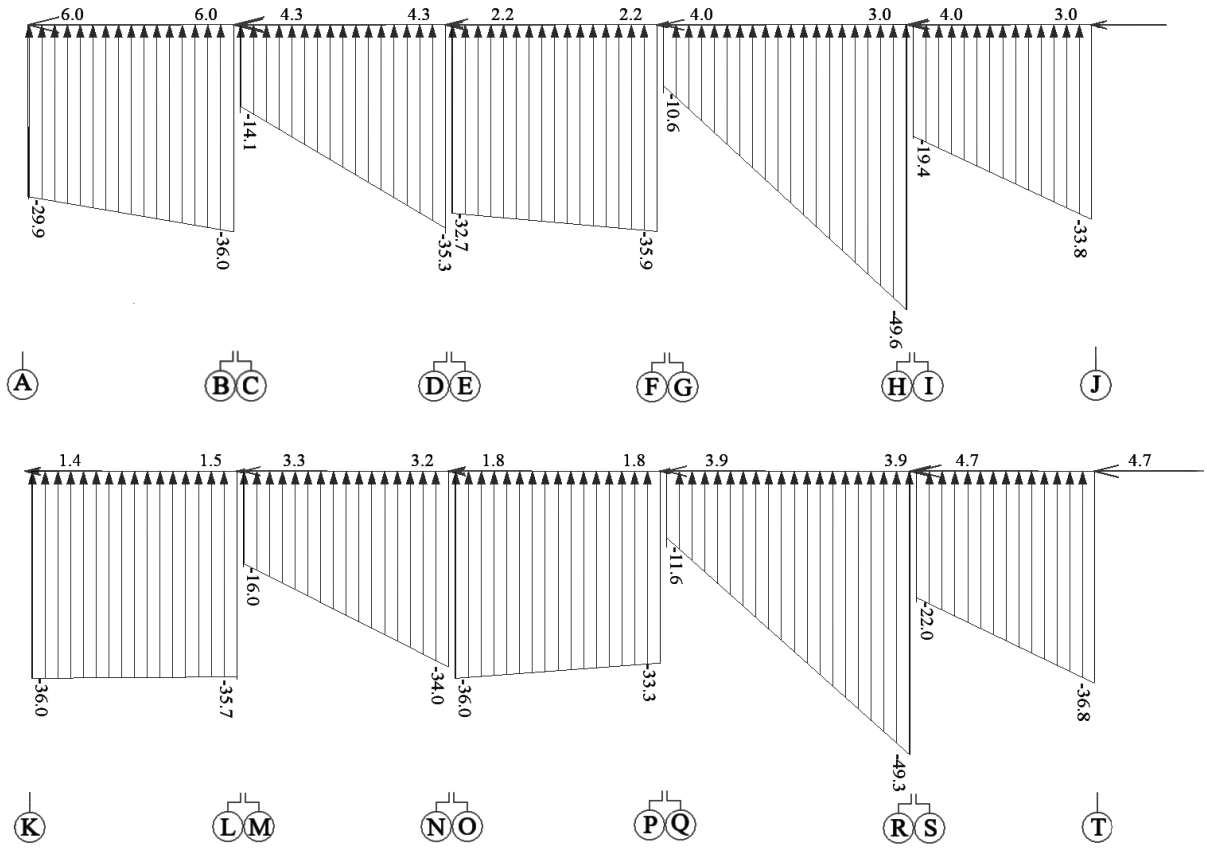

Figure C.3: Line support reaction forces [kN/m] and point support reaction forces [kN] along axis U (assuming a linear line load distribution).

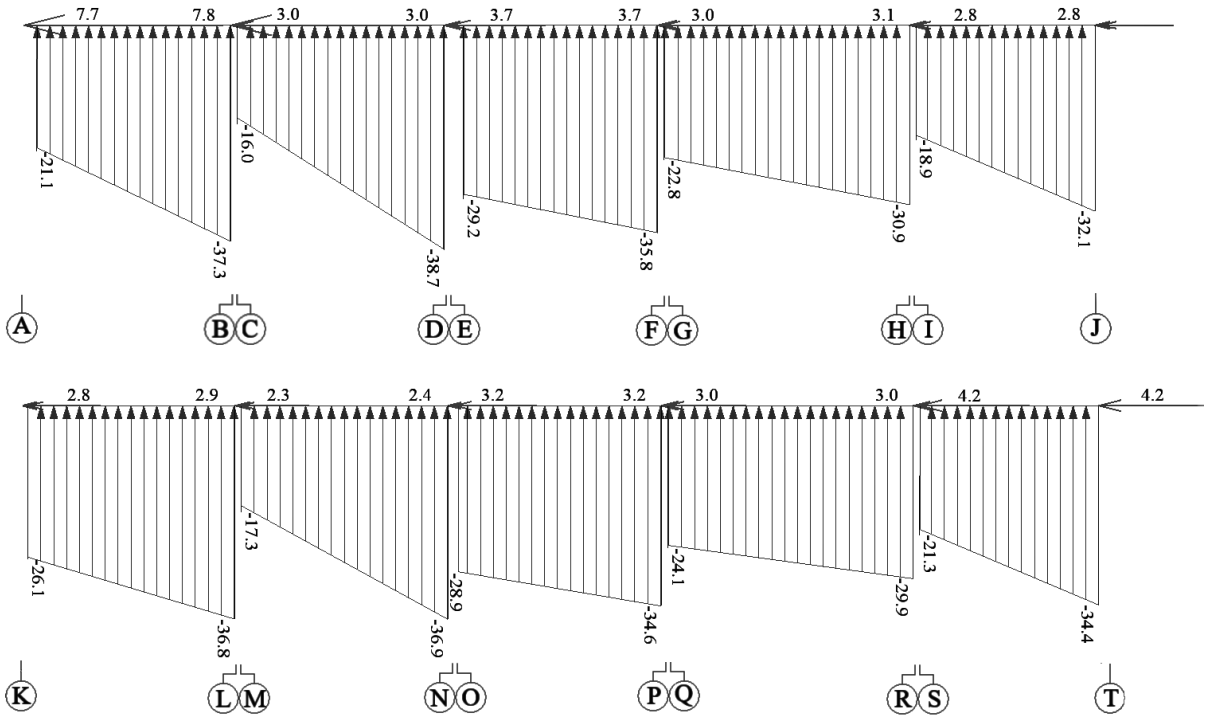

Figure C.4: Line support reaction forces [kN/m] and point support reaction forces [kN] along axis V (assuming a linear line load distribution).

C.2 Displacements

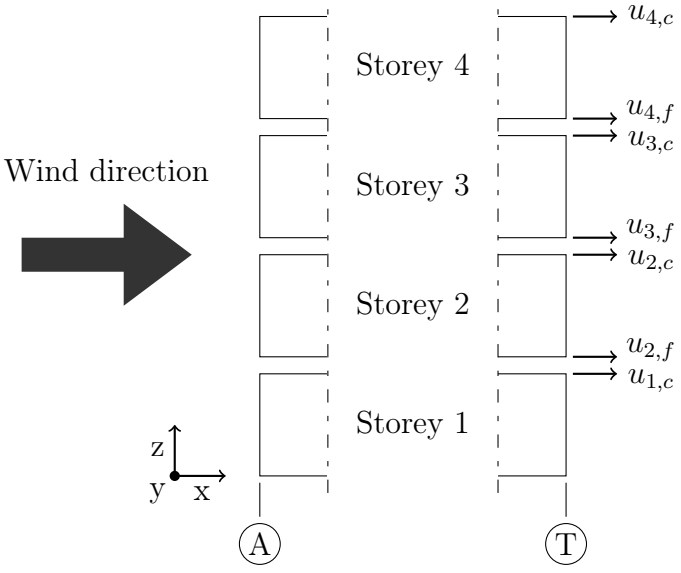

Figure C.5: Illustration of displacement measuring positions in the ceiling truss (u_c) and floor truss (u_f).

Table C.1: Horizontal in-plane (u_x) and out-of-plane (u_y) displacements [mm] for the analyses on wind loads towards the short side of the building.

Configuration	Complete		Complete, only shear walls	
Axis	U	V	U	V
$u_{1,c,x}$	16	16	28	24
$u_{1,c,y}$	-1	-1	-30	-30
$u_{2,f,x}$	18	19	32	29
$u_{2,f,y}$	-2	-2	-30	-30
$u_{2,c,x}$	34	34	65	63
$u_{2,c,y}$	-3	-3	-51	-51
$u_{3,f,x}$	36	36	69	67
$u_{3,f,y}$	-3	-4	-51	-51
$u_{3,c,x}$	48	47	99	94
$u_{3,c,y}$	-4	-4	-71	-71
$u_{4,f,x}$	50	48	181	157
$u_{4,f,y}$	-4	-5	-71	-70
$u_{4,c,x}$	63	56	216	161
$u_{4,c,y}$	-5	-5	-86	-87

C.3 Connection forces

C.3.1 Vertical connection force distributions

Axis U

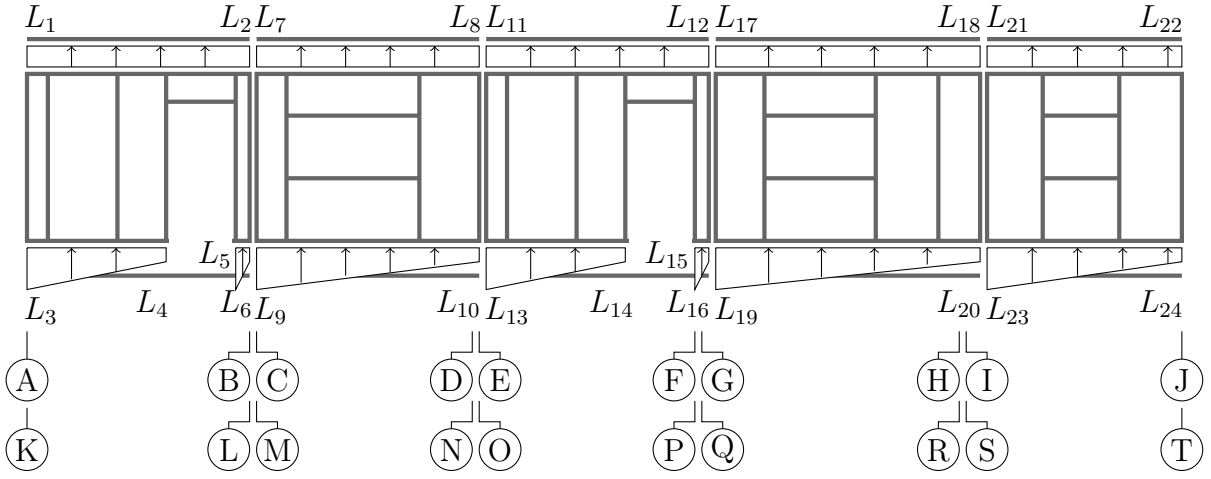

Figure C.6: Illustration of vertical force distribution (linearized) in the connections between shear walls and horizontal diaphragms on each floor along axis U.

Table C.2: Vertical line connection forces [kN/m] (linearized distribution) along axis U for the complete analysis.

	Axis A-J				Axis K-T			
Storey	1	2	3	4	1	2	3	4
L_1	-8.0	-3.5	-2.1	0.7	-8.5	-3.7	-2.6	-0.3
L_2	-4.4	-2.9	-0.4	1.6	-4.9	-3.2	-0.3	2.1
L_3	-4.2	-3.3	-2.4	0.2	-5.9	-4.0	-2.9	-1.1
L_4	-15.0	-8.7	-4.7	-1.5	-14.1	-8.8	-4.9	-1.0
L_5	-23.7	-8.1	-4.0	-22.4	-4.9	-8.4	-4.0	-0.1
L_6	-20.9	-18.7	-9.3	-0.3	-19.6	-19.3	-9.2	-0.1
L_7	-4.1	-2.7	-2.5	-0.1	-4.0	-2.6	-2.5	0.2
L_8	-4.4	-1.8	0.3	2.5	-4.6	-1.8	0.3	2.1
L_9	-2.5	-2.2	-1.7	-0.3	-3.7	-2.3	-1.8	-0.4
L_{10}	-9.8	-4.4	-1.8	-0.9	-8.7	-5.7	-1.8	-0.8
L_{11}	-8.6	-4.1	-2.7	-1.3	-8.8	-4.2	-2.9	-0.5
L_{12}	-4.9	-3.1	-0.5	2.5	-5.2	-3.3	-0.6	1.4
L_{13}	-5.3	-4.2	-2.9	-1.3	-6.1	-4.2	-3.3	-1.9
L_{14}	-14.9	-9.0	-5.2	-1.5	-14.4	-9.0	-5.3	-1.9
L_{15}	-23.6	-8.4	-4.3	-0.2	-23.2	-8.7	-4.4	-0.6
L_{16}	-20.6	-19.2	-9.9	-0.6	-20.1	-20.0	-10.0	-1.3
L_{17}	-1.8	-2.8	-1.7	-0.1	-3.3	-2.6	-1.1	0.9
L_{18}	-12.2	-5.7	-1.6	2.6	-10.6	-5.5	-1.7	1.7
L_{19}	-2.4	-2.4	-1.3	-0.1	-3.9	-4.8	-2.6	-0.8
L_{20}	-15.1	-8.1	-5.6	-1.1	-13.6	-6.4	-3.7	-0.3
L_{21}	-2.8	-2.2	-1.3	-1.0	-3.0	-2.2	-1.1	-1.0
L_{22}	-3.9	-1.8	-0.3	1.9	-4.2	-1.9	-0.7	1.6
L_{23}	-2.3	-1.8	-1.2	-1.4	-2.3	-1.6	-1.1	-0.4
L_{24}	-8.0	-5.3	-3.5	-0.8	-8.6	-5.8	-3.7	-2.2

Table C.3: Vertical line connection forces [kN/m] (linearized distribution) along axis U for the complete analysis with only shear walls.

	Axis A-J				Axis K-T			
Storey	1	2	3	4	1	2	3	4
L_1	-34.8	-25.1	-14.9	-3.3	-39.3	-28.4	-22.3	-18.9
L_2	-33.8	-22.4	-11.6	-2.2	-36.6	-26.7	-11.7	-5.4
L_3	-31.2	-29.5	-18.4	-6.1	-38.3	-34.4	-25.8	-6.6
L_4	-62.8	-40.1	-23.5	-7.2	-66.5	-45.4	-28.0	-9.9
L_5	-115.1	-39.3	-21.6	-7.4	-121.1	-45.2	-22.8	-5.0
L_6	-115.9	-98.2	-53.7	-18.4	-121.3	-112.8	-56.4	-11.9
L_7	-22.0	-17.2	-13.7	-4.8	-23.1	-17.2	-13.6	-5.4
L_8	-32.4	-18.0	-0.7	10.8	-32.4	-18.2	-1.6	10.7
L_9	-20.7	-15.8	-10.9	-3.6	-23.1	-17.2	-11.5	-4.2
L_{10}	-39.0	-32.4	-9.0	-0.7	-37.6	-24.6	-9.1	4.2
L_{11}	-36.6	-28.2	-20.8	-19.6	-40.6	-27.5	-22.6	-17.3
L_{12}	-35.7	-23.1	-9.9	9.4	-32.8	-24.9	-9.1	6.2
L_{13}	-34.5	-33.1	-22.9	-1.5	-23.2	-16.1	-11.3	-4.2
L_{14}	-64.8	-42.5	-26.1	-8.5	-70.0	-42.6	-26.6	-7.5
L_{15}	-119.1	-39.9	-21.2	0.0	-112.8	-42.2	-20.3	-1.7
L_{16}	-119.6	-99.4	-52.8	1.1	-113.1	-105.1	-50.1	-2.6
L_{17}	-5.6	-12.7	-11.0	-5.5	-7.1	-12.0	-10.8	1.9
L_{18}	-63.3	-35.6	-16.8	-2.1	-62.6	-35.3	-17.8	-6.3
L_{19}	-12.7	-5.6	-12.7	-11.0	-14.0	-7.1	-12.6	-1.8
L_{20}	-61.4	-42.3	-23.5	-7.2	-61.0	-41.8	-23.7	-7.9
L_{21}	-23.5	-18.7	-11.2	-4.6	-27.7	-21.8	-11.5	0.8
L_{22}	-36.1	-19.3	-5.0	10.3	-38.9	-23.1	-11.6	-2.2
L_{23}	-23.4	-19.1	-11.0	-3.3	-26.5	-22.6	-13.6	-0.8
L_{24}	-40.9	-23.7	-9.9	4.2	-44.8	-27.0	-14.2	-5.3

Axis V

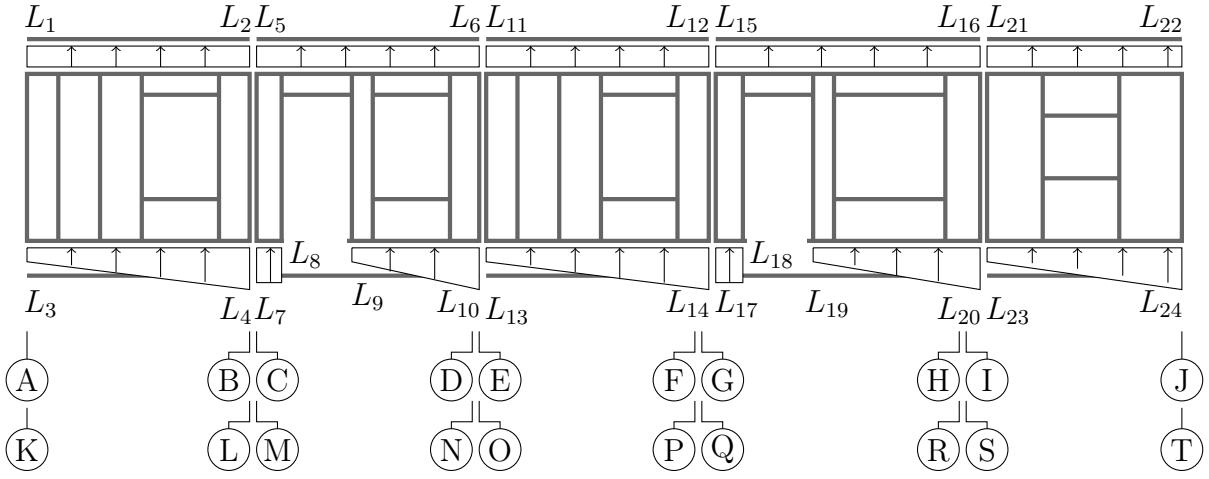

Figure C.7: Illustration of vertical force distribution (linearized) in the connections between shear walls and horizontal diaphragms on each floor along axis V.

Table C.4: Vertical line connection forces [kN/m] (linearized distribution) along axis V for the complete analysis.

	Axis A-J				Axis K-T			
Storey	1	2	3	4	1	2	3	4
L_1	-3.0	-1.1	-1.3	0.3	-5.6	-3.8	-2.1	-0.2
L_2	-5.4	-5.8	-0.8	1.7	-5.5	-2.5	-0.7	1.8
L_3	-2.4	-1.6	-1.6	-0.4	-4.9	-2.9	-2.4	-1.2
L_4	-11.3	-6.8	-3.3	-0.7	-10.3	-6.1	-2.9	-0.4
L_5	-3.4	-4.8	-1.6	-0.9	-3.5	-4.8	-1.6	-0.3
L_6	-8.7	-2.3	-2.6	1.5	-8.3	-2.3	-2.5	1.2
L_7	-9.6	-12.1	-8.0	-4.2	-10.7	-12.4	-8.1	-3.2
L_8	-10.5	-5.7	-3.4	-1.9	-11.0	-5.3	-3.4	-1.3
L_9	-9.0	-5.1	-3.1	-0.9	-9.0	-5.1	-3.1	-0.8
L_{10}	-11.3	-6.7	-4.1	-1.6	-10.4	-6.3	-4.1	-1.6
L_{11}	-5.4	-1.4	-1.6	0.3	-5.7	-4.9	-2.0	0.5
L_{12}	-5.8	-6.2	-1.0	1.4	-5.8	-2.7	-0.9	1.0
L_{13}	-4.1	-2.2	-2.0	-0.8	-4.9	-3.5	-2.7	-1.4
L_{14}	-11.4	-7.0	-3.4	-0.6	-10.6	-6.3	-2.9	-0.4
L_{15}	-5.0	-3.6	-2.4	0.2	-5.9	-3.7	-1.3	1.3
L_{16}	-6.9	-4.4	-1.1	1.9	-6.0	-3.9	-1.6	1.1
L_{17}	-9.4	-10.4	-7.9	-2.6	-11.3	-13.5	-7.9	0
L_{18}	-8.0	-3.8	-2.9	-0.9	-9.1	-3.7	-2.1	0
L_{19}	-10.5	-6.9	-3.9	-0.2	-10.8	-7.6	-3.9	0.1
L_{20}	-8.5	-4.8	-2.5	0	-7.6	-4.4	-2.5	-0.7
L_{21}	-3.4	-1.8	-1.5	-0.7	-3.0	-2.5	-1.3	-0.6
L_{22}	-3.8	-2.2	-0.3	1.5	-3.9	-2.2	-0.7	0.8
L_{23}	-2.6	-1.4	-1.6	-1.0	-2.0	-1.7	-1.5	-0.9
L_{24}	-8.2	-6.1	-3.7	-1.5	-8.5	-6.1	-3.7	-2.1

Table C.5: Vertical line connection forces [kN/m] (linearized distribution) along axis V for the analysis with only shear walls.

	Axis A-J				Axis K-T			
Storey	1	2	3	4	1	2	3	4
L_1	-20.0	-8.4	-11.0	-2.2	-31.0	-22.5	-18.1	-12.6
L_2	-39.1	-30.7	-8.1	3.2	-35.5	-23.8	-8.2	6.5
L_3	-20.0	-12.5	-9.8	-3.3	-29.5	-20.7	-16.9	-9.9
L_4	-44.7	-32.2	-14.9	-1.3	-42.5	-31.1	-14.9	-1.8
L_5	-16.3	-28.5	-16.4	-11.8	-18.2	-26.9	-15.5	-12.5
L_6	-53.3	-20.6	-12.3	3.3	-51.1	-21.9	-13.0	4.0
L_7	-65.0	-78.1	-62.3	-34.5	-70.8	-70.4	-60.0	-34.5
L_8	-56.6	-31.1	-20.9	-12.3	-60.1	-27.4	-20.4	-11.4
L_9	-49.1	-32.3	-19.1	-8.2	-49.0	-32.5	-18.8	-7.9
L_{10}	-55.8	-39.2	-21.9	-4.9	-53.3	-39.6	-22.6	-5.2
L_{11}	-26.9	-11.0	-14.3	-5.1	-31.4	-25.8	-17.4	-4.5
L_{12}	-37.0	-32.8	-9.1	2.2	-33.8	-19.3	-7.4	0.3
L_{13}	-24.7	-16.3	-12.8	-5.8	-28.9	-22.6	-16.6	-6.8
L_{14}	-44.8	-33.0	-16.1	-2.7	-41.9	-26.0	-13.7	-3.6
L_{15}	-24.0	-19.9	-17.1	-7.0	-26.2	-19.4	-11.6	-2.6
L_{16}	-37.8	-23.9	-8.5	-0.3	-36.0	-24.8	-14.3	-5.2
L_{17}	-55.7	-56.1	-49.5	-22.9	-60.0	-59.1	-38.7	-13.5
L_{18}	-37.9	-17.2	-14.5	-7.2	-40.4	-17.0	-11.0	-4.2
L_{19}	-50.5	-35.2	-22.0	-8.5	-51.5	-35.8	-22.4	-7.1
L_{20}	-38.4	-28.6	-14.6	-3.8	-36.8	-28.0	-16.9	-8.8
L_{21}	-23.7	-18.5	-11.0	-4.1	-27.3	-22.1	-13.5	2.6
L_{22}	-36.3	-19.6	-5.8	8.6	-38.8	-22.4	-12.0	-4.4
L_{23}	-24.4	-18.5	-10.8	-2.7	-27.3	-22.4	-14.9	-5.8
L_{24}	-40.7	-21.7	-11.0	2.2	-43.8	-27.2	-13.3	-0.5

C.3.2 Horizontal force distributions in shear walls

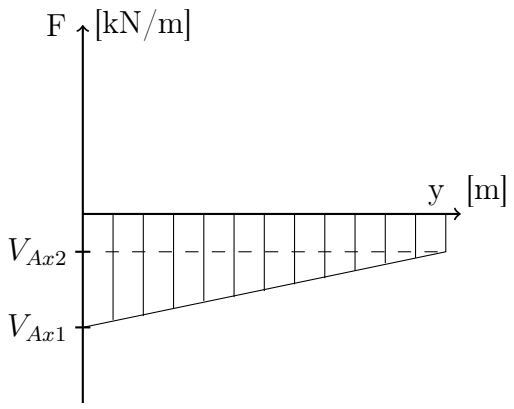

Figure C.8: Illustration of horizontal force distribution (linearized) in connections between ceilings and shear walls.

Table C.6: Horizontal line connection forces [kN/m] (linearized) between the shear walls and the ceiling for the complete analysis.

Axis	Storey	Ax1	A	C	E	G	I	K	M	O	Q	S
		Ax2	B	D	F	H	J	L	N	P	R	T
U	4	V_{Ax1}	0	1.2	0	0.8	0.2	0.2	0.3	0	0.3	0.9
		V_{Ax2}	0.8	0	0.9	0.6	0.2	0.1	0.5	0.2	0.2	0.9
	3	V_{Ax1}	0.9	1.6	1.0	0.6	0.7	0.9	1.4	1.2	0.3	1.0
		V_{Ax2}	0.3	0.3	0.3	1.4	0.7	0.4	0.4	0	0.4	0.4
	2	V_{Ax1}	1.8	1.2	1.7	0.9	1.0	1.6	1.0	2.1	0.1	1.3
		V_{Ax2}	0.5	1.2	0.5	2.1	1.0	0.5	1.2	0.3	0.3	0.8
	1	V_{Ax1}	2.3	1.7	1.7	0	1.2	1.4	1.1	1.4	0.2	1.7
		V_{Ax2}	1.6	1.9	0.4	3.4	1.2	1.0	1.3	0.8	3.1	1.0
V	4	V_{Ax1}	0.6	1.3	0.2	0.6	0.3	0.5	0.1	0.2	0.4	0.5
		V_{Ax2}	0.6	0.5	0.5	0.1	0.7	0.3	0.6	0.1	0.5	0.1
	3	V_{Ax1}	0.7	0.7	0.6	1.0	0.7	0.6	0.5	0.7	0.3	0.8
		V_{Ax2}	1.2	0.6	1.2	0.1	0.7	1.2	0.8	0.8	0.2	0.4
	2	V_{Ax1}	3.1	1.8	2.9	0.9	1.1	0.8	1.6	1.0	0.2	1.3
		V_{Ax2}	0.1	0	0.1	0.6	1.1	1.5	0.2	1.9	0.1	0.9
	1	V_{Ax1}	2.3	1.2	1.5	1.1	1.2	1.2	0.7	1.0	0.9	1.7
		V_{Ax2}	2.1	1.3	2.7	0.7	1.3	2.1	1.1	1.9	0.8	1.0

Table C.7: Horizontal line connection forces [kN/m] (linearized) between the shear walls and the ceiling for the complete analysis with shear walls only.

Axis	Storey	Ax1	A	C	E	G	I	K	M	O	Q	S
		Ax2	B	D	F	H	J	L	N	P	R	T
U	4	V_{Ax1}	1.0	0.1	0.5	1.3	1.9	0.6	0.8	0.6	0.2	1.2
		V_{Ax2}	0.9	1.4	2.7	0.4	1.1	1.9	2.1	0.4	0.6	0
	3	V_{Ax1}	0.6	1.8	1.3	1.3	0.6	0.6	1.8	0.9	0.9	0.2
		V_{Ax2}	0.3	0.3	0.5	0.5	0.5	0.4	0	0.9	2.0	0.1
	2	V_{Ax1}	1.5	1.7	1.5	1.9 0	1.0	1.0	1.7	0.7	1.5	0.9
		V_{Ax2}	0.4	1.7	0	4.0	0.9	0.1	1.6	0.1	3.9	0.7
	1	V_{Ax1}	2.8	2.8	2.2	0.2	2.0	1.7	2.1	2.2	0.6	2.6
		V_{Ax2}	1.0	2.7	0.4	4.5	2.4	0	2.1	0.1	4.8	2.5
V	4	V_{Ax1}	1.0	2.0	0.8	0.7	0.8	1.9	0.8	0.6	0.5	1.8
		V_{Ax2}	0.7	0.4	0.8	0.1	0.8	1.0	1.8	0.4	1.3	2.9
	3	V_{Ax1}	1.2	0.6	1.2	1.9	0.8	0.7	1.3	0.5	0.8	0.1
		V_{Ax2}	2.2	0.8	2.1	0.1	0.8	1.7	0.4	1.7	0.1	0.3
	2	V_{Ax1}	4.0	3.9	2.7	2.1	1.2	1.4	3.9	1.1	1.1	1.1
		V_{Ax2}	0.4	0	0.4	1.1	1.3	1.5	0.1	1.9	0.7	1.0
	1	V_{Ax1}	3.3	0.9	1.2	2.0	1.8	1.3	0.6	1.4	1.9	2.3
		V_{Ax2}	3.0	3.7	3.5	1.1	2.2	2.4	2.2	2.6	1.2	2.0

C.3.3 Horizontal connections between TVEs

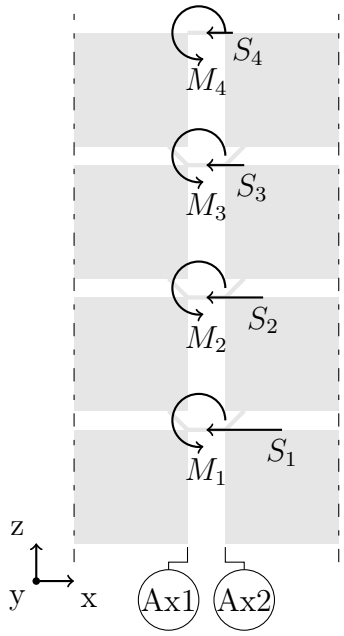

Figure C.9: Illustration of horizontal point connections (steel plates) between TVEs .

Table C.8: Forces, F [kN], and moments, M [kNm], in point connections between TVEs for the complete configuration.

Ax1/Ax2	Axis U							
	V_1	V_2	V_3	V_4	M_1	M_2	M_3	M_4
B/C	-7.8	-9.1	-9.9	-6.8	-1.6	-2.3	-2.7	0
D/E	-5.7	-7.7	-8.2	4.5	-1.9	-1.9	-2.3	0
F/G	-3.7	-6.1	-6.7	-3.1	0	-2.0	-2.1	-3.1
H/I	-3.1	-3.9	-5.1	0	-1.5	-1.6	-1.9	0
J/K	-2.5	-2.5	-2.7	0	0	-0.4	-0.3	0
L/M	-1.7	-0.9	-0.7	0	0	0	0	0
N/O	-1.5	0	1.5	1.9	0	0	0	0
P/Q	-1.7	2.8	4.4	1.3	0	0	0	0
R/S	4.4	3.1	5.1	0	0	3.1	0.2	0
A1/A2	Axis V							
	V_1	V_2	V_3	V_4	M_1	M_2	M_3	M_4
B/C	-7.8	-8.9	-9.8	-6.8	-3.1	-2.9	-3.1	0.6
D/E	-6.1	-7.6	-8.6	-5.5	-1.2	-1.3	-1.8	0.5
F/G	-3.9	-5.4	-6.4	-4.0	-2.0	-2.1	-2.4	-0.3
H/I	-3.3	-4.2	-4.5	-3.1	0	-0.9	-1.5	0
J/K	-2.6	-2.7	-3.0	-1.1	0	0	0	0.4
L/M	-1.6	-1.1	-0.7	0.8	0	0	0	0.3
N/O	-1.6	0	0.8	2.4	0	0	0	0.4
P/Q	1.3	2.9	3.8	3.2	0	0	0	0
R/S	3.6	2.6	3.1	3.9	0	0	0	1.6

Table C.9: Forces, F [kN], and moments, M [kNm], in point connections between TVEs for the complete configuration with only shear walls.

A1/A2	Axis U							
	V_1	V_2	V_3	V_4	M_1	M_2	M_3	M_4
B/C	-8.2	-9.7	-9.5	-8.6	-4.3	-4.1	-5.5	0
D/E	-4.8	-7.7	-8.2	-6.3	-3.1	-4.8	-4.8	0
F/G	-2.9	-8.4	-8.9	-2.8	-0.3	-5.3	-4.4	0
H/I	-5.8	-3.9	-5.3	0	-1.2	-3.1	-4.4	0
J/K	-2.4	-2.9	-4.8	0	0	-3.2	-2.7	0
L/M	-1.5	-2.5	-5.2	2.3	0	0	-2.6	0
N/O	0	0	-4.3	4.0	0	0	-0.3	0
P/Q	2.5	-2.1	0	3.0	0	0	0	0
R/S	0	2.8	6.1	0	0	0	0	0
A1/A2	Axis V							
	V_1	V_2	V_3	V_4	M_1	M_2	M_3	M_4
B/C	-6.8	-11.0	-8.5	-6.6	-8.6	-3.4	-4.8	-0.4
D/E	-7.3	-7.0	-8.7	-4.7	0	-5.2	-3.6	0.8
F/G	-3.5	-8.5	-5.9	-3.0	-0.4	-4.8	-3.6	0.5
H/I	-3.9	-6.1	-3.3	-1.0	0	-1.9	-2.9	-2.7
0 J/K	-1.9	-4.9	-3.2	0.9	-0.2	-3.2	-2.0	0.7
L/M	0	-4.2	-3.8	4.7	0.8	0	0.1	1.5
N/O	-2.2	-0.8	-5.3	9.2	0	0	-0.2	2.6
P/Q	-0.7	0.5	-2.2	9.2	-0.3	-0.3	0	3.2
R/S	1.8	2.3	-2.0	-11.9	0	0	0	2.9

C.3.4 Vertical connections between TVEs

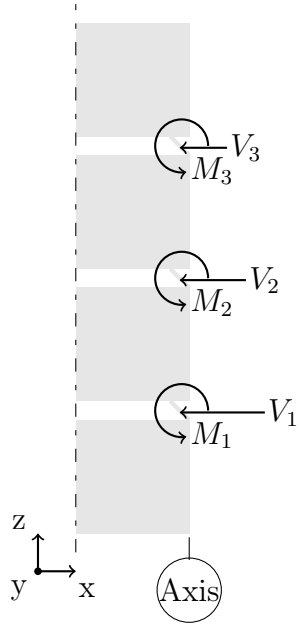

Figure C.10: Illustration of point connections between TVEs (stops).

Table C.10: Forces, F [kN], and moments, M [kNm], in point connections between TVEs for the complete configuration.

Axis	Axis U						Axis V					
	V_1	V_2	V_3	M_1	M_2	M_3	V_1	V_2	V_3	M_1	M_2	M_3
A	0	0	-0.9	0	0	0.1	0	0	-0.9	0	0	0.1
B	-12.4	-11.6	-9.1	-1.2	-1.2	-1.7	-12.4	-11.0	-9.1	-1.2	-1.5	-1.7
C	-4.1	-5.0	-7.4	-2.5	-2.0	-2.0	-4.1	-5.0	-7.4	-2.5	-2.0	-2.0
D	-8.8	-9.1	-9.1	0	0	-0.4	-8.8	-9.1	-9.6	0	0	-0.4
E	-1.7	-4.6	-5.6	-8.8	-0.7	0	-1.7	-4.6	0	-1.0	-0.7	0
F	-7.9	-8.4	-8.0	-0.8	-0.8	-1.2	-7.9	-8.4	-8.0	-0.8	-0.8	-1.2
G	-0.7	-2.9	-4.6	-1.9	-1.7	-1.7	-0.7	-2.9	-4.6	-1.9	-1.7	-1.7
H	-5.5	-6.1	-5.9	0.8	0	-0.6	-5.5	-6.1	-5.9	0.8	0	-0.6
I	-4.9	-1.4	-2.5	0	-0.8	-1.2	0	-1.4	-2.5	0	-0.8	-1.2
J	-4.9	-4.8	-4.4	0.7	0.7	0.6	-4.9	-4.8	-4.4	0.7	0.7	0.6
K	0	-0.3	-1.1	0	-0.4	-0.2	0	0	-0.8	0	0	0
L	-4.4	-3.0	-1.9	0.7	0.5	0.3	-5.4	-3.9	-2.3	0.8	0.6	0.4
M	0	0	0	0	0	0	0	0	0	0	0	0
N	-4.7	-3.6	-1.4	0.6	0.6	0.3	-4.6	-3.2	-1.7	0.7	0.5	0.3
O	0	0	0	0	0	0	0	0	0	0	0	0
P	-5.0	-2.7	0	0.6	0.2	0	-6.1	-3.1	0	0.8	0.4	0
Q	0	0	0	0	0	0	0	0	0	0	0	0
R	0	0	0	0	0	0	0	0	0	0	0	0
S	0	0	0	0	0	0	0	0	0	0	0	0
T	-7.4	-5.6	-5.8	1.1	0.8	0.8	-7.7	-5.5	-3.9	1.1	0.8	0.6

Table C.11: Forces, F [kN], and moments, M [kNm], in point connections between TVEs for the complete analysis with only shear walls.

Axis	Axis U						Axis V					
	V_1	V_2	V_3	M_1	M_2	M_3	V_1	V_2	V_3	M_1	M_2	M_3
A	0	-0.8	-1.8	0	0	0.2	0	0	0	0	0	0
B	-8.6	-7.3	-6.8	-0.3	-3.1	-4.4	-11.3	-11.7	-8.7	-6.7	-1.7	-3.4
C	-3.3	-6.7	-8.7	-3.9	-3.2	-4.1	-3.6	-6.3	-6.6	-8.0	-2.6	-3.8
D	-7.8	-10.0	-10.5	-0.2	-3.3	-3.2	-10.8	-8.8	-9.5	1.2	-3.9	-2.3
E	-1.8	-7.0	-6.2	-2.9	-3.7	-3.8	0	-6.3	-6.0	0	-4.1	-2.7
F	-5.1	-10.1	-10.3	0.4	-3.8	-2.9	-2.8	-11.4	-8.0	0	-3.1	-2.4
G	0	-0.9	-4.4	0	-5.1	-3.8	0	-3.7	-3.5	0	-4.2	-3.1
H	-11.5	-7.6	-7.7	0.2	-2.1	-3.3	-5.8	-7.5	-4.4	0.8	-0.9	-2.3
I	-1.0	-2.8	-4.9	-1.2	-2.7	-3.7	0	-3.6	-2.3	0	-1.4	-2.5
J	-3.3	-4.4	-6.1	0.3	-2.5	-1.8	-3.8	-5.8	-4.4	0.4	-2.3	1.4
K	0	-1.3	-3.0	0	-3.0	-2.3	0	-2.0	0	0	-2.9	-2.0
L	-1.9	-2.6	-4.9	0.2	0.2	-1.9	-4.6	-6.2	-4.7	-0.2	0.8	0.5
M	0	0	-2.5	0	0	-2.2	0	0	0	0	0	0
N	-4.4	-2.8	-4.2	0.4	0.2	0.2	-7.0	-2.8	-4.6	0.7	0	0.4
O	0	0	0	0	0	0	0	0	0	0	0	0
P	0	0	0	0	0	0	-5.8	-2.8	0	0.4	0	0
Q	0	0	0	0	0	0	0	0	0	0	0	0
R	-13.9	-7.2	0	1.8	0.8	0	0	0	0	0	0	0
S	0	0	0	0	0	0	0	0	0	0	0	0
T	-4.5	-2.6	0	0.6	0.3	0	-5.5	-2.9	0	0.8	0.4	0